ABSTRACT

Title of Document: CONDUCTIVE POLYMER NANOTUBE PATCH FOR FAST AND CONTROLLED *IN VIVO* TRANSDERMAL DRUG DELIVERY.

Thao Minh Nguyen, Doctor of Philosophy, 2012

Directed By: Professor Sang Bok Lee
Department of Chemistry and Biochemistry

Transdermal drug delivery has created new applications for existing therapies and offered an alternative to the traditional oral route where drugs can prematurely metabolize in the liver causing adverse side effects. Opening the transdermal delivery route to large hydrophilic drugs is one of the greatest challenges due to the hydrophobicity of the skin. However, the ability to deliver hydrophilic drugs using a transdermal patch would provide a solution to problems of other delivery methods for hydrophilic drugs. The switching of conductive polymers (CP) between redox states cause simultaneous changes in the polymer charge, conductivity, and volume—properties that can all be exploited in the biomedical field of controlled drug delivery. Using the template synthesis method, poly(3,4-ethylenedioxythiophene (PEDOT) nanotubes were synthesized electrochemically and a transdermal drug delivery patch was successfully designed and developed. *In vitro* and *in vivo* uptake and release of hydrophilic drugs were investigated. The relationship between the strength of the

applied potential and rate of drug release were also investigated. Results revealed that the strength of the applied potential is proportional to the rate of drug release; therefore one can control the rate of drug release by controlling the applied potential. The *in vitro* studies focused on the kinetics of the drug delivery system. It was determined that the drug released mainly followed zero-order kinetics. In addition, it was determined that applying a releasing potential to the transdermal drug delivery system lead to a higher release rate constant (up to 7 times greater) over an extended period of time (~24h). In addition, over 24 hours, an average of 80% more model drug molecules were released with an applied potential than without. The *in vivo* study showed that the drug delivery system was capable of delivering model hydrophilic drugs molecules through the dermis layer of the skin within 30 minutes, while the control showed no visible drugs at the same depth. Most importantly, it was determined that the delivery of drugs into the blood stream was stable within 20 minutes.

The functionalization of CP was also studied in order to enhance the properties and drug loading capabilities of the polymers. The co-polymerization of poly(3,4-(2-methylene)propylenedioxythiophene) (PMProDot) with polystyrene (PS) and polyvinylcarbazole (PVK) through the highly reactive methylene group was achieved. The modified PMProDot nanotubes demonstrated response times that were two times faster than without modification. The modification of PEDOT nanotubes with polydopamine, a biocompatible polymer, was also investigated and achieved. In depth characterization of functionalized CP demonstrate the ability to fine tune the

properties of the polymer in order to achieve the required therapeutic drug release profile.

A novel transdermal drug delivery system (TDDS) was developed in this thesis to deliver hydrophilic drugs of specific doses in a fast and controlled manner. The low cost, facile fabrication, painlessness, and safety of the patch demonstrate a promising success in research, clinical, and industrial fields. Ideally, a universal transdermal system utilizing PEDOT nanotubes to controllably delivery therapeutic and imaging payloads of multiple drug molecules, irrespective of their charge or hydrophobicity, can be achieved.

CONDUCTIVE POLYMER NANOTUBE PATCH FOR FAST AND CONTROLLED *IN VIVO* TRANSDERMAL DRUG DELIVERY

By

Thao M. Nguyen

Dissertation submitted to the Faculty of the Graduate School of the
University of Maryland, College Park, in partial fulfillment
of the requirements for the degree of
Doctor of Philosophy
2012

Advisory Committee:
Professor Sang Bok Lee, Chair
Professor Neil Blough
Professor Kyu Yong Choi
Professor Catherine Fenselau
Professor Zhihong Nie

"*It always seems impossible until it's done*." – Nelson Mandela

Dedication

This thesis is dedicated to my one and only, ba me

Acknowledgements

I would first like to thank my advisor, Dr. Sang Bok Lee. Not many professors have the patience that he had with me. His guidance and support was instrumental in my graduate research. With his encouragement, I was allowed to do what few graduate students have done, study abroad. I thank him for believing greater things in me than I thought I could ever achieve. He is a great scientist, innovator, professor, and above all, advisor. I would also like to thank my committee members, Professor Kyu Youg Choi, Catherine Fensleau, Neil Blough, and Zhihong Nie for your support and precious time. Thank you to Dr. Lei Zhu and Dr. Seulki Lee from the National Institutes of Health for being so generous in sharing their instrumentation and ideas and answering my questions. I would also like to thank Dr. Mark Choi and Dr. Andy Yun from MGH and Harvard Medical School for providing the platform for my *in vivo* research, for allowing me to use their state of the art two-photon microscope, and for answering my questions. Special thanks to Mark for those much needed after work beer sessions after a long day of experiments in Boston. I would also like to extend my sincere thanks to Dr. Seungil Cho for teaching me everything I needed to know, and much more, about conductive polymers and their electrochromic properties. I want to give many thanks to Larry Lai and Dr. Wei Chiou for their help in characterizing my nanotubes. I would like to express the utmost appreciation for Tim Maugel and Jan Endlich for their assistance with the electron microscope and allowing last minute scope time, but particularly for their personal conversations, foodie-gossip,

and endless jokes. I would like to thank Matt Hurley for helping me sneak into gen chem labs to obtain IR spectra of my polymers. Thank you to Dr. Haeshin Lee for being my mentor at KAIST and opening his lab to me. I would also like to extend a thank you from the bottom of my heart to the wonderful group members at KAIST: Jihyun Seok, Dongheun (a.k.a. Oopa) Kim, Sunhee Lee, and the adopted member Joseph Park. You guys treated me like one of your own and provided me the most memorable experiences in Korea. I would like to give many thanks to my past and current group members for their valuable support, intellectual conversations, and guidance. Thank you to Dr. Sungkyoung Kim for showing me patience and having the answers to all my scientific dilemmas. I probably would not have survived without Stef by my side through the years. She is the best "lab-buddy"/friend/secretary any person can ask for. Thanks to Lauren for being such a model protégée and becoming a wonderful friend, keep Friday Jam Sessions alive! Finally, I would like to give the greatest thanks to my family and Joseph. I would not be where I am as the person I am without you guys guiding me every step of the way.

Table of Contents

List of Tables

List of Figures

Schemes

List of Acronyms

transdermal Drug Delivery Systems (TDDS)
transdermal Drug Delivery (TDD)
gastrointestinal (GI)
dimethyl sulfoxide (DMSO)
lipid-protein partitioning (LPP)
poly(3,4-ethylenedioxythiophene (PEDOT)
3,4-ethylenedioxythiophene (EDOT)
of poly(3,4-(2-methylene)propylenedioxythiophene) (PMProDot)
polystyrene (PS)
polyvinylcarbazole (PVK)
gonductive polymers (CP)
light emitting diodes (LEDs)
polypyrrole (PPy)
polyaniline (PANi)
poly(vinyl alcohol) (PVA)
layer-by-layer (LbL)
Prussian Blue (PB)
polystyrene (PS)
anodic aluminum oxide (AAO)
Iron (III) tosylate ($Fe(OTs)_3$)
polycarbonate membrane (PC)
lithium perchlorate ($LiClO_4$)
poly(methylmethacrylate (PMMA)
polyethylene glycol (PEG)
quartz crystal microbalance (QCM)
scanning electron microscope (SEM)
transmission electron microscope (TEM)
fluorescein isothiocyanate (FITC)
Sodium chloride (NaCl)
poly(styrenesulfonate) (PSS)
nerve growth factor (NGF)
polyethylene glycol (PEG)
dimethylformamide (DMF)
3,4-(2-methylene)propylenedioxythiophene (MProDot)
Poly(3,4-(2-methylene)propylenedioxythiophene) (PMProDot)
photomultiplier tube (PMT)
polyvinylcarbazole (PVK)
transmission electron microscope (TEM)
surface electron microscope (SEM)
atomic force microscopy (AFM)
indium tin oxide (ITO)
4-dihydroxyl-L-phenylalanine (DOPA)
energy-dispersive X-ray spectroscopy (EDS)

Chapter 1: Introduction

The first transdermal system for systemic delivery—a three-day patch to release scopolamine to treat motion sickness—was approved for use in the United States in 1979. Between 1979 and 2002, a new patch was approved on average every 2.2 years. From 2003 to 2007, that rate has more than tripled to a new transdermal delivery system every 7.5 months. It is estimated that more than one billion transdermal patches are currently manufactured each year.[1] The annual US market for transdermal patches is more than $3 billion.[2]

1.1 Transdermal Drug Delivery Systems (TDDS)

In the past thirty years, there has been an explosion in the creation and discovery of new medicinal agents. Innovations in drug delivery have not only enabled successful implementation of these pharmaceuticals, but also promoted the developments of new medical treatments with existing drugs. The creation of a transdermal drug delivery system (TDDS) has been one of the most important innovations. Transdermal products for cardiovascular disease, Parkinson's disease, Alzheimer's disease, depression, anxiety, skin cancer, and post-menopausal bone loss are at various stages of formulation and development.[3] This chapter will outline the advantages of TDDS, current methods of transdermal drug delivery and its future.

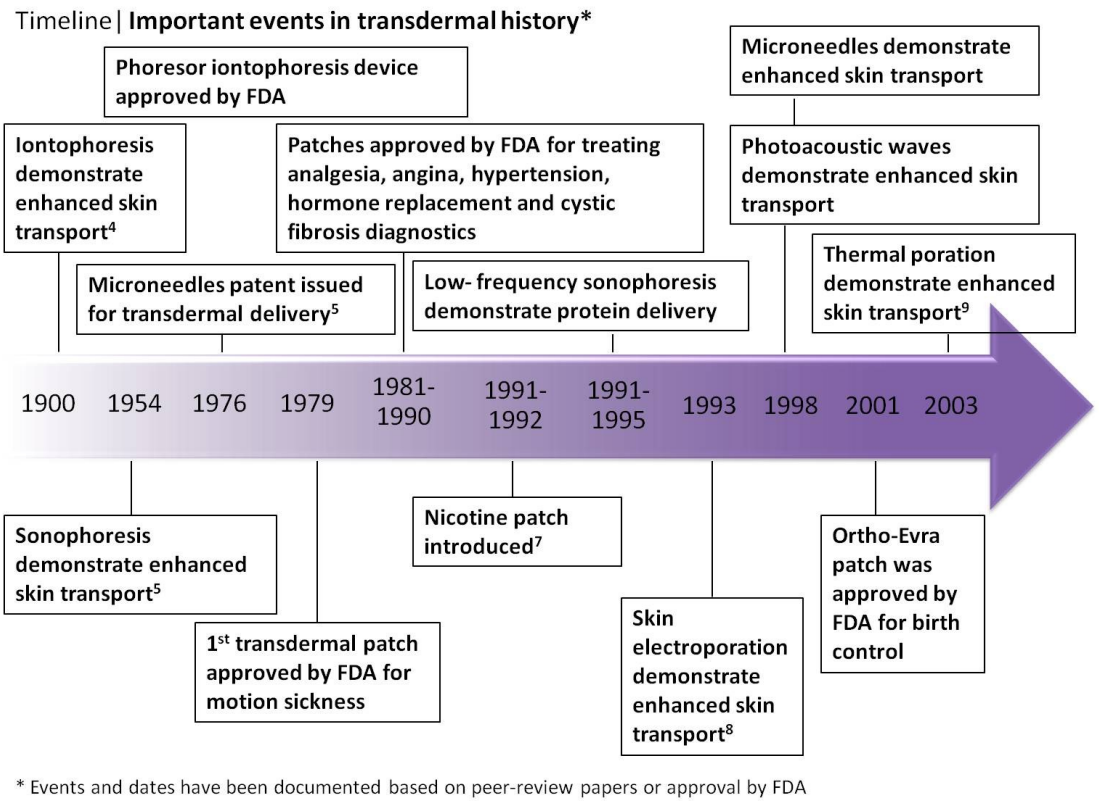

Figure 1.1 Timeline of important events in transdermal history. Reprinted from Prausnitz et al.[2]

1.1.1 Advantages of TDDS

Transdermal delivery have created new applications for existing therapies and offered an alternative to the traditional oral route where drugs can prematurely metabolize in the liver causing adverse side effects. For example, oestradiol patches can be used by patients where oral dose cause liver damage.[10] While hypodermic injections are painful, generate dangerous medical waste, and pose a risk of transmission through the reuse of needles, particularly in developing countries, transdermal delivery is painless, noninvasive, and self administered.[11] The use of transdermal patch can lengthen the duration of drug release and

therapeutic action, reduce administration frequency, and improve patience compliance, all at a fairly inexpensive production cost.

Opening the transdermal delivery route to large hydrophilic drugs is one of the greatest challenges due to the hydrophobicity of the skin. However, the ability to be able to deliver hydrophilic drugs through a transdermal patch would also provide a solution to problems of other delivery methods for hydrophilic drugs, most notably, those involving the gastrointestinal (GI) tract. Due to their low absorption by the GI tract, hydrophilic drugs need to be administered orally in very large doses. This increases the cost of the drug and may carry harmful side effects. Increased efficacy of hydrophilic drugs in TDDS appeals to drug makers, physicians, and patients alike. The development of an effective TDDS, particularly for hydrophilic drugs, will increase the availability of drugs to patients and bring new hydrophilic drugs to the markets which were previous not viable due to their poor bioavailability with oral dosing.

Despite current successes, the numbers of drugs that can be administered with conventional patches are limited. Presently, the drugs that can pass through the skin share three constraining properties: low molecular mass (<500 Da), high lipophilicity, and small required dose (up to milligrams).[2]

1.1.2 Anatomy of the skin

Human skin has a multifunctional role. One of the most important roles is to act as a protective barrier against foreign materials and the loss of excessive endogenous materials (i.e. water). The functionality of the skin is reflected in its multilayered structure with each layer representing different cellular or epidermal

differentiation (Figure 1.2). The stratum corneum (~15µm) is the uppermost layer of the skin comprised of a hierarchical structure of a lipid-rich matrix embedded with 10-15 layers of corneocytes.[12-14] The corneocytes are composed of cross linked keratin fibers (~0.2-1.5µm thick, 36-46µm in diameter), and held together by corneodesmosomes providing structural support.[15] The "brick and mortar" architecture of the lipid bilayers serve as the primary barrier of the stratum corneum. The corneocytes (bricks) are in an intercellular matrix (mortar) of long chain ceramides, free fatty acids, triglycerides, cholesterol and sterol/wax esters.[16] The renewal period for the stratum corneum is two to four weeks, however it is actively repaired by cellular excretions following disruptions to the barriers.[17]

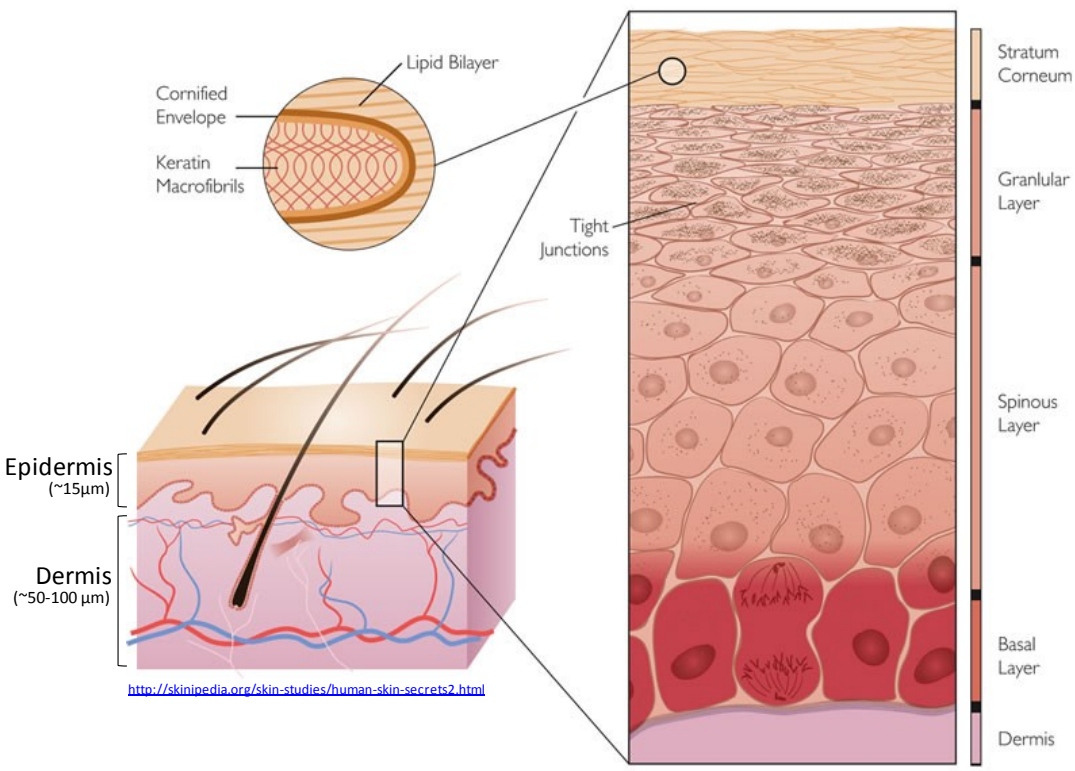

Figure 1.2 Anatomy and physiology of skin.[18]

Directly below the epidermis is the dermis (~50-100 μm) which contains viable tissue but is devoid of blood vessels. Further below the dermal-epidermal junction, the dermis begins to contain capillaries that can take up transdermally administered drugs for systemic distribution. A successful transdermal delivery patch must penetrate to the dermis in order to deliver drugs systemically.

In order to understand how the physiochemical properties of drugs can influence transdermal drug delivery, it is necessary to determine the predominant route of drug permeation through the stratum corneum. Drug molecules that come in contact with the skin can penetrate through three pathways (Figure 1.3): 1) through the sweat ducts, 2) via hair follicles and sebaceous glands, or 3) directly across the stratum corneum. It is generally accepted that the sweat ducts provide minimal contribution (permeation of ~0.1%) to the steady flux of most drugs, therefore the majority of skin penetration enhancements have focused on transporting drugs across the stratum corneum.[19] However, drug molecules must travel a very intricate and specific pathway through the stratum corneum. A molecule that transverse through the stratum corneum must partition into and diffuse through the corneocytes. In order to move to the next corneocyte, the drug molecule must migrate through multiple lipid layers in between each corneocyte. The partitioning into and diffusion across continuous hydrophilic and hydrophobic domains is unfavorable for most drugs. As a result, the majority of techniques and methods used to optimize transdermal drug delivery are directed towards the manipulation and alteration of the well ordered stratum corneum.

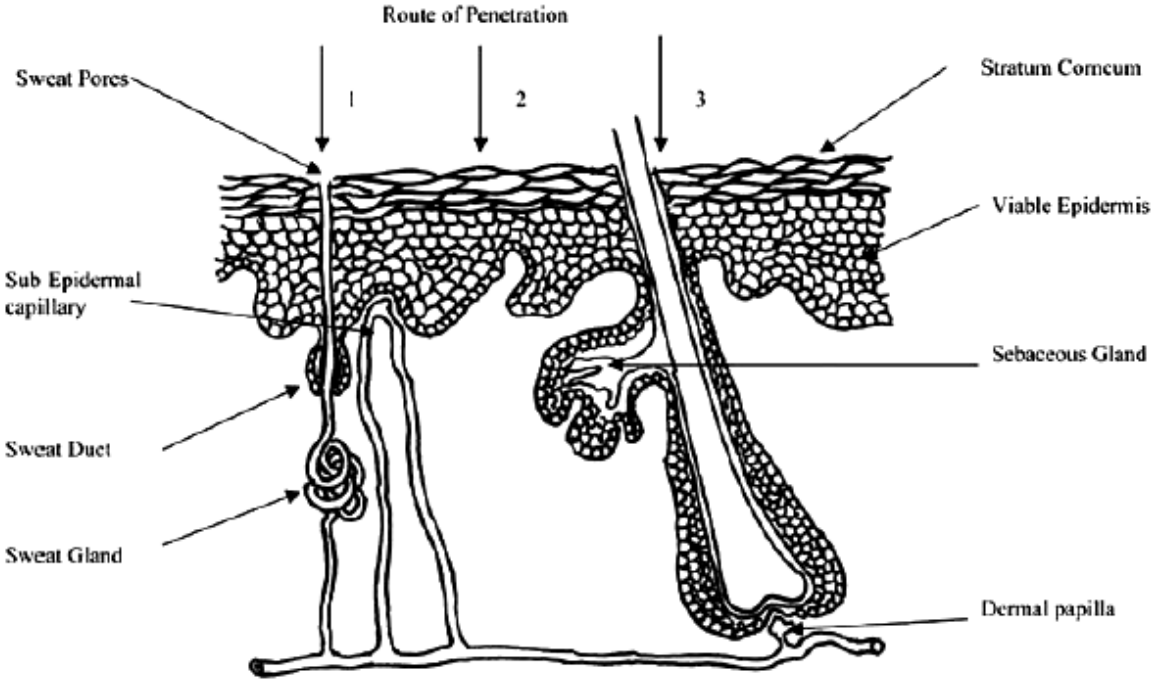

Figure 1.3 Simplified illustration of skin showing routes of penetration: 1) through sweat ducts; 2) through stratum corneum; 3) via hair follicles. Reprinted from Benson et al.[3]

Drug permeation across the stratum corneum obeys Fick's first law (Equation 1.1). The steady-state flux (J) is related to the diffusion coefficient (D) of the drug over the membrane thickness (h), the partition coefficient (P) between the stratum corneum and drug vehicle, and drug concentration (C_0) which is assumed to be constant. Since the skin thickness and drug concentration are considered constant, techniques used to successfully increase the rate of drug release through the stratum corneum focus on increasing D and P. More importantly, the combination of enhancing both D and P will result in multiplicative effect.

$$J = \frac{D C_0 P}{h}$$ Equation 1.1

1.1.3 Current methods of transdermal drug delivery

There are many methods currently used to bypass the skin's protective barriers ranging from chemical enhancers, which have a broad range of chemical additives to thermal poration, which locally heat and ablate holes in the stratum corneum to increase permeability.[20] In this chapter we will focus on the four methods which have had the largest impact on controlled transdermal drug delivery: Chemical enhancers, iontophoresis, electroporation, and microneedles.

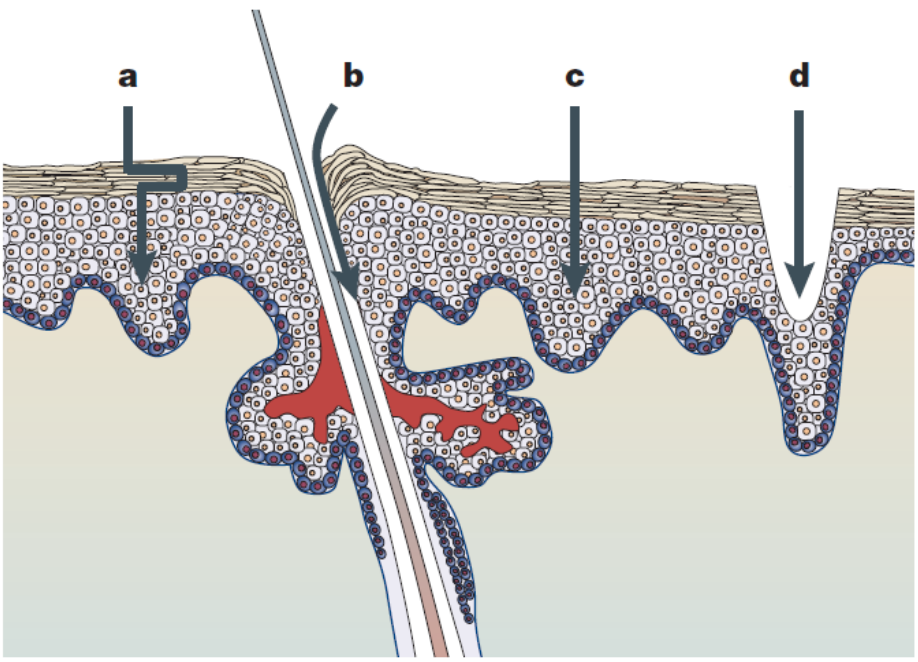

Figure 1.4: Schematic representation of cross section of human skin. a) Transdermal diffusion, with the presence of a chemical enhancer, can take a tortuous route across the stratum corneum. b) Low-voltage applied during iontophoresis can increase transport pathways through hair follicles and sweat

ducts. c) High-voltage applied during electroporation has been shown to disrupt lipid bilayers to create transcellular pathways. d) Microneedles create micron-scale holes in the skin to provide direct pathways for drug transport. Reprinted from Prausnitz et al.[2]

1.1.3.1 Chemical Enhancers

The enhancement of skin has been tested with water, surfactants, essential oils, dimethyl sulfoxide (DMSO), and alcohols. Barry and coworkers proposed the lipid-protein partitioning (LPP) theory to describe how enhancers affect skin permeability. By disrupting the intercellular bilayer lipid structure and interacting with intracellular proteins of the stratum corneum, chemical enhancers improve the partitioning of a drug, coenhancer, or cosolvent into the stratum corneum.[21-23]

One of the safest and most widely used chemical enhancer to increase permeation is water. It is hypothesized that the increased hydration of the skin may lead to swelling and to the opening of the structure which can increase permeation.[3] Other types of enhancers have shown increase in permeability by disordering the lipid structure of the stratum corneum. The diffusion coefficient (D in Equation 1.1) of the drug is increased as microcavities are formed in the lipid bilayers. In other cases, enhancers can create permeable "pores" that provide less resistance for polar molecules.[24-26] Penetration of chemical enhancers has also been found to interact with the keratin in the corneocytes. The surfactants interact and bind with keratin to disrupt the order within the corneocytes thereby D.

One of the major side effects of chemical enhancers is irritation to the skin at potent levels, which is not surprising since the chemicals disrupt organized lipid structures, cell membranes, and their components.[27] The toxicity associated with many enhancers have limited their usefulness in clinical applications, however there has been a move towards investigating potential generally regarded as safe (GRAS) enhancers by the FDA, such as essential oils and terpenes .[28, 29]

1.1.3.2 Iontophoresis

This method of transdermal drug delivery involves low level electric current applied either directly or indirectly to the skin in order to enhance its permeation.[30-34] The electrical charge primarily drives drug molecules through the skin via sweat ducts since they provide less electrical resistance than the stratum corneum.[3] The reason for the increased permeation can be attributed to one or all of the following: electrophoresis (for charged solutes), electro-osmosis (for uncharged solutes), and electropertubation (for both charged and uncharged solutes). Figure 1.5 shows a simplified illustration of the diffusion of solutes during iontophoresis. Electrophoresis drives charge molecules across the skin by direct interaction with the applied electric field, therefore small highly charged particles are delivered more rapidly. In electroosmosis, the delivery of molecules occurs as they are dragged by the electrically induced solvent flow.[35] The flow of the solvent is induced by the net flux of cations from the anode to the cathode. The electroosmotic flow of water is generated by the preferential movement of mobile cations in the cells (i.e. Na^+) instead of fixed anions proteins in the skin.[35]

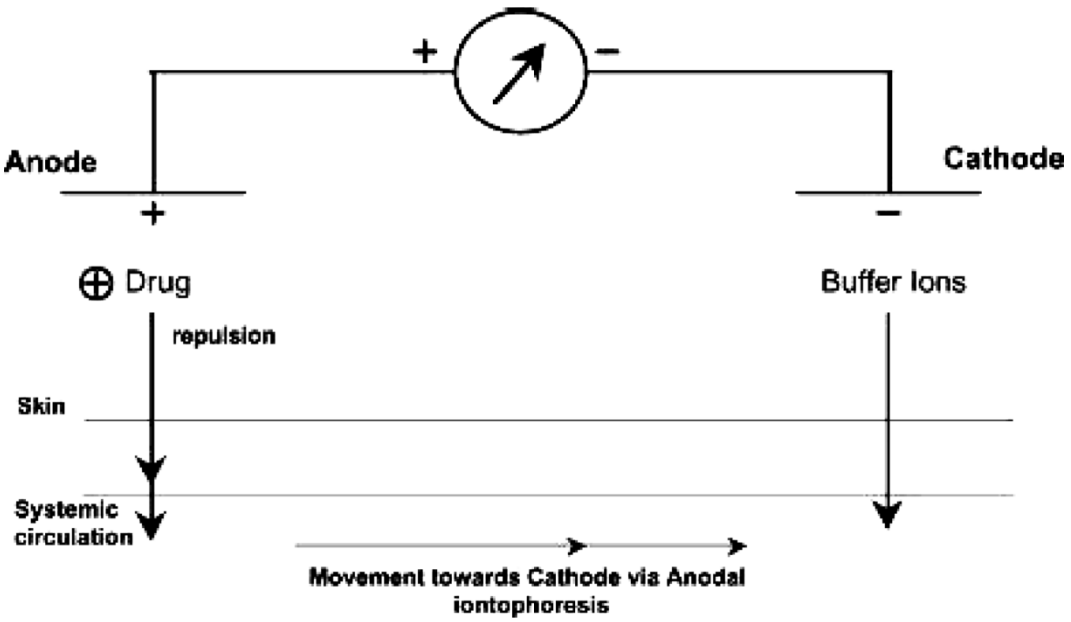

Figure 1.5 Basic iontophoretic set-up illustrates direction of solute movement with respect to electrode type. Reprinted from Wang et al.[36]

Typically, a few milliamperes of current are applied to a small area of the skin, generating no pain beyond mild erythema.[37] The Phoresor™ was the first iontophoretic system approved by the FDA in the late 1970s as a therapeutic device. Currently, iontophoretic systems are approved for administering drugs into the body for specialized medical purposes, such as diagnosis of medical conditions and glucose monitoring. Despite the straight forward application, many parameters can affect the design of an iontophoretic device, including but not limited to electrode type, current intensity, pH of system, and competitive ion effect.[34] Currently, there are many requirements for a successful iontophoretic device. For example, the device must: (1) be sufficiently high powered to provide desired delivery rate; (2) not produce any permanent harmful effects on skin permeability; (3) establish proportionality between flux and applied

current/voltage; and (4) maintain constant current/voltage over time.[38] In addition, iontophoresis is limited by the electric current that can be used on humans (regulated at 0.5mA/cm^2)

1.1.3.3 Electroporation

This method of transdermal delivery is similar to iontophoresis, in which it uses electrical current to aid the delivery of drug molecules through the skin. In the case of electroporation, extremely high voltage pulses, rather than milliamperes of current, are used to induce skin perturbation. The high voltage creates transient pores which may account for the skin permeability.[39] The increased skin permeability is related to the electroporation process, which is the formation of aqueous pathways across the lipid bilayer by a pulsed electric field.[39-41, 30] This technology can enhance the skin permeability to molecules of greater hydrophilicity and sizes compared to other methods.

High voltages (≥100 V) over short durations (milliseconds) are normally applied. The pulses can be administered painlessly using closely spaced electrodes to minimize the electric field in the nerve-free stratum corneum. With the application of high voltages, transdermal transport can be reduced to a few seconds opening opportunities for rapid-response delivery systems.[41] Transdermal transport has been shown to increase by orders of magnitude with partial to full reversibility within minutes to hours.[40, 42] However, with the use of high voltage, there is a greater chance of cell damage if the pulses duration or

intensity is too great.[39, 43] In addition, electroporation requires specialized and cumbersome equipment.[41]

1.1.3.4 Microneedles

This method of transdermal drug delivery involves piercing the skin with very short needles. Solid microneedles (~50-100μm) encapsulated or coated with drug formulations for controlled or rapid release. Microneedles increase permeability and delivery of drugs transdermally by creating micron-scale pathways into the skin, driving drugs into the skin as coated cargo. Their effects are targeted in the stratum corneum, although they do pierce across the epidermis and into superficial dermis.[44] Microneedles treatment have been reported to be painless by volunteers and generally well tolerated.[44] This technique has great promise because they appear to be capable of delivering a broad range of drugs. A notable limitation is the diffusion rate of large compounds through micron-scale pathways. When rapid delivery is required, it may be necessary use an additional force to drive the drugs into the skin.

1.2 Conductive polymer for controlled drug delivery systems

Conductive polymers (CP) are organic polymers with electrical, magnetic, and optical properties. The flexible mechanical properties allows for easy processing. They have found applications in a wide variety of areas including but not limited

to light emitting diodes (LEDs), smart mirrors, electromagnetic shielding, antistatic coatings, and various sensing devices.[45] In the biomedical field, CPs have been used for biosensing, nerve regeneration, and drug delivery systems.[46-49]

Controlled drug delivery systems offer many advantages over conventional therapies, such as implantable devices, by maintaining therapeutic bioavailability of drugs, providing specific dose requirements for treatment, and minimizing side effects. Implantable systems can release drugs over an extended period of time, however the release of the drugs is at a pre-programmed rate and cannot be altered without removing and resetting the device. Another limitation of implantable devices is the inability to maintain a steady release rate due to the diminishing drug concentration gradient. The intrinsic electronic properties of CPs offer the use of an external stimulus which can be modified to appropriately monitor the release rate of a drug.

1.2.1. Electrically controlled drug delivery systems

Over the last few decades, one of the greatest challenges for polymer-controlled release systems is the delivery of drugs in a pulsatile or staggered release profile.[50] Current methods developed for controlled delivery responds to changes in the local environment such as enzymatic and hydrolytic degradation, pH fields and temperature. Despite these methods, responses to changes in electric field offer the unique advantage of providing on-demand release due to the availability of equipment allowing precise control of delivery with regards to magnitude of current, duration and interval of pulses.

Conductive polymers are electrically conductive due to the continuous and ordered pi-conjugated backbone. When conductive polymers are oxidized, "holes" are created along the backbone through the removal of electrons. The conjugated backbone provides a path for neighboring electrons to move freely through these "holes". The progression of charge through the "holes" explains their conductivity. CPs can undergo controllable and reversible redox reactions. The switching between redox states results in simultaneous changes in the polymer charge, conductivity, and volume. The change in volume is due to the charging and discharging of the polymeric composition (Figure 1.6). The packed polymer structure is due to the strong Van der Waals interaction during oxidation. The electrons are removed from the chains due to π bond redistribution from the influx of cations. Then the polymer undergoes conformational changes to provide volume for the balancing counteranions from the solution. By exploiting these properties, the rate of drug release from CPs can be controlled.

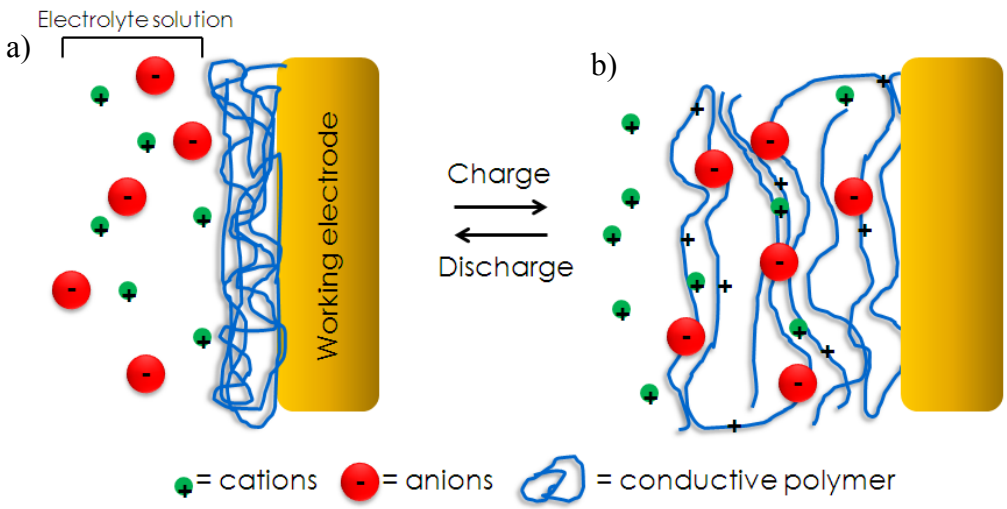

Figure 1.6 Reverse electrochemical reactions promote a) shrinking and b) swelling of polymer.

There are several factors determining if a drug is suitable for use in CP drug delivery systems such as potency, half life, bioavailability, and most importantly electroactive properties. The drugs can be incorporated into the polymer during or following the polymerization process. The mechanism of drug incorporation during polymer synthesis involves the combination of electrostatic and hydrophobic interactions between the drug (dopant) and polymer, along with physical entrapment.[48] However, the drugs can interfere with the polymerization growth of the monomer; therefore most research focuses on incorporating the drugs into the CP following polymerization. This technique allows flexibility in polymer preparation without the limitations due to drug incorporation.

1.2.2. Conductive polymer films for drug delivery systems

The first reported controlled release system based on electrostatic release of anionic drugs was reported by Zinger and Miller in 1984 when glutamate anions were released on the reduction of polypyrrole (PPy) (Figure 1.7).[51] Fourteen times more glutamate was released at a reducing potential of -1.0V than with no applied potential. Massoumi and Entezami constructed a CP bilayer to control the release of anions.[52, 53] The bilayer released drugs on reduction of the polymer and reincorporated them upon oxidation. Pyo et al. also demonstrated the controlled release of adenosine 5'-triphosphate from PPy.[54] Michniak et al. utilized a porous polyaniline (PANi) membrane as a drug delivery system as well as an electrode in iontophoretic TDD.[55]

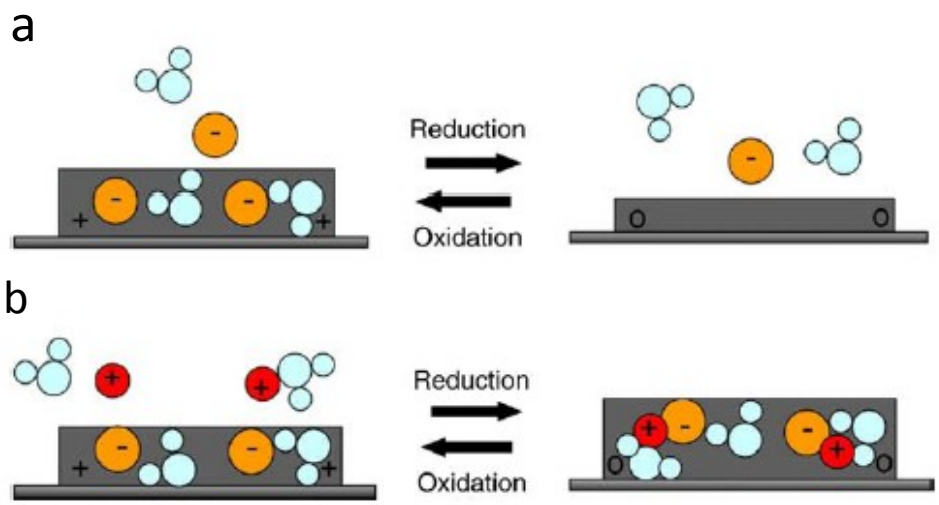

Figure 1.7 a) PPy released mobile anions on reduction of the polymer. b) PPy prepared with immobilized anions will incorporate cations based on the reduction of the polymer, the cations can then be released upon oxidation. Reprinted from Zinger et al.[51]

Overcoming limitations in the choice of dopant and molecular weight of delivered drug, Langer et al. took a different approach by attaching molecules to PPy through biotin-streptavidin coupling.[56] After the molecule of interest is attached to the biotin dopant, drug release is triggered through electrical stimulation. The reduction of PPy is believed to trigger the release of biotin and the attached payload (Figure 1.8). Kang et al. also took a similar approach by covalently immobilizing poly(vinyl alcohol) (PVA)-heparin hydrogel onto PPy film and studied the release behavior of heparin from PPy with and without electrical stimulation.[57]

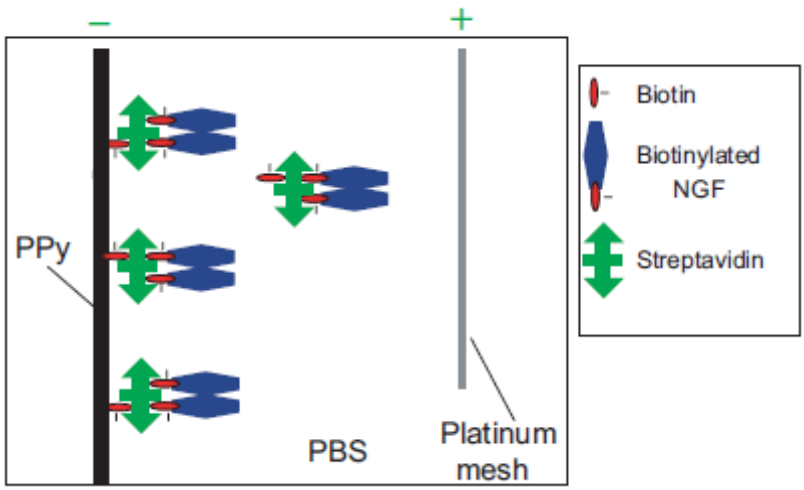

Figure 1.8 Voltage applied across the polymer in PBS solution causes the release of biotin from the PPy surface. Reprinted from George et al.[56]

Most recently, Hammond et al. utilized the layer-by-layer (LbL) assembly technique to create polymer films of thickness in the 100-500 nm range. The group reported the fabrication of nanoscale films that can release drugs in response to an anodic potential of at least +0.5 V (vs. Ag/AgCl). The films contained negatively charged Prussian Blue (PB) particles and positively charged gentamicin, a small hydrophilic antibiotic. The dosing and rate of drug delivery was controlled by tuning the film thickness as well as applied potential.

Current technology has made it possible to finely tune polymer film thickness down to the nanometer range, however, the amount of therapeutic drugs that can be delivered from nanometer films needs to be improved further. To efficiently load drugs and provide fast and controlled transdermal delivery in electrical systems, polymeric nanostructures need to be investigated.

1.2.3 Conductive polymer nanostructure for drug delivery systems

Despite the emerging researched based on CPs for drug delivery, several limitations have prevented the broad use of CP films in controlled drug delivery. One reason is due to the small surface area and thus limited capacity for clinical drug loading. In addition, CPs release drugs most efficiently from their surface, as opposed to bulk polymer, which can hinder the release of embedded drugs and affect the ability of the polymer to fine-tune the release rate of the drugs. The easiest and most efficient way of overcoming these limitations is to increase the surface area of the CPs. Nanostructures have intrinsically high surface area to volume. Polymer nanostructures can respond quickly to electrical stimulations, increase the payload capacity of the system, and provide the innovative template for small, attractive, and easily marketable transdermal patches.

Cui et al. developed an approach to increase the surface area of conductive polymers and increase the drug loading capacity of traditional films.[59] Nanoporous PPy films embedded with fluorescein were synthesized using a polystyrene (PS) modified electrode (see Figure 1.9).[58] A potential of -2.0 V was applied in 10 s increments to reduce and remove the charge from PPy, releasing negatively charged dye molecules. The group reported that nanoporous PPy films released about 10 times more than conventional PPy films. In a similar experiment, the group reported the upload of both fluorescein and dexamethasone into the nanopores protected by a thin layer of PPy on top. Both fluorescein and dexamethasone were released after electrical stimulation however the accumulated drug release was only in the nanograms range.

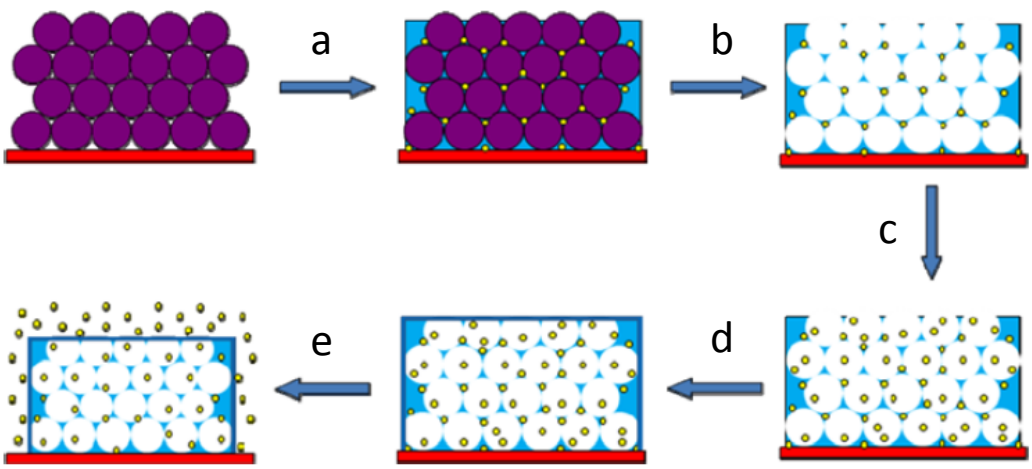

Figure 1.9 Schematic process of synthesis and drug release of nanostructured PPy film. a) Immerse modified template in PPy solution containing drugs of interest and electrochemically polymerized. b) Dissolution of polystyrene nanobeads. b) An additional drug is added. d) A thin layer of PPy is deposited. e) Application of potential released loaded drug. Reprinted from Luo et al.[59]

Electrochemical actuators have been synthesized with conducting polymers based on the principle of expansion and contraction due to the number and size of ions exchanged.[60] Martin et al. reported the fabrication of poly(3,4-ethylenedioxythiophene) (PEDOT) nanotubes around drug incorporated biodegradable polymer for precise controlled drug released.[60] Nanofibers were first electrospun onto the surface of neural probes followed by the electrochemical deposition of PEDOT around the fibers. The nanotube wall thickness varied between 50-100 nm, while the diameter ranged from 100-600 nm. The drug loaded PEDOT was actuated by applying a potential of 1 V. The contraction of the PEDOT nanotubes created a pressure within the nanotubes which expelled the drug molecules and degraded the biopolymers. A potential of 0 V was applied in

the control experiment which showed that the model drug did not significantly diffuse through the PEDOT nanotube walls.

1.3 Conductive nanotubes for fast and controlled release

The Martin group has pioneered the versatile template synthesis method that can be implemented to fabricate cylindrical metal, metal oxides, or organic nanostructures.[61-63] Mallouk et al. have synthesized poly(3,4-ethylenedioxythiophene) gold capped PEDOT nanowires utilizing anodic aluminum oxide (AAO) as the template membrane.[64] Hernandez et al. also used AAO to electrochemically synthesize porous PPy nanowires.[65] The ease in fabrication of cylindrical conductive polymer nanostructures and their enhanced electrochemical properties makes them an ideal candidate for controlled delivery.

1.3.1 Enhanced electrochemical properties

Nanostructured materials provide intrinsically high surface areas leading to a shorter diffusion distance for ion transport and thus faster charge/discharge rates. Nanotubular conductive polymers are the ideal structure for enhance drug delivery because the wall thickness and length can be used to control the rate of upload and release. The beauty of nanotubes is the ability to utilize the inner hollow tubular structure for drug upload while the outside can undergo further modifications to enhance the materials, targeting capabilities, and stability. Our group has previously pioneered the electrochemical synthesis of PEDOT nanotubes and demonstrated their enhanced properties in applications such as fast electrochemical devices and energy storage.[66-71]

Electrochromics is one of the most fascinating properties of conductive polymers. The effect of electrochromism has been known for many years and it is based on the fact that certain materials change color depending on their redox states.[72] Lee et al. pioneered the electrochromic studies of PEDOT nanotubes which achieved an extremely fast electrochromic response (<10 ms), compared to their film counter parts (~seconds).[71] The ability to respond to electrical changes within milliseconds makes conductive polymers ideal for fast and controlled transdermal drug release.

1.3.2 Tunable chemical and physical properties

Surface modifications of CP through the incorporation of biomolecules have lead to changes in chemical and physical properties. Changes to the chemical properties of CPs have occurred through the doping of biomolecules or the immobilization of bioactive polymers on the surface of the materials.[73-74] Physical modifications can create well ordered polymer backbones which can increase the charge/discharge rate of the polymers. One type of modification process, copolymerization with other polymers, is addressed later in this thesis.

Chapter 2: Synthesis of PEDOT Nanotube Transdermal Patch

The Materials and Methods in this chapter has been reproduced in part with permission from: Xiao, R., Il Cho, S., Liu, R. & Lee, S.B. Controlled electrochemical synthesis of conductive polymer nanotube structures. *Journal of the American Chemical Society* 129, 4483-4489 (2007)

2.1 Introduction

Preparations of conducting polymers involve the oxidative polymerization of the monomer ions. By controlling the amount and rate of charge passed, the polymerization process can be optimized to produce a polymer with desired morphological and electromechanical properties.

The synthesis of poly(3,4-etheylenedioxythiophene) (PEDOT) can be achieved through two main types of polymerization: oxidative chemical reagents or electrochemical processes. Chemical polymerization of EDOT can be carried out using several methods and oxidants. The classical method employs oxidizing agents such as $FeCl_3$ and Fe (III) tosylate ($Fe(OTs)_3$).[75-76] This method results in black, insoluble, and infusible PEDOT. On the contrary, electrochemical polymerization is favored to create drug delivery systems as it requires only a small amount of monomer, no harsh oxidizing or reducing agents, short polymerization times, and yields both electrode-supported and free standing polymers. During electrochemical polymerization, a positive potential is applied at the electrode causing the monomer to be oxidized to a delocalized radical cation.[77] As seen in Scheme 2.1, the radical cation induces radical-radical coupling generating dimerization of the monomer radicals through deprotonation at the α-position. Following the generation of a the neutral dimer through the removal of two H^+ ions, chain propagation occurs through the oxidation of neutral

dimers into dimer radicals. The dimer radicals will than react with monomers or dimers in solution and resulting in the elongation of the polymer backbone. The oxidation potential of the monomer is higher than that of the polymer, therefore the newly formed polymer is slightly oxidized in its neutral form.[78]

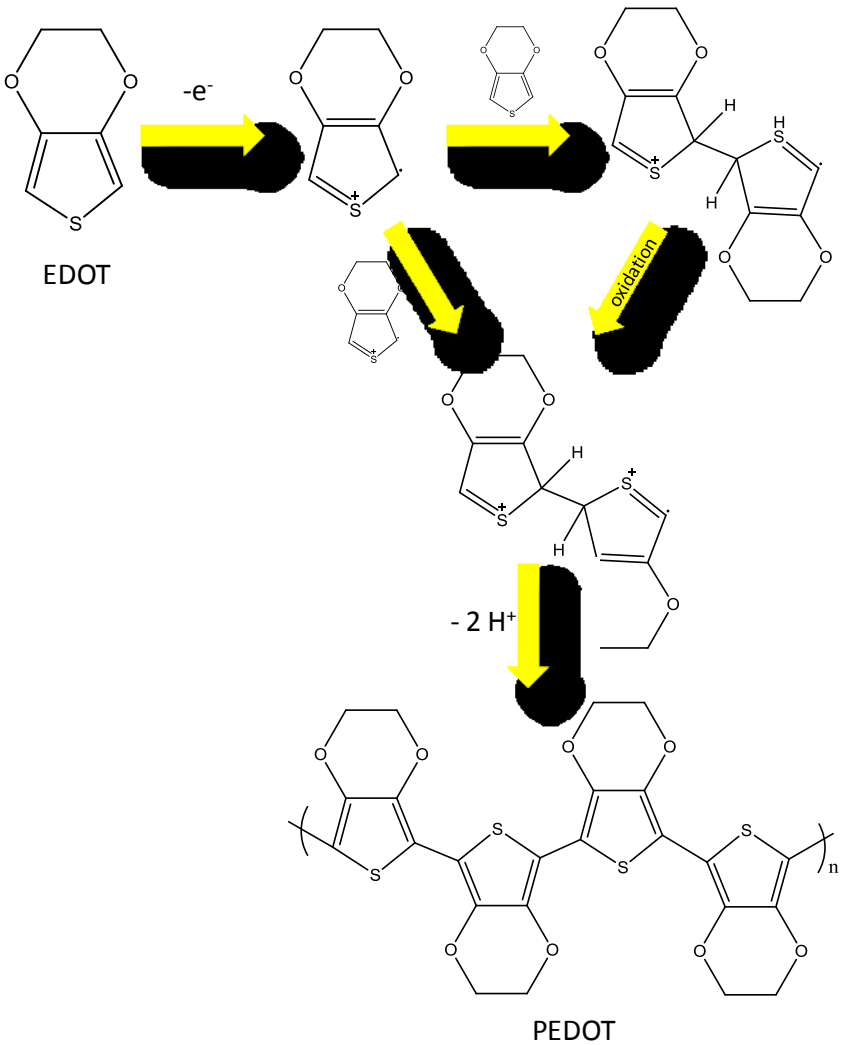

Scheme 2.1 Electrochemical polymerization of EDOT to PEDOT.

The synthesis of conductive polymer nanotubes has been performed chemically or electrochemically using various templates.[79-81] Martin and co-workers have pioneered the synthesis of conductive polymers in pores of

polycarbonate or alumina membranes.[79-81] The template synthesis method utilizes membranes with tunable pore diameters and length resulting in well defined, robust, and monodisperse PEDOT nanotubes. PEDOT nanotubes have attracted intensive attention in the fields of energy storage and drug delivery due to their ultra fast electrochemical responses, conductivity, and long term stability.[58, 59, 83-84] PEDOT nanotubes have several advantages over their film counterparts, as well namely, (i) the nanotube structure feature an inner void for accommodating molecules such as ions, drugs, biomolecules, enzymes, etc. (ii) The increased surface area of nanotube compared to film provides a much larger amount of drug loading and (iii) the thin walls of the nanotubes provide a short diffusion distance for ions. Lee and coworkers have used these concepts to synthesize capacitors, electrochromic windows, and energy storage devices.

In this chapter, a method is designed to develop the TDDS. The drug reservoir for the system consists of PEDOT nanotubes embedded in a polycarbonate membrane (PC). The synthesis of PEDOT nanotubes in a porous template was originally reported by Xiao and co-workers.[67] Figure 2.1 illustrates the transdermal delivery patch which consists of a working electrode, drug reservoir (PEDOT nanotubes), electrochemically active gel electrolyte, and counter electrode. The chapter will conclude with proof-of-concept results for the drug release in PBS buffer solution in a three electrode system.

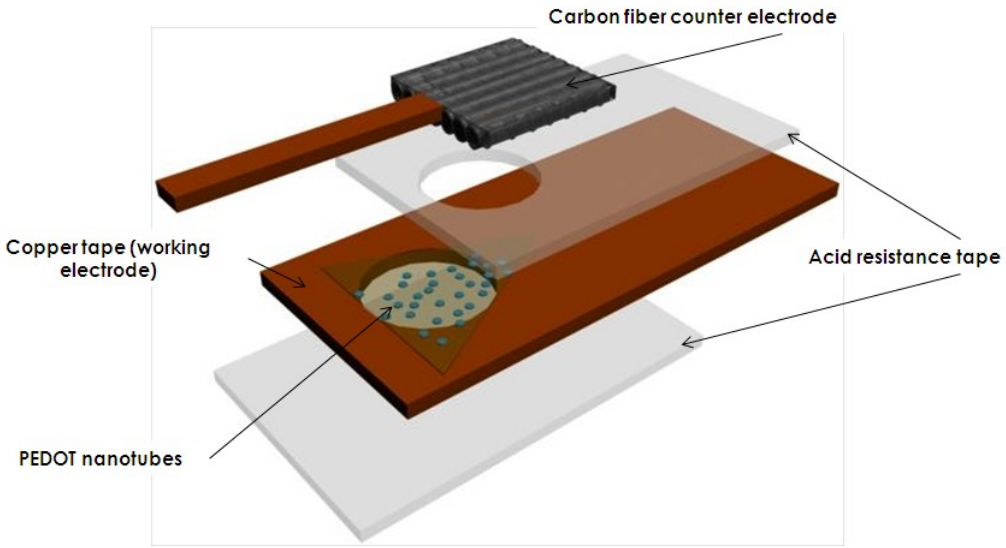

Figure 2.1 Deconstructed representation of transdermal patch.

2.2. Materials and Methods

2.2.1 Chemical and Materials

3,4-ethylenedioxythiophene (EDOT, Sigma Aldrich), acetonitrile (Fisher Scientific), and lithium perchlorate ($LiClO_4$, Acros) were used to synthesized PEDOT nanotubes within gold sputtered alumina (200 nm diameter, 60 µm thickness, Whatman) and polycarbonate membrane (PC, 220 nm diameter, GE Osmonics) with Pt foil (99.99%, Alfa Aesar) as the counter and Ag/AgCl as the reference electrode. Anhydrous propylene carbonate (Sigma), ethylene carbonate (Sigma Aldrich) and poly(methylmethacrylate (PMMA, Sigma Aldrich) were used to synthesize the electrolyte gel for hydrophobic dyes. Sodium chloride (NaCl, J.T. Baker), polyethylene glycol (PEG, Sigma Aldrich), and millipore water obtained by a Milli-Q A10 system was used to synthesized the electrolyte gel for hydrophilic dyes. The PEDOT nanotubes were sandwich between copper

tape (3M) and acid resistant tape (3M). Finally, the patch was finished with a carbon fiber mesh (fuelcellstore.com) as counter electrode.

2.2.2 Template synthesis of PEDOT nanotubes

Two different types of commercial membranes were used to synthesize PEDOT nanotubes. Commercial alumina templates (AAO), with 200 nm diameter and 60 μm thickness, were used to synthesize PEDOT nanotubes for structural analysis and characterization due to the ease of preparation for characterization. PC membranes, with 200 nm diameter and 47 μm thickness, were used for PEDOT synthesis of the transdermal drug delivery patch due to its flexibility. A Denton Vacuum Desktop III was used to sputter a thin layer of gold (ca. 100 nm thick) on one side of the membrane template. Copper tape (3M) was attached to the gold to provide contact with the working electrode. Silicon, Teflon, and corrosive resistant clamps were used to keep the electrochemical cell in place. The three electrode cell set up is illustrated in Figure 2.2. An electroactive window with a 60% porosity (1.26 cm^2) was defined by using acid resistant tape. The entire cell is placed in a 50 mM solution of EDOT in 100 mM $LiClO_4$ in acetonitrile. A potential of 1.2 V is applied to the system until the charge reached 200 mC.[67] All electrode potentials were measured relative to a Ag/AgCl reference electrode using Pt foil as a counter electrode, if not specified otherwise. The deposited mass of PEDOT nanotubes was controlled by fixing the total charge passed during electropolymerization.

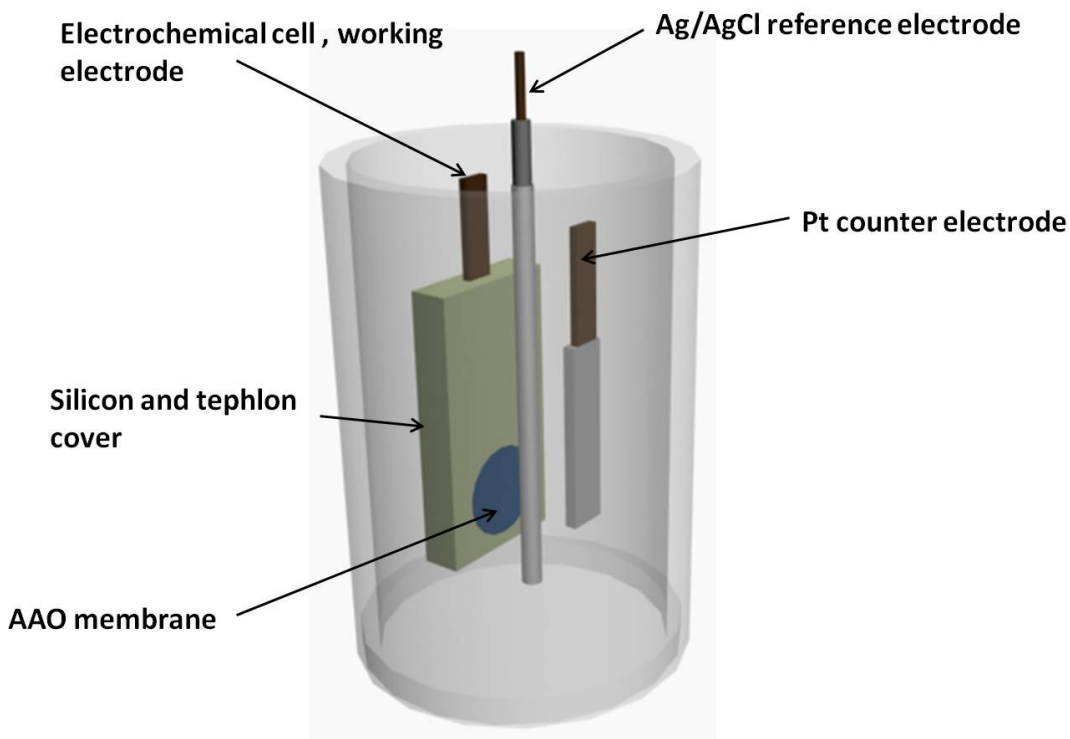

Figure 2.2 Three electrode cell set up for the electrochemical synthesis of PEDOT nanotubes.

2.2.3 Construction of PEDOT nanotubes transdermal patch

We have previously established the electrochemical stability of PEDOT nanotubes embedded in the membrane and therefore the tubes were kept within the pores for the TDDS.[70] Prior to the loading of anionic molecules, PEDOT was cycled between -0.500 V and 1.0 V in a solution of the desired drug at 10 mV/s in order to remove any PEDOT monomers or polymers from the membrane and to exchange perchlorate ions with model drugs. The PEDOT patch was placed in a 600 mM solution of amaranth (Figure 2.3). A potential of 1.2 V was applied to the working electrode until 200 mC/cm^2 of the amaranth was loaded (~30 µg). To evaluate the amount of model drug loaded, we used a quartz crystal microbalance

(QCM; Stanford Research Systems) to measure the weight change of PEDOT over time (Figure 2.4).

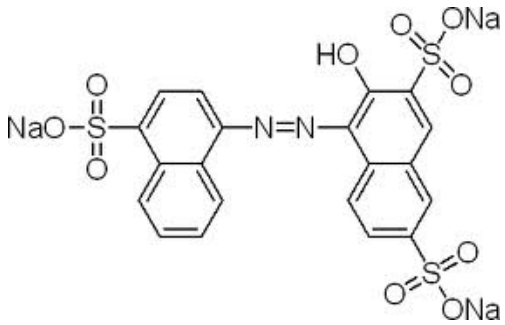

Amaranth

Figure 2.3 Structure of amaranth.

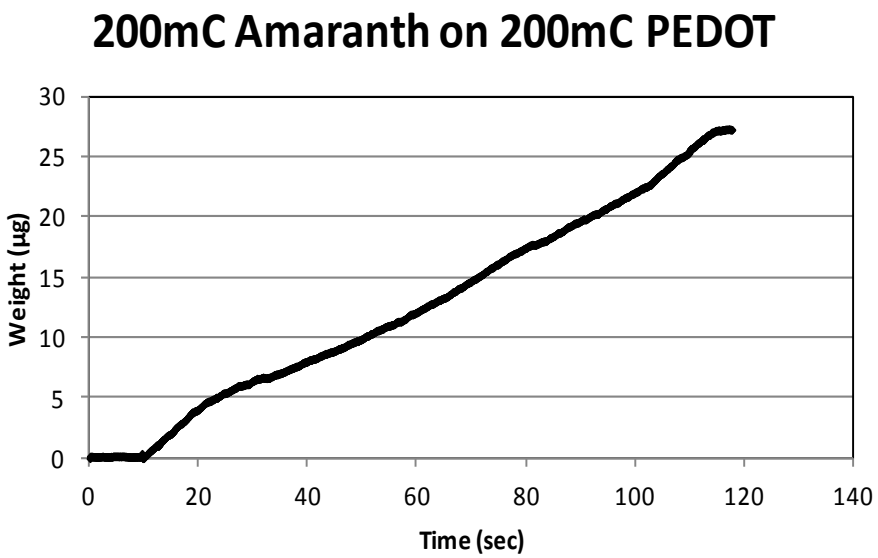

Figure 2.4 QCM graph of change in mass over time for 200 mC of amaranth uploaded into on 200mC PEDOT.

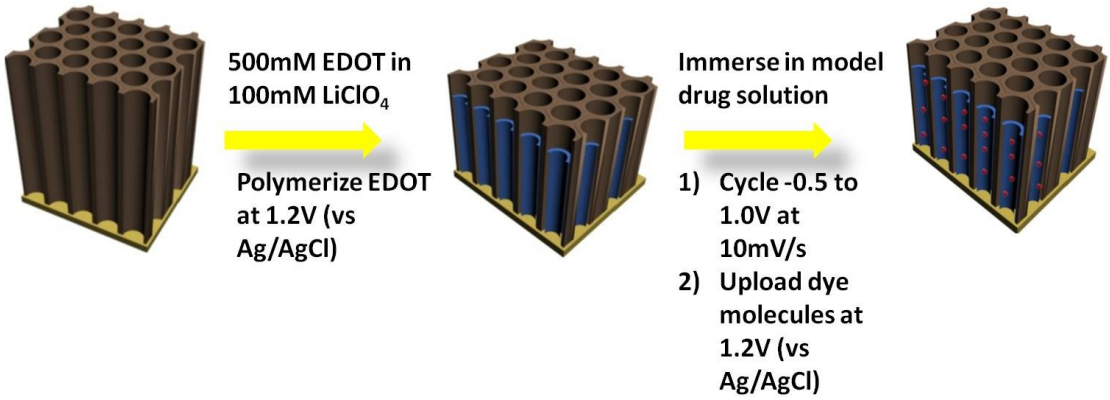

Scheme 2.2 Electropolymerization of EDOT and uploading of model dyes in AAO/PC membrane.

In order to create a contact between the PEDOT nanotubes and the gel electrolyte, the PEDOT nanotube patch was placed in 100 mM solution of NaCl or $LiClO_4$ and 200 mC of electrolyte was deposited. The next layer of the PEDOT patch consisted of a solid electrolyte matrix that was in contact with the surface of the flexible template. The solid electrolyte matrix for amaranth consisted of 100 mM sodium chloride and polyethylene glycol (7.5%wt/wt) dissolved in water and heated slowly under strong stirring until the gel was homogeneous. Finally, 1 cm by 1cm piece of carbon fiber paper was placed on top of the electrolyte gel and the edges of the patch were sealed with epoxy (See Scheme 2.3).

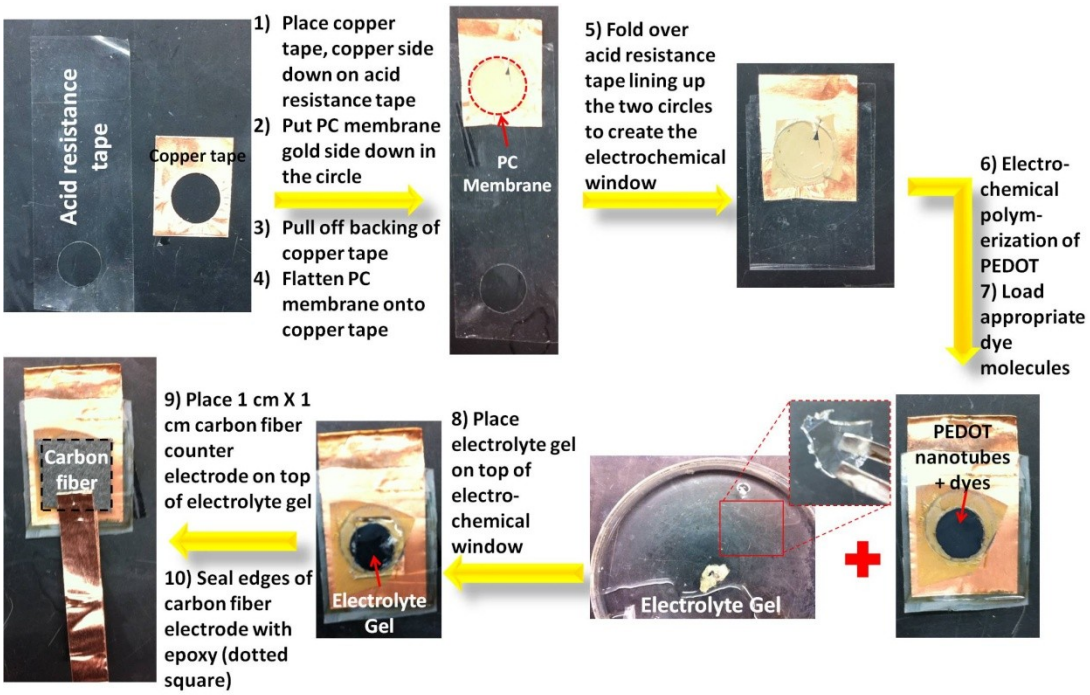

Scheme 2.3 Step by step construction of PEDOT nanotube transdermal patch.

2.2.4 Characterization of PEDOT nanotubes and uploading capabilities of model drugs

The PEDOT nanostructures were investigated using a field-emission scanning electron microscope (SEM; Hitachi S-4700, operated at an acceleration voltage of 5 keV) and transmission electron microscope (TEM; Zeiss EM10CA, operated at 80 keV). TEM and SEM sampling methods were previously described in detail.[70, 67, 85] Briefly, the template was dissolved in 3 M NaOH for 15 minutes to expose the PEDOT nanotubes. After rinsing them with de-ionized water repeatedly, the samples were dispersed in ethanol and sonicated. The nanotubes precipitated to the bottom of the microvial. For SEM sampling, 6 µL of the nanotube solution were dropped on carbon tape and dried in air before observation. For TEM

sampling, 6 μL of the nanomaterial solution was dropped and dried on a TEM grid.

The uploading and release capabilities of the nanotube patch were performed in a three electrode system. The patch was placed in a solution of PBS (pH 7.4) after the model drugs were loaded into the nanotube. A constant potential of -1.0 V was applied to the patch for 24h. Sampling amounts of 1mL aliquots of PBS buffer were taken out and stored in 1.5mL microvials every hour for 5 hours, at hour 10, and once again at 24 hours. The beaker was replenished with fresh PBS after each sampling interval. The absorbance of amaranth was measured at wavelengths of 216, 255, and 520 nm. The multiple absorbance peaks correlate to the multiple negative charges provided by the sulfonic groups.[86]

2.3. Results and Discussion

2.3.1 Electron microscope characterization of PEDOT nanotubes

The specified conditions for the growth of PEDOT nanotubes are based on our previously published mechanism.[67] The gold sputtered on the bottom of the AAO and PC membranes form a ring-shaped electrode that defines the tubular shape of the nanotubes. In addition, the limited amount of EDOT monomer at low concentrations prevents the formation of solid nanowires. Controlling the amount of charge per unit area during electropolymerization regulates the amount of PEDOT loaded in the pores of the template. Figure 2.5 shows the SEM image of PEDOT nanotubes following the removal of the membrane template. Without the template to support the nanotubes, the structures collapse and aggregate from the

strong surface tension generated at the interface between the nanotubes and solvent during evaporation. Although the top of the nanotubes are aggregated, the open porous structure of the nanotubes remains evident.

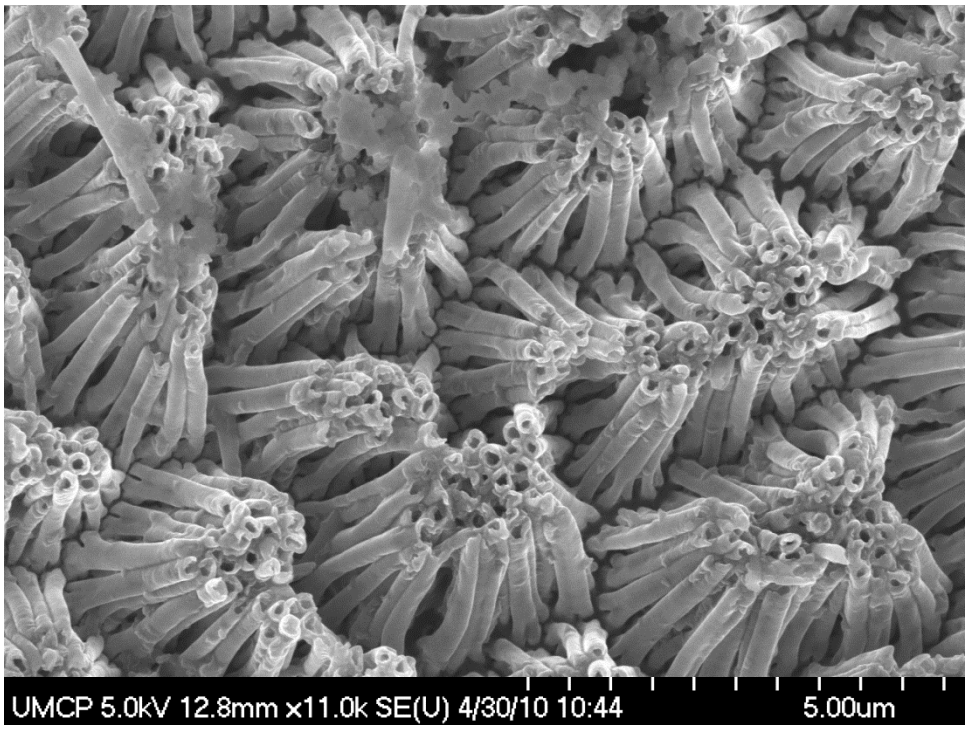

Figure 2.5 Electron microscopy images of PEDOT nanotubes electrodeposited with a charge density of 200 mC/cm^2 and subsequent removal of the membrane template.

2.3.2 Theory for upload and release of drugs from PEDOT patch

There have been many studies over the past twenty five years to overcome problems associated with skin delivery. Although new methods, like those discussed in *Section 1.1.3*, have emerged over the years, those techniques can be divided into two main categories: passive and active. Passive methods include conventional means of applying drugs to the skin such as ointments, creams, gels,

etc. Passive methods are limited by the amount of drug that can be delivered due to the fact that the fundamental barrier properties of the skin are not changed. On the other hand, active methods use external energy to act as a driving force to reduce the barrier structure of the stratum corneum. All of the current TDDS covered in *Section 1.1.3*, including our PEDOT nanotube patch, are active methods.

Currently, there are four main categories that transdermal patches can be classified in: single-layer, multilayer, reservoir-type and matrix-type, with the last two being predominant (see Figure 2.6). Single and multi-layered transdermal patches have the same working principle for the drugs are contained in the adhesive layer. The advantage of the multilayer release is that it may contain two layers, one for immediate release and the other for controlled release.[87] A reservoir-type holds the drugs in a solution or gel thus drug delivery can be governed by rate-controlling membrane position between the drug reservoir and skin. By contrast, matrix-types are an all-in-one patch that combines the drug, adhesive and mechanical backbone of the patch and does not involve a rate-controlling membrane. The delivery rate in all-in-one patches is governed by the permeability of the skin. Reservoir-type patches involve a greater design complexity, however they offer an advantage over matrix-type patches in terms of formulation flexibility, and tighter control over drug delivery rates, although an initial burst of drug delivery is evident.[2] Stimulus-responsive polymers are attractive for reservoir-type drug release systems due to the fact that drugs can be triggered by polymer structure changes in responses to stimuli such as pH,

temperature, and electricity.[60, 84, 88] Herein we discuss a new electrical release method involving the intrinsic electronic properties of conductive polymers, specifically PEDOT.

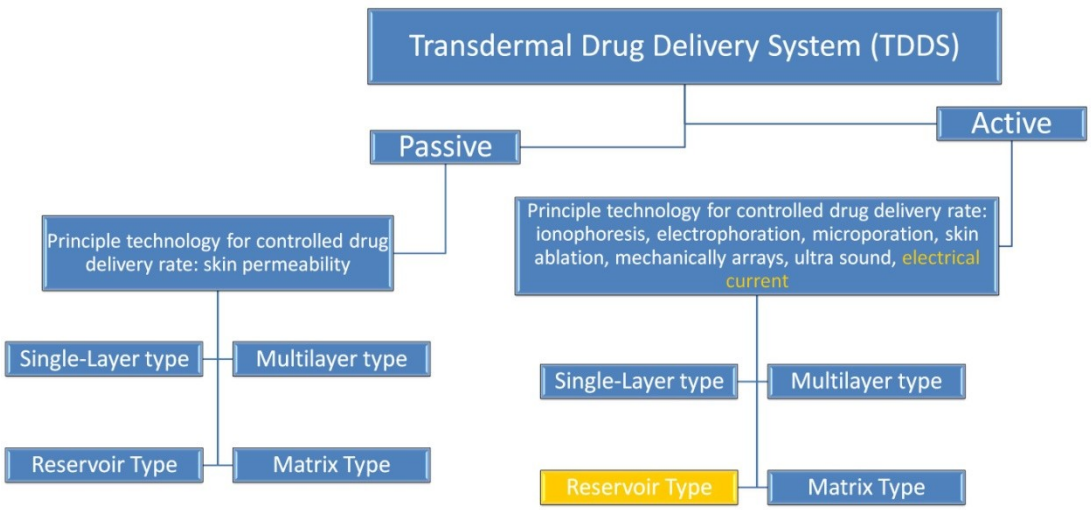

Figure 2.6 Classification chart for transdermal drug delivery systems.

Electrochemical switching of PEDOT (Figure 2.7) is accompanied by charge compensation through ion movement into or out of a membrane. A practical application of this property would be the upload and controlled release of anionic drugs from PEDOT backbone. The drugs can accumulate in the polymer during oxidation and then be released by electrochemically controlled reduction of the polymer.

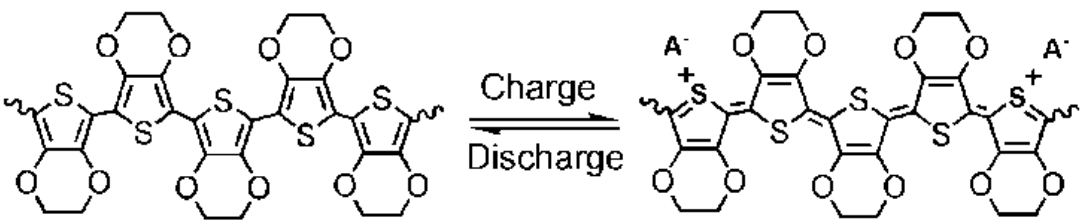

Figure 2.7 Charge (oxidation) and discharge (reduction) of PEDOT polymer backbone.

Responses to electrochemical oxidation can also produce changes in conductivity, color, and volume.[89-91] A change in the electronic charge is accompanied by an equivalent change in ionic charge, which requires a mass transport between the polymer and dopant ions.[92] When the counterions enter the polymer it physically expands and contracts depending on the number of ion exchanges (Figure 1.6).

The electronic properties of PEDOT allow for the uptake and release of drugs by varying the applied electrical potential (Scheme 2.4). The design criterion of the patch is based on the electrostatic interaction between hydrophilic model drugs and the oxidized and reduced forms of PEDOT nanotubes. When an oxidative potential is applied, the PEDOT backbone becomes positively charged therefore a variety of anionic molecules can be utilized. In order to controllably release the dye, a potential can be applied causing electrostatic repulsion or attraction between the dyes and charged PEDOT. Applying a positive potential (i.e.: charge) will prevent the delivery of drugs (Scheme 2.4c), while a negative potential (i.e.: discharge) will release the drugs, accordingly (Scheme 2.4d). At 0 V, PEDOT is only slightly negative therefore migration of dyes molecules through diffusion can occur. In addition to electrostatic repulsion, the physical swelling and shrinking of the nanotubes can forcefully expel the drug molecules from the nanotubes.

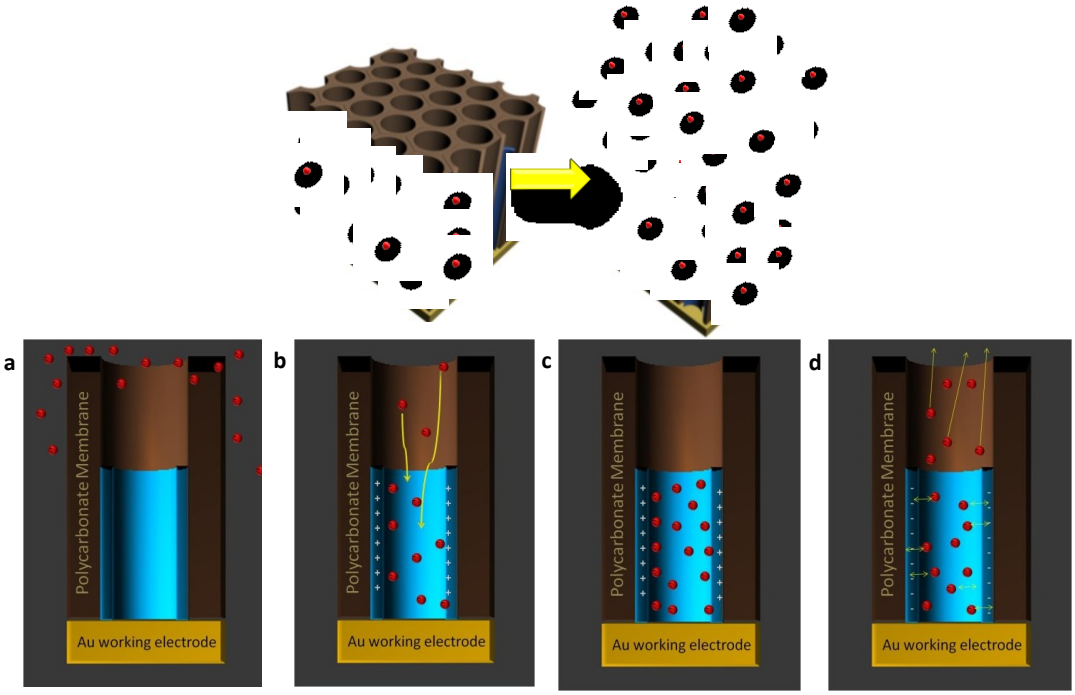

Scheme 2.4 Schematic depicting the main steps of the controlled released delivery system. The controlled drug delivery system is assembled by a) placing the template-embedded PEDOT nanotubes in drug solution b) then loading anionic drugs into the pores of PEDOT nanotubes. c) After optimal loading the d) desired potential is applied to release the drugs either in step-wise or steady doses.

2.3.3 Release kinetics of PEDOT nanotubes TDDS in PBS

In Chapter 1, general drug release experiments where a diversity of molecules was incorporated into various CP materials to be released following electrical stimulation were addressed.[52, 83, 93-97] However, drug loading within films are subject to size requirements of dopant molecules and therefore are inefficient for the uploading and release of drugs. The Langer group circumvented issues involving dopant ions by attaching drug molecules directly to the surface of polypyrrole (PPy) through biotin-streptavidin coupling.[56] Following the attachment of the desired molecule, electrical stimulation triggers the release of

the molecule. By incorporating biotin as a dopant, it is believed that an electrical pulse triggers the release of the biotin and the attached payload. However, CPs release most efficiently from the surface compared to the polymer bulk. Drugs loaded within the deeper layers of the film can take up to days to be release while those mainly on the superficial layers are prematurely release.[56-57]

The most effective way to increase drug release efficiency is to increase the surface area of the polymer film. The Cui group was one of the first to explore conductive polymer "nanostructures" for electrical stimulus responsive release.[58, 59] The group electrochemically polymerized PPy and fluorescein on a glassy carbon electrode modified with multilayers of PS nanobeads (mean diameter 46±2nm). The removal of the PS beads after the polymerization of PPy provided a porous morphology to the film thus increasing the surface area and increased the release of fluorescein in PBS buffer by almost 9 times , compared to a conventional film (Figure 2.8).

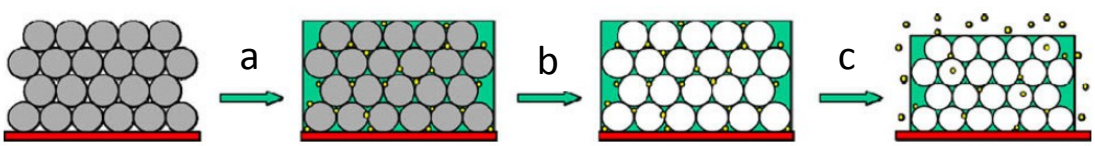

Figure 2.8 Synthesis of nanoporous PPy film for electrochemical controlled drug release. a) Immersion of PS template modified electrode into pyrrole solution containing fluorescein and polymerize; b) dissolve PS nanobeads; c) apply potential to release fluorescein. Reprinted from Luo et al.[59]

To overcome these issues, we developed a transdermal drug delivery patch with PEDOT nanotubes. With an external stimulus to control the potential, doses can be delivered to match clinical requirements.

For proof of concept, we analyzed the controlled release of a model drug molecule from PEDOT nanotubes in a buffered solution (25°C, pH 7.4). The PEDOT embedded nanotubes were immersed directly into PBS buffer solution following the upload of Amaranth. We applied a steady potential of -1.0 V, 0 V, and +1.0 V (vs. Ag/AgCl) for 24 h (similar set up to Figure 2.2). The absorbance of amaranth in PBS was measured over time and expressed as the cumulative percentage of the total amount of model drug released from PEDOT nanotubes. An observed correlation between the cumulative percent of drug release and strength of applied potential was evident (Figure 2.9).

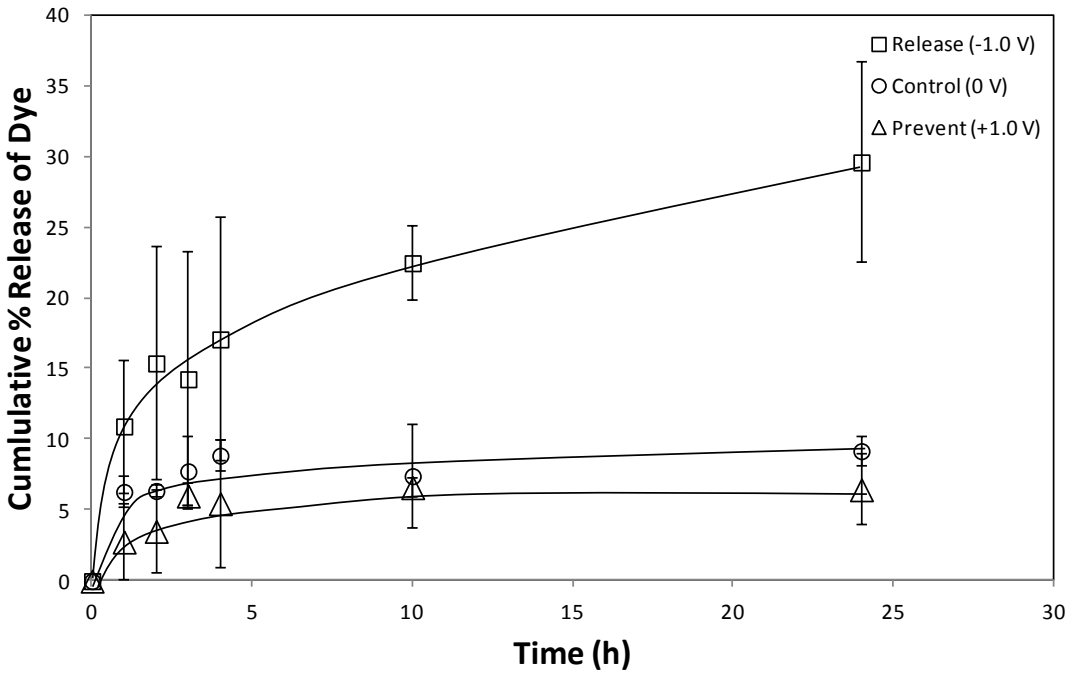

Figure 2.9 Release of amaranth in PBS buffer solution in three electrode system. a) A constant potential of -1.0V, 0 V, and +1.0 V (vs. Ag/AgCl) was applied for 24h and 1mL aliquots were taken out and measured with UV-Vis at 1h, 2,h, 3h, 4h, 5 h, 10h, and at 24h. After the measurements, 1mL of fresh PBS buffer was used to replenish the beaker. The experiment was repeated three separate times and data sets are averaged with standard deviation error bars (N=3±SD).

Following a reduction potential, the negatively charged PEDOT backbone caused electrostatic repulsion releasing the dyes into the solution. With an oxidative potential (+1.0 V), the cumulative percent of drug release was found to be much lower than both -1.0 V and 0V. Approximately 7 times more dye molecules were released with an applied potential than without. In addition, applying a positive potential prevents the diffusion of dye molecules. These

preliminarily studies demonstrated that the strength of the potential affects the rate of model drug release.

2.4 Conclusion

In this chapter, the PEDOT nanotube transdermal patch was designed and synthesized. Approximately 30 μg of model drug molecules were loaded within the patch system and released accordingly. As a proof of concept experiment, the PEDOT nanotubes loaded with dye molecules were placed in a solution of PBS buffer and variable potentials were applied. Cumulative percentage of release over time showed that the rate of drug release can be controlled by the strength of the applied potential. The feasibility and efficiency of the template synthesis method provides an easy fabrication route for the PEDOT nanotube TDDS making it an ideal candidate for industrial manufacturing.

Chapter 3: Transdermal drug delivery analysis

3.1. Introduction

The most familiar means of transdermal drug delivery is through passive methods, such as ointments and passive patches (e.g., nicotine, birth control patches). The main restrictions with passive delivery is the property of the stratum corneum which limits drug delivery to those of low-molecular weights that are hydrophobic and effective at low doses.[2] Active delivery methods involve an external energy source to help drive the drug across the skin thereby facilitating the delivery of smaller, hydrophobic molecules in addition to larger charged and hydrophilic molecules. Many active methods were discussed in Chapter 1, such as iontophoresis and electroporation for electrical stimulation and microneedles and abrasions for mechanical stimulations.[20] In this section we will focus on the *in vivo* release kinetics of the PEDOT nanotube TDDS using the active delivery method.

3.2. Materials and methods

3.2.1. Chemical and materials

3,4-ethylenedioxythiophene (EDOT, Sigma Aldrich), acetonitrile (Fisher Scientific), and lithium perchlorate ($LiClO_4$, Acros) were used to synthesized PEDOT nanotubes within gold sputtered alumina (200 nm diameter, 60 μm thickness, Whatman) and polycarbonate membranes (PC, 220 nm diameter, GE

Osmonics) with Pt foil (99.99%, Alfa Aesar) as the counter electrode and Ag/AgCl as the reference electrode. Indium tin oxide (ITO) glass (R_s=4-8 ohms, thickness 1.1 mm) for PEDOT films was commercially available from Delta Technologies Limited. The model dye molecules used for *in vitro* analysis were amaranth (Sigma-Aldrich) and Cy5.5 (G.E. Health). Fluorescein isothiocyanate (FITC) (Invitrogen) was used for *in vivo* drug delivery analysis. Anhydrous propylene carbonate (Sigma), ethylene carbonate (Sigma-Aldrich) and poly(methylmethacrylate) (PMMA, Sigma-Aldrich) were used to synthesize the electrolyte gel for hydrophobic dyes. Sodium chloride (NaCl, J.T. Baker), polyethylene glycol (PEG, Sigma-Aldrich), and Millipore water was obtained by a Milli-Q A10 system was used to synthesized the electrolyte gel for hydrophilic dyes. The electrochemical windows were dictated by copper tape (3M), acid resistance tape (3M), and parafilm. Finally, the patch was topped with a porous carbon fiber mesh (Fuel Cell Store) as counter electrode. Epoxy was used to seal the entire TDDS.

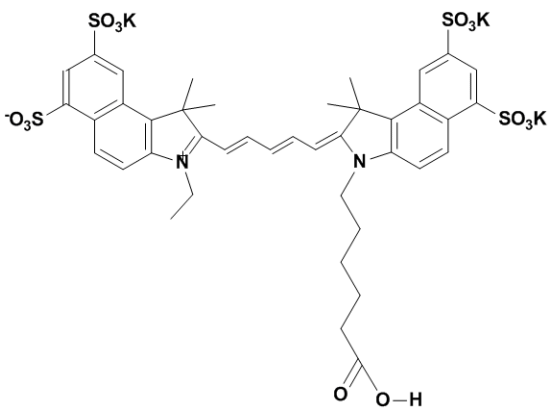

Cy5.5

Figure 3.1 Cy 5.5 molecular structure.

3.2.2. Synthesis of PEDOT film for comparative studies

PEDOT film was synthesized on ITO. Copper tape was attached to the electroactive side of the ITO. Acid resistance tape was used to secure the copper tape on the ITO and create a symmetric square electroactive area (see Figure 3.2). 1.26 cm^2 of ITO was placed in 500 mM of EDOT in 100 mM $LiClO_4$ in acetonitrile. The three electrode cell set up as illustrated in Figure 2.2 was utilized. The entire ITO surface is placed in a 50 mM solution of EDOT in 100 mM $LiClO_4$ in acetonitrile. A potential of 1.2V is applied to the system until the charge reached 200 mC.[67] All electrode potentials were measured relative to a Ag/AgCl reference electrode using Pt foil as a counter electrode, if not specified otherwise. Next, the PEDOT film was placed in a solution of 600 mM amaranth and cycled between -1.0 V and 1.0 V to flush out any EDOT monomers and perchlorate ions. After adequate flushing, 200 mC charge of amaranth was passed into the PEDOT film by applying 1.2 V. Following the upload of amaranth into the film, the PEDOT film was rinsed very carefully with water. Next, the electrolyte gel was spread on the PEDOT film and the carbon fiber counter electrode was placed on top of the gel to complete the delivery system. The PEDOT film patch was then placed in a Franz Diffusion Cell and release studies were performed under the same conditions as for the nanotube patch system. Briefly, 1.2 V, 0 V, and -1.2 V (vs. carbon fiber counter electrode) were applied for 24 h. Sample amounts of 1mL aliquots were taken at specified intervals. The receptor cell volume was 10mL and was replenished with fresh 1 mL aliquots of PBS after each sampling period.

Figure 3.2 ITO 1.26 $cm^2$with copper and tape after polymerization of PMProDot.

3.2.3. Set up for *in vitro* analysis

The construction of the PEDOT nanotube patch is as mentioned in Section 2.2.3. Prior to the loading of Cy5.5 and Amaranth, PEDOT was cycled between -0.500 V and 1.0 V in a solution of the amaranth or Cy5.5 at 10 mV/s in order to remove any EDOT monomers and to exchange perchlorate ions with the dye molecules. After adequate flushing of PEDOT nanotubes with the dye molecules, the dye molecules were uploaded in PEDOT nanotubes by immersing the membrane-embedded nanotubes in a fresh solution of either 600 mM amaranth or 10mM Cy5.5. A potential of 1.2 V (vs. Ag/AgCl) was applied to the PEDOT nanotubes. 200 mC of amaranth is approximately equivalent to 30 µg (See Figure 2.2) and 200 mC of Cy5.5 correlates to approximately 14 µg (See Figure 3.3). To evaluate the amount of molecules loaded, a QCM (Stanford Research Systems) was used to measure weight change of PEDOT over time.

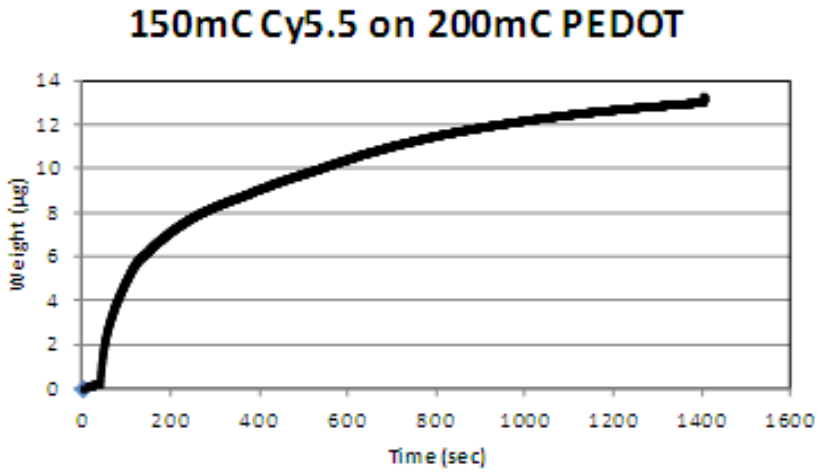

Figure 3.3 QCM analysis provides a change in weight over time graph for the upload of 150 mC Cy 5.5 into 200 mC PEDOT is measured at approximately 14 µg.

Following the upload of the dye molecules into the nanotubes, the patch was thoroughly rinsed with Millipore water to remove surface dye molecules and a layer of solid gel electrolyte was placed on top of the electrochemical window. The final PEDOT patch structure consisted of a solid electrolyte matrix that was sandwiched between the surface of the PC membrane embedded with PEDOT nanotubes and a carbon fiber counter electrode. The solid electrolyte matrix for amaranth consisted of 100 mM sodium chloride and polyethylene glycol (7.5%wt/wt) dissolved in water then heated slowly under strong stirring until the gel was homogeneous. Since Cy5.5 is less hydrophilic than amaranth, a solid electrolyte matrix of higher hydrophobicity was prepared as published by Kumar et al. with modifications.[98] Briefly, 1.0 M $LiClO_4$ was mixed in 1:1 (vol:vol) ethylene carbonate and propylene carbonate for 8 hours at 25°C. PMMA was

added to the solution at 3:1 (wt:wt) ratio of solution to PMMA. PMMA was fully incorporated in the solution by heating at 70°C then slowly cooling in the oven. The thickness obtained was approximately 0.69 mm. The solid gel electrolyte matrices were sealed between the PEDOT nanotubes and carbon fiber counter electrode with epoxy. The patch was used immediately after the epoxy hardened.

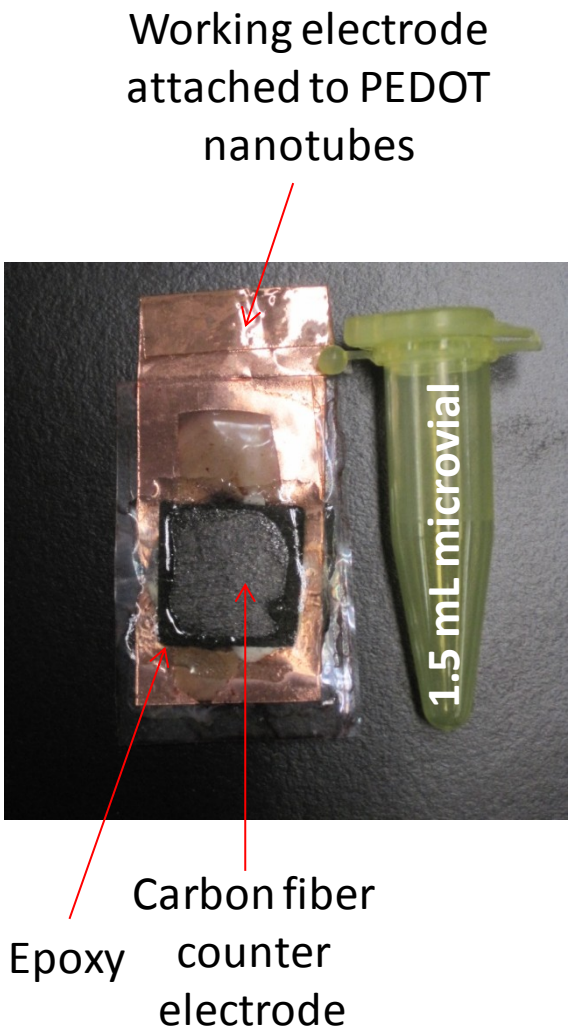

Figure 3.4 PEDOT nanotube patch. Detailed scheme of construction is provide in Scheme 2.4.

Porcine ears used for *in vitro* studies were obtained from a local slaughter house and cleaned under cold water. The whole skin was removed carefully from the outer region of the ear and separated from the underlying cartilage. The method of Klingman and Christopher with slight modifications was used to separate the porcine epidermis from the whole skin.[99] The skin was incubated over night at 37°C in 0.5% trypsin solution in PBS (pH 7.4). The tissue was smoothed out and soft epidermis was removed with cotton tipped applicator. The samples were immediately stored at -20°C until use.

A two compartment Franz Diffusion Cell setup was used to evaluate the rate of drug delivery through the excised porcine skin (Figure 3.5). A potential of -1.2 V (vs. carbon fiber counter electrode) was applied for release of amaranth through the skin while, 0 V and +1.2 V (vs. carbon counter electrode) were applied for the control and preventative release studies, respectively. The release, open circuit, and preventative experiments for Cy5.5 were performed achieved at -1.45 V, 0 V, and +1.45 V (vs. carbon fiber counter electrode) respectively. Samples were collected at 0, 1, 2, 3, 4 or 5, 10, and 24 h and then analyzed with UV-Vis spectroscopy. A full absorption spectrum for Cy5.5 (Figure 3.1) was obtained and 280 nm peak was used for analysis.

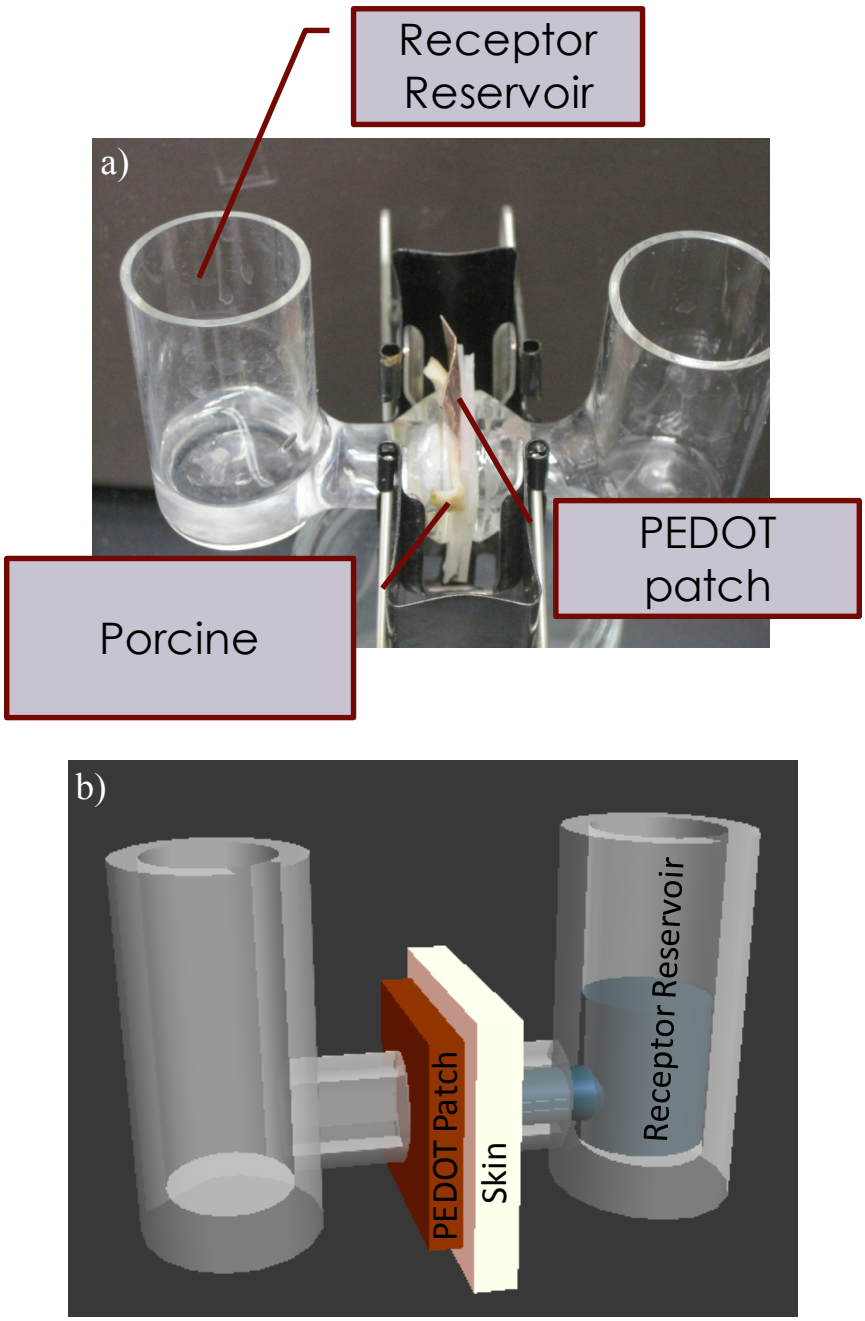

Figure 3.5 *In vitro* delivery of amaranth and Cy 5.5 through porcine skin via Franz Diffusion Cell. a) photo of set up b) illustration of set up. Porcine skin was sandwiched between PEDOT patch and receptor reservoir. Dye molecules transverse through the skin and into the reservoir to be measured and analyzed. The skin thickness is approximately 2.5 mm.

3.2.4. Set up for *in vivo* analysis

3.2.4.1. Live fluorescence imaging

Fabrication of the PEDOT nanotube patch and upload of Cy 5.5 are as described in section 3.2.3. The patch was placed on the chest of the nude mouse since the chest is the area of least autofluorescence.

Optical imaging acquirement and analysis were done using Maestro 2.10 imaging system (Cambridge Research & Instrumentation, Woburn, MA; excitation = 675 nm, emission = 695 nm). The patch was placed on the chest of nude mouse that was anesthetized with 2.5% isoflurane in oxygen delivered at a flow of 1.5 L/min (See set up in Figure 3.6). For the control experiment, 0 V was applied to the patch, while -1.45 V was applied in the working experiment. A potential of -1.45 V was applied over 60 minutes and the mouse was subjected to optical imaging at 0, 15, 30, 45 and 60 minutes. For example, -1.45 V was applied for 15 minutes, the patch was taken off the mouse, and the moue was subject to optical fluorescence imaging. The same procedure was repeated at time 30, 45, and 60 minutes. After image acquisition, deconvolution yielded the pseudocolored images of the pure spectrum of Cy5.5. All images were normalized and analyzed using Maestro software. For quantitative comparison, regions of interest (ROIs) were drawn, and the average signal ($x10^6$phot/cm^2/s) for each area was measured.

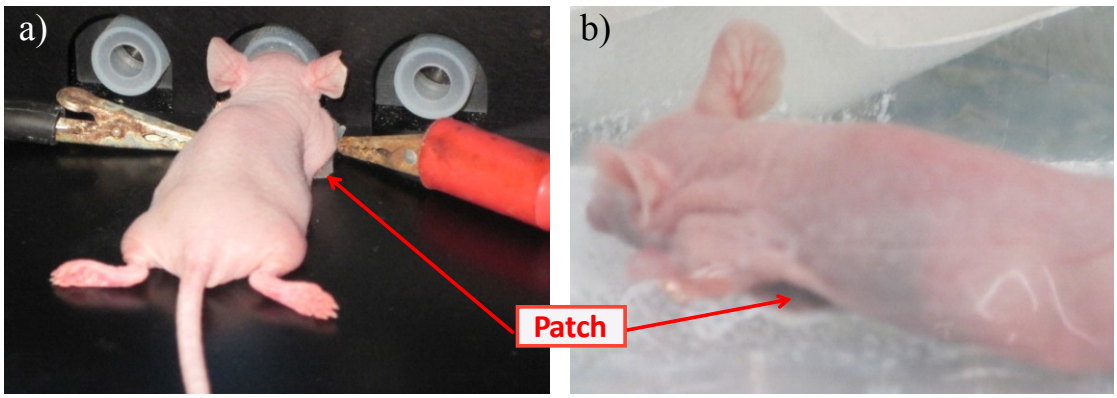

Figure 3.6 Set up for live fluorescence imaging of live nude mouse for the a) working experiment, b) control.

3.2.4.2. *In vivo* microscopy in mice

Fabrication of the PEDOT nanotube patch and upload of Cy5.5 dye molecules are as described in 3.2.3.

Fluorescein isothiocyanate (FITC) was the used *in vivo* imaging studies (See Figure 3.7). FITC was used for because of its high fluorescence quantum yield and ability to diffuse freely through tissues and blood vessels making it beneficial for live *in vivo* imaging. In addition, FITC have been used in transdermal drug delivery experiments and exhibit limited degradation.[100] FITC is negatively charged at neutral pH, therefore it was uploaded and released from the PEDOT nanotubes through electrostatic interactions as well. FITC was loaded into the PEDOT nanotube patch in the same manner as amaranth and Cy5.5. Briefly, a PC membrane with embedded PEDOT nanotubes was immersed in 600 mM FITC in ethanol. A potential of 1.2 V (vs. Ag/AgCl) was applied until 200 mC of FITC was deposited. The patch was then thoroughly rinsed with ethanol followed by water. Due to the hydrophobicity of FITC, the electrolyte gel used in

the TDDS was the same as mentioned in section 3.2.3 for Cy 5.5. A porous carbon fiber counter electrode (1 cm by 1 cm) was placed on top of the electrolyte gel. The entire system was sealed with epoxy and used immediately after the epoxy hardened.

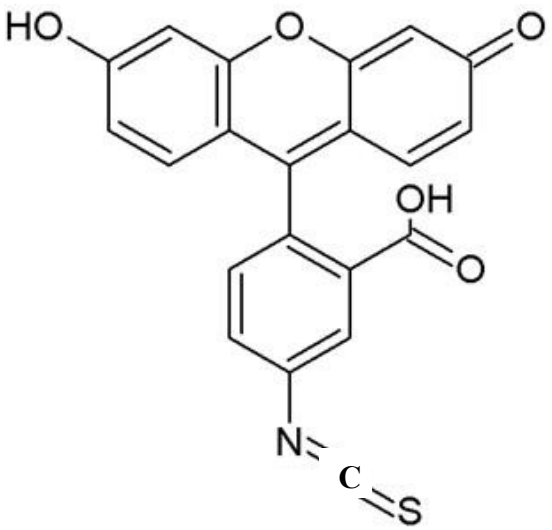

Figure 3.7 FITC molecular structure.

6–8 week old male C57B6/L mice (Jackson Laboratory) were used for the *in vivo* imaging experiments. After anesthesia with intraperitoneal injection of ketamine-xylazine (90 mg/kg and 9 mg/kg respectively), the dorsal part of the back skin was clipped and residual hair was removed using a hair removal cream. Approximately 1 cm by 1 cm of the epithelial side was attached to the transdermal patch. FITC was delivered transdermally at -1.45V (vs. carbon fiber counter electrode) for 30 minutes. Acquisitions were obtained from a custom-made two-photon laser scanning microscope with a tunable Ti:Sapphire laser (Mai-Tai DeepSee, Spectra-Physics) and a water immersion objective lens (20X, 1.0 NA).

The laser was tuned to 800 nm. The average laser power at the sample was set to < 25 mW. All animal experiments were performed in compliance with institutional guidelines and approved by the subcommittee on research animal care at the Massachusetts General Hospital.

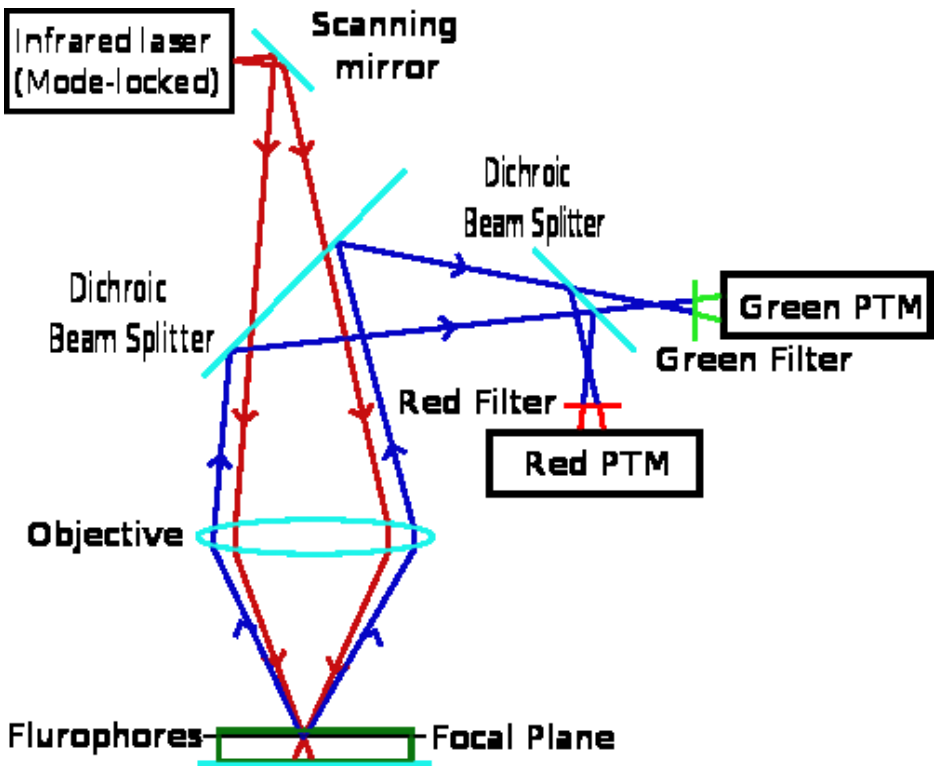

Figure 3.8 Schematic of general two-photon laser scanning microscopes.[101]

3.3. Results and discussion

3.3.1. Release rates from PEDOT films for comparative studies

The limitations of PEDOT films for transdermal drug delivery were addressed in Chapter 2. In addition to dopant restrictions and variable release rates, depending on the depth that the drug is embedded in the film, PEDOT films have been found to respond to potential changes within 1 to 2 s.[89, 98] The slow interconversion rate

is a main obstacle for applications of films for devices requiring fast charge/discharge capability such as controlled TDDS. The observations from the comparative film studies further support the advantage of using PEDOT nanotubes over film for controlled drug delivery.

As seen in Figure 3.9, there was an initial release of dyes from the PEDOT film with an applied potential of -1.2 V, however there was almost no difference in the cumulative percent of dye released over 24 hours between -1.2 V and 0 V. It is hypothesized that the initial release corresponds to dye molecules on or very close to the surface of the PEDOT film. However, as seen from the release rate constant in Supplemental Figure 5, there is minimal long term release. This is most likely due to the long diffusion time of the dyes deeply embedded within the cross linking polymer. As the dyes take longer to travel to the surface of the polymer films they have a greater amount of non-specific interactions (H-bonding, Van der Waals, etc) to overcome.

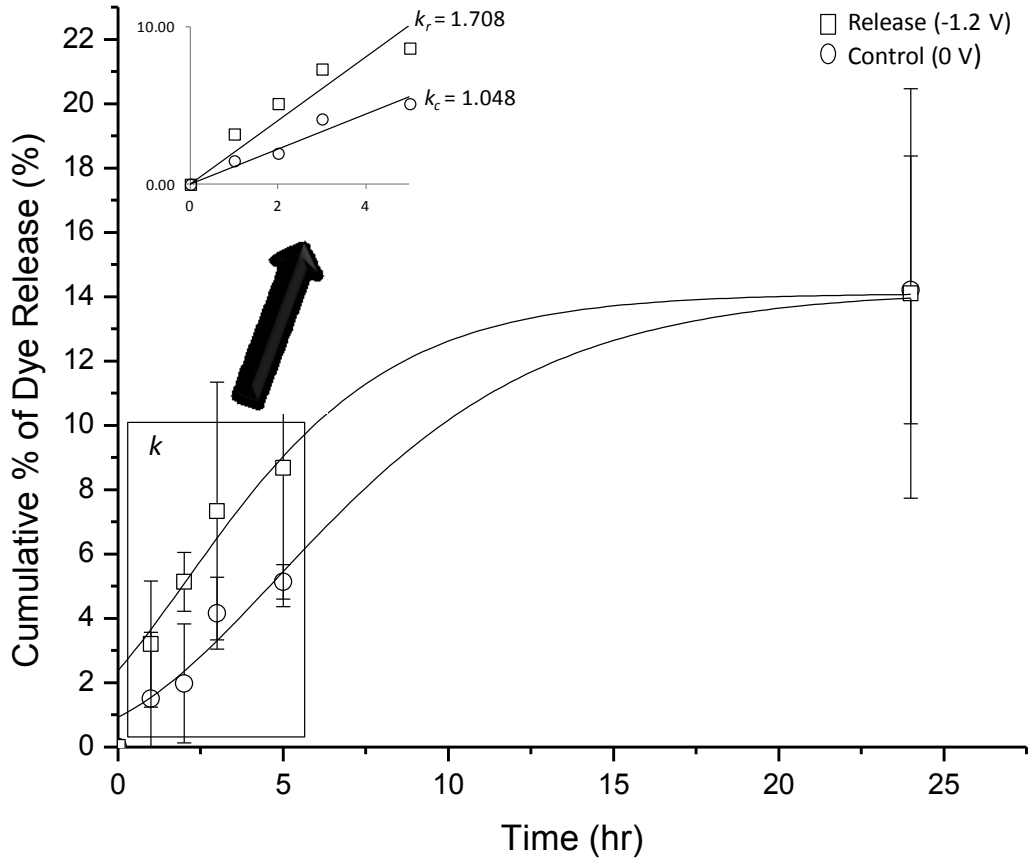

Figure 3.9 Graph depicts the cumulative percent dye release of amaranth from PEDOT film on ITO surface. The PEDOT film was placed in a Franz Diffusion Cell and release studies were performed under the similar conditions as for the nanotube patch system. Briefly, -1.2 V and 0 V (vs. carbon fiber counter electrode) were applied to two systems independently for 24 h. Sample amounts of 1mL aliquots were taken at specified intervals. The receptor cell volume was 10mL and was replenished with fresh 1 mL aliquots of PBS after each sampling period. (1.2 V r^2value from 0 h to 5 h = 0.867; 0V r^2 value from 0 h to 5 h = 0.938). The experiment was repeated three separate times and data sets are averaged with standard deviation error bars (N=3±SD).

3.3.2. *In vitro* analysis

Although excised human skin is regarded as a "gold standard" for *in vitro* transdermal experiments, it is not sufficiently available and there is large variability among samples in relation to gender, race, age, and anatomical donor site.[101-107] Many animal skin models from various mammals, rodents, and reptiles have been used as surrogates for human skin, however animal skin tends to be more permeable than human.[107, 108] Generally, monkey and pig skin are better models than rodents, however for ethical reasons primate research is restricted. Therefore pig skin is the preferred replacement.[109] In addition, based on morphological and functional data, domestic pig skin seems to be the closest to human skin, and therefore it was specifically chosen to be utilized in the *in vitro* analysis.[110-111]

One way to study the effectiveness of a transdermal patch is through the use of a Franz Diffusion Cell (Figure 3.5). The system is used to determine the permeation amount of specific molecules on a certain type of membrane, which in this case is porcine skin. A Franz Diffusion Cell system is composed of a receptor and donor cell. The permeated amount through the skin is independent of initial concentration, concluding that these studies are zero order release.

In order to release the dye molecules, a potential of either -1.2 V or -1.45 V (vs. carbon fiber counter electrode) was applied causing electrostatic repulsion between the dye molecules and charged PEDOT. Amaranth was released at -1.2 V, while +1.2 V was applied to prevent the release (See Figure 3.10). Applying a negative potential will release the drugs (Figure 3.10a), while applying a positive

potential prevents the release of drug molecules (Figure 3.10b). Figure 3.10c, d, and e shows excised porcine skin following applied potential of -1.2 V (Figure 3.10c), +1.2 V (vs. carbon fiber counter electrode) (Figure 3.10d), and 0 V (Figure 3.10e) over 24h. The visible discoloration of the porcine skin corresponds to the release of amaranth at -1.2 V. In addition, since PEDOT backbone is slight negative at 0 V, some release of amaranth dye can also be detected.

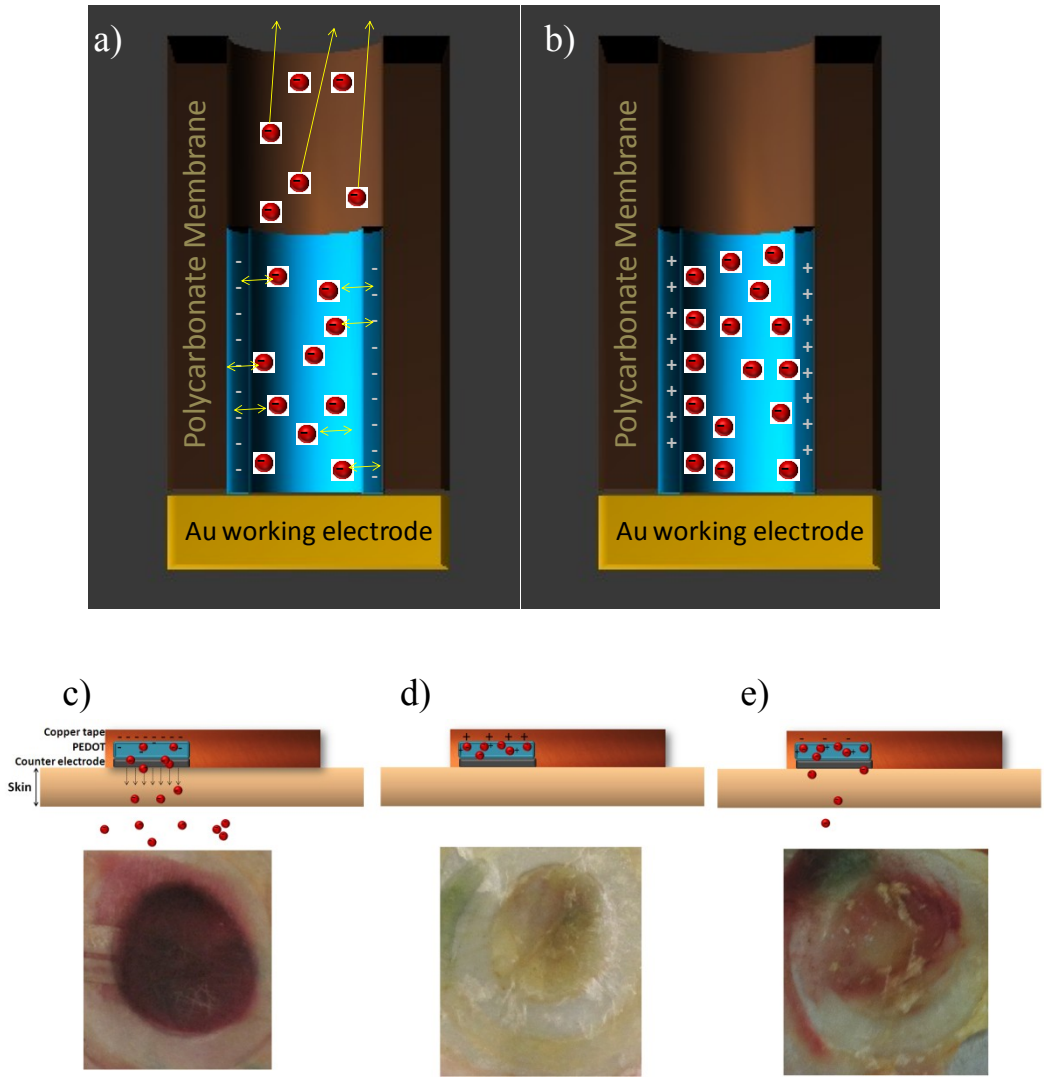

Figure 3.10 By controlling the potential of the PEDOT patch, we can control the amount and duration of the drugs delivered. a, c) Applying a negative potential will deliver the drugs in a fast and controlled manner, while applying b, d) a positive potential will result in minimal release of drugs molecules. Excised porcine skin following applied potential of c) -1.2 V, d) +1.2 V and e) 0 V for 24 h. The visible discoloration corresponds to the release of amaranth at -1.2 V. Since PEDOT backbone is slightly negative in the neural state, some releases of dye molecules can also be seen (e).

It is hypothesized that the dyes are released through two main mechanisms. The first is the electrostatic attraction and repulsion following the oxidation and reduction of the PEDOT nanotubes (See Figure 3.11). The oxidation of PEDOT allows for electrostatic attraction to upload and keep the dye molecules within the TDDS. When a reduction potential is applied, electrostatic repulsion cause the dye molecules to leave the PEDOT nanotubes and transverse through the gel electrolyte towards the counter electrode. Through this mechanism, most of the dye molecules may remain in the counter electrode since it becomes positively charged when PEDOT is negatively charge. In order for the dye molecules to transverse past the counter electrode and into the skin, the second hypothesized mechanism is similar to the delivery mechanism of iontophoresis. The second mechanism is demonstrated in Figure 3.12 which shows an electrical charge causes volume flow in the direction of the counterions flow. Electroosmosis occurs in the direction of the counterions migration when an electrical potential difference is applied across the skin. The electrophoresis and electroosmosis aids the delivery of the dye molecules through the counter electrode and into the dermis.

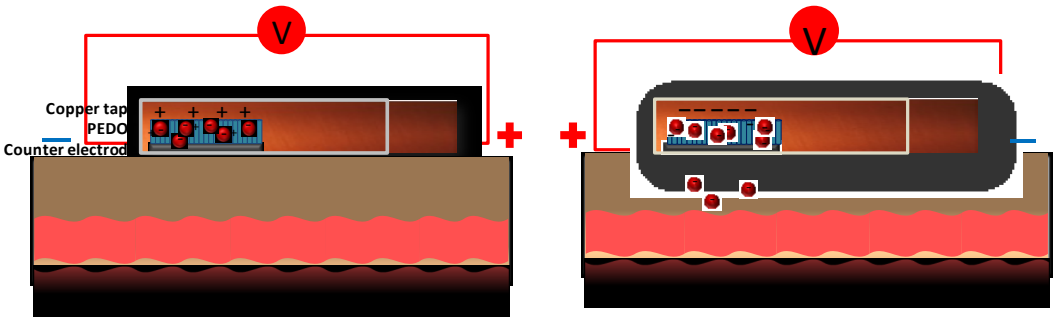

Figure 3.11 a) The oxidation of PEDOT allows for electrostatic attraction to upload and keep the dye molecules within the TDDS. b) When a reduction potential is applied, electrostatic repulsion cause the dye molecules to leave the PEDOT nanotubes and transverse through the gel electrolyte towards the counter electrode.

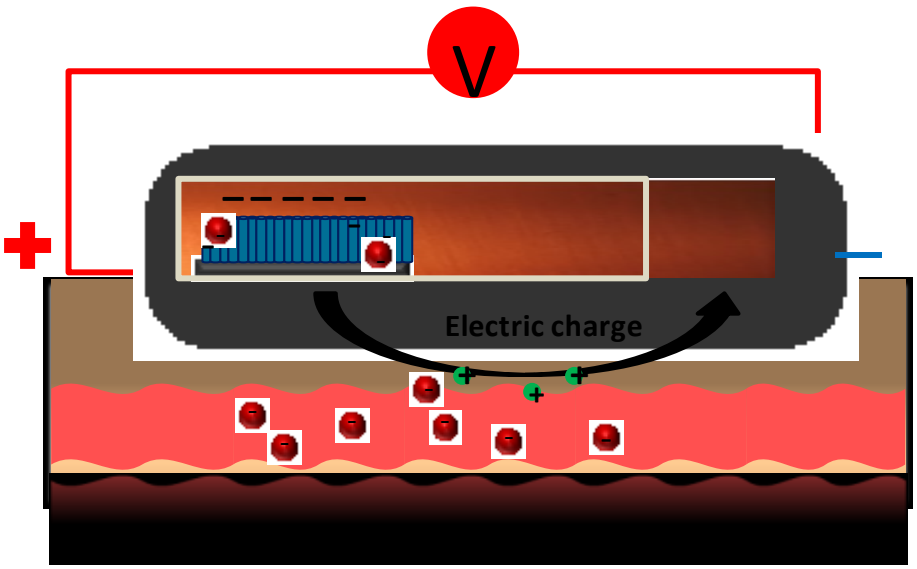

Figure 3.12 The second mechanism for drug delivery in the PEDOT patch results from the contact of the counter electrode and working electrode on the skin. The electrical potential difference applied across the skin from the working electrode and counter electrode creates a volume flow that allows for the electroosmotic and electrophoretic flow of anionic dye molecules and counter ions through the skin and into the dermis.

More importantly, we analyzed the release rates with an applied potential and release payload of hydrophilic model drugs from the PEDOT nanotube TDDS through porcine skin to demonstrate that both can be fine tuned to deliver the desired therapeutic concentration. These observations were supported by the results shown in Figure 3.13 and 3.14. A Franz Diffusion Cell was used to measure the cumulative amount of dye release over time. Amaranth and Cy5.5 have different charges -3 and -1 at pH 7.4, respectively, and partition coefficients (*Log P*) values, -14.594 and -14.122 (octanol/water), respectively. Cy5.5 is slightly less hydrophilic than amaranth and therefore required a higher potential to be released. Over 24 h, the cumulative percent of drug release for amaranth and Cy5.5 were 88% and 70%, respectively, compared to the control (0 V). The cumulative amount of dyes released at 0 V is due to the diffusive mass transport of dyes out of the negligibly charged PEDOT polymer, therefore leakage of dye from positively charged PEDOT needed to be assessed as well. Figure 3.13 clearly shows the prevention of a migrational flux as a result of a positive applied potential for amaranth, however the difference between the diffusive flux at 0 V and migrational flux at +1.45 is not as distinct for Cy5.5 (see Figure 3.14). We hypothesized that this is a result of the lower net charge of Cy5.5 compared to Amaranth. In addition, the high hydrophobicity of Cy5.5 can result in stronger hydrophobic interactions between the dye molecules and porcine skin. This observation demonstrates the capability of controlled transdermal delivery through applied potential.

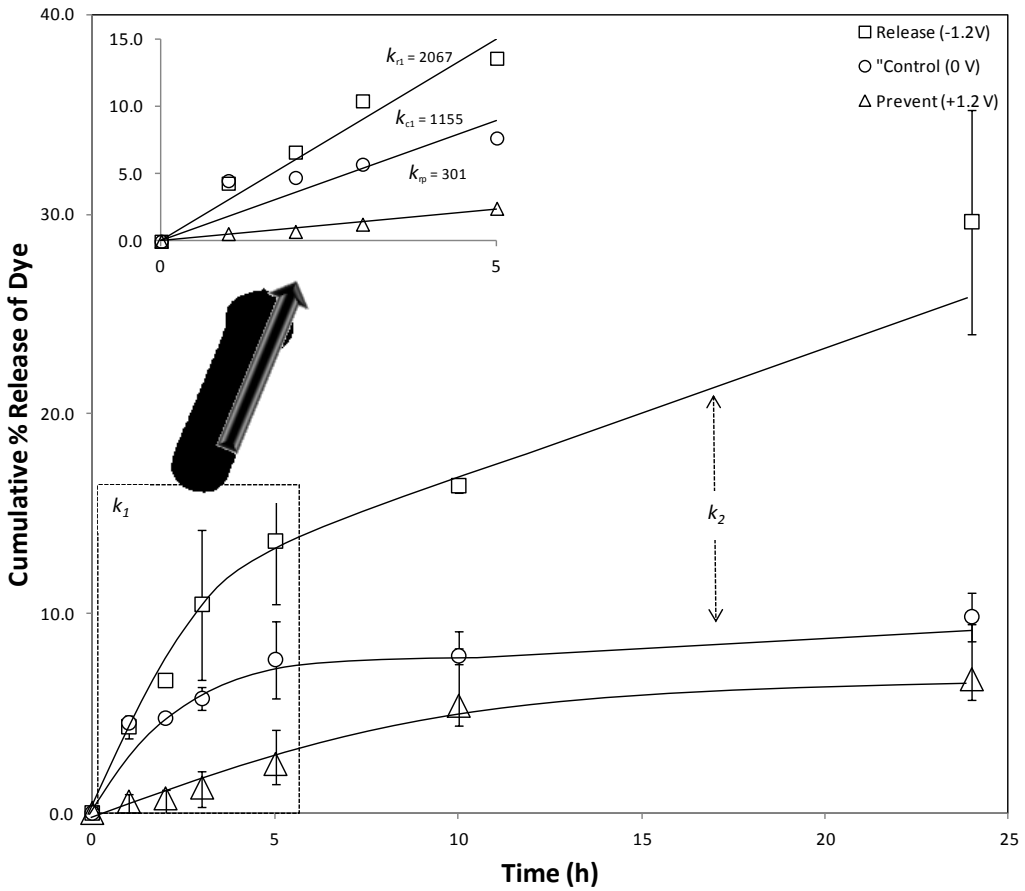

Figure 3.13 Graph depicts the cumulative percent of amaranth molecules released from PEDOT nanotube patch through porcine skin. The PEDOT nanotube patch was placed in a Franz Diffusion Cell. Release studies were performed under -1.2 V, 0 V, and +1.2 V (vs. carbon fiber counter electrode) for 24 h. A different patch was used for all the experiments. Sample amounts of 1mL aliquots were taken at specified intervals. The receptor cell volume was 10mL and was replenished with fresh 1 mL aliquots of PBS after each sampling period. (-1.2 V r^2value from 0 h to 5 h = 0.945; 0V r^2 value from 0 h to 5 h = 0.671; +1.2 V r^2value from 0 h to 5 h = 0.976). The experiment was repeated three separate times and data sets are averaged with standard deviation error bars (N=3±SD).

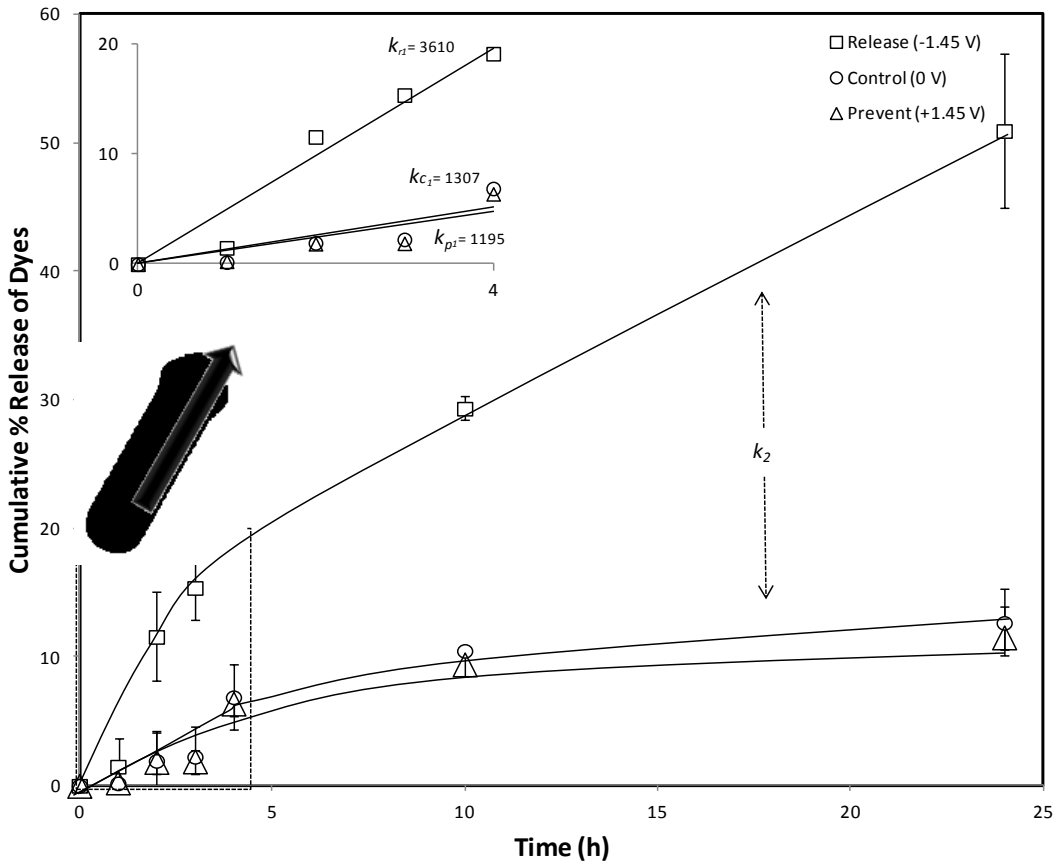

Figure 3.14 Graph depicts the cumulative percent of amaranth molecules released from PEDOT nanotube patch through porcine skin. The PEDOT nanotube patch was placed in a Franz Diffusion Cell. Release studies were performed under -1.45 V, 0 V, and +1.45 V (vs. carbon fiber counter electrode) for 24 h. A different patch was used for all the experiments. Sample amounts of 1mL aliquots were taken at specified intervals. The receptor cell volume was 10mL and was replenished with fresh 1 mL aliquots of PBS after each sampling period. (-1.45 V r^2value from 0 h to 5 h = 0.951; 0V r^2 value from 0 h to 5 h = 0.750; +1.45 V r^2value from 0 h to 5 h = 0.750). The experiment was repeated three separate times and data sets are averaged with standard deviation error bars (N=3±SD).

Mathematical models were used to evaluate the kinetics and mechanism of drug release from the PEDOT nanotube transdermal drug delivery patch. The

model that best fits the data is selected based on the correlation coefficient (r), therefore the model that gives the highest "r" value is considered the best fit for the release data. Traditional mathematical models for TDDS include: 1) zero order release, 2) first order release, 3) Higuchi release model.

Simplified equations of the different mathematical models are provided as Equation 3.1a, b, and c. Q_0 is the initial amount of drug, Qt is the cumulative amount of drug, k is the release rate constant, and t is time in hours. In a zero order graph (Equation 3.1a), the cumulative percent of drug release is plotted against time. In a 1st order release model (Equation 3.1b), the drug release is dependent on the concentration and the log cumulative percent of drug release is plotted versus time. Finally, the Higuchi release model (Equation 3.1c), in which the cumulative prevent release is plotted against the square route of time, suggests that the drugs are released by diffusion.

(a) $$Q_t = Q_0 + k_t t$$

(b) $$Log\ Q_t = Log\ Q_0 + \frac{k_t}{2.303}$$ Equations 3.1

(c) $$Q = K_H t^{1/2}$$

After plotting the cumulative percent of drug release using Equation 3.1a, b, and c, it was determined that the PEDOT transdermal patch system most closely follow a zero order release in a simplified model. The *r*-values obtained from this model for the release data up to 5 h are 0.9451 and 0.9509 for amaranth and

Cy5.5, respectively, and 0.9218 and 0.9258 for up to 24 h (See Figure 3.13 and 3.14).

In a zero order release, the cumulative amount (Q_t, μg) of dye released from the patch was plotted as a function of time (t). The linear release rate, which is calculated as the slope in a zero order release, was represented as the constant (k). As seen in Figure 3.13 and 3.14 and Table 3.1, the average release rate constants (k_r) were approximately 3 times greater than the control (k_c). Over longer periods of delivery, the total amount of dye molecules released in experiments with an applied potential were up to 4 times greater than those without potential (0 V).

The release profile in Figure 3.13 and 3.14 suggests a bi-phase release system that includes two zero order releases. k_1 is referred to the release constant from 0 h to 5 h, while k_2 corresponds to 5h to 24 h. It is hypothesized that during the initial release, the dye molecules near the surface are exchanging with counter ions in the gel electrolyte. After the dye molecules diffuse through the gel electrolyte and into the counter electrode, it can penetrate through the skin at a much faster rate, thus k_2 is faster than k_1 in both experiments. In addition, the k_1 for the release, control, and preventative experiments show similar trends, however at zero and positive potential, the k_2 slows down to almost 0. This trend supports the fact that applying a potential may accelerates this exchange process and forcefully expel the dye molecules from the patch. This observation demonstrates the ability of the patch to deliver drugs at a fast and controllable rate not only in short bursts of time but also over longer periods. This ability

efficiently utilizes the loaded drugs and is essential to maintaining their bioavailability. Although these are promising results, further research is warranted to optimize for a wide range of drugs molecules with various properties.

Release dye and method	Potential (V)	k, Release Constant	k_r/k_c	C_r/C_c
Ex vivo release Amaranth through porcine skin	-1.2 V	2067.2 μg $cm^{-2}hr^{-1}$	1.79	3.0
Ex vivo release Amaranth through porcine skin	0 V (control)	1155.2 μg $cm^{-2}hr^{-1}$		
Ex vivo release Amaranth through porcine skin	+1.2 V	301.4 $cm^{-2}hr^{-1}$		
Ex vivo release Cy5.5 through porcine skin	- 1.45 V	3610.0 μg $cm^{-2}hr^{-1}$	2.76	3.96
Ex vivo release Cy5.5 through porcine skin	0 V (control)	1307.2 μg $cm^{-2}hr^{-1}$		
Ex vivo release Cy5.5 through porcine skin	+1.45 V	1194.5 μg $cm^{-2}hr^{-1}$		

Table 3.1 Comparison of linear release rate constants (k_r) of PEDOT nanotube patches with corresponding applied potential and control experiments. The ratios between the release constant and control constant are given. k_r is under the assumption that there is only release rate. The ratio between the cumulative % release of dyes for the release and control experiments are also given (C_r/C_c).

3.3.3. *In vivo* analysis

3.3.3.1. Live fluorescence optical imaging

Molecular imaging is a newly emerging and rapidly developing imaging field that can transform internal biological and physiological change at a cellular and molecular level into a visual and measureable macroscopic change.[111-114] Optical molecular imaging utilizes optical probes to track and report biological

changes. Unlike conventional imaging techniques such as X-ray computed tomography (CT) and magnetic resonance imaging (MRI), small animal optical imaging is non-radiative and has a high cost-effectiveness.[112, 114-117] Unlike fluorescence microscopy, *in vivo* fluorescence imaging detects bulk signals from thousands of cells at a much higher resolution. The photons detected from this imaging experiment are generated from the fluorescent dye molecule Cyanine (Cy5.5) which emits in the NIR region, where photons can travel several centimeters through tissue with limited biological absorption. Despite the low absorption in the electromagnetic spectrum, a very small quantity of photons arrives at the surface of the animal therefore a high sensitivity detector, such as cooled charged-coupled device (CCD) camera and photomultiplier tube (PMT) are used. The mouse was placed in a dark imaging chamber to prevent interference from ambient light. To maintain normal physiological functioning, the mouse is kept under anesthesia on a thermostat platform.

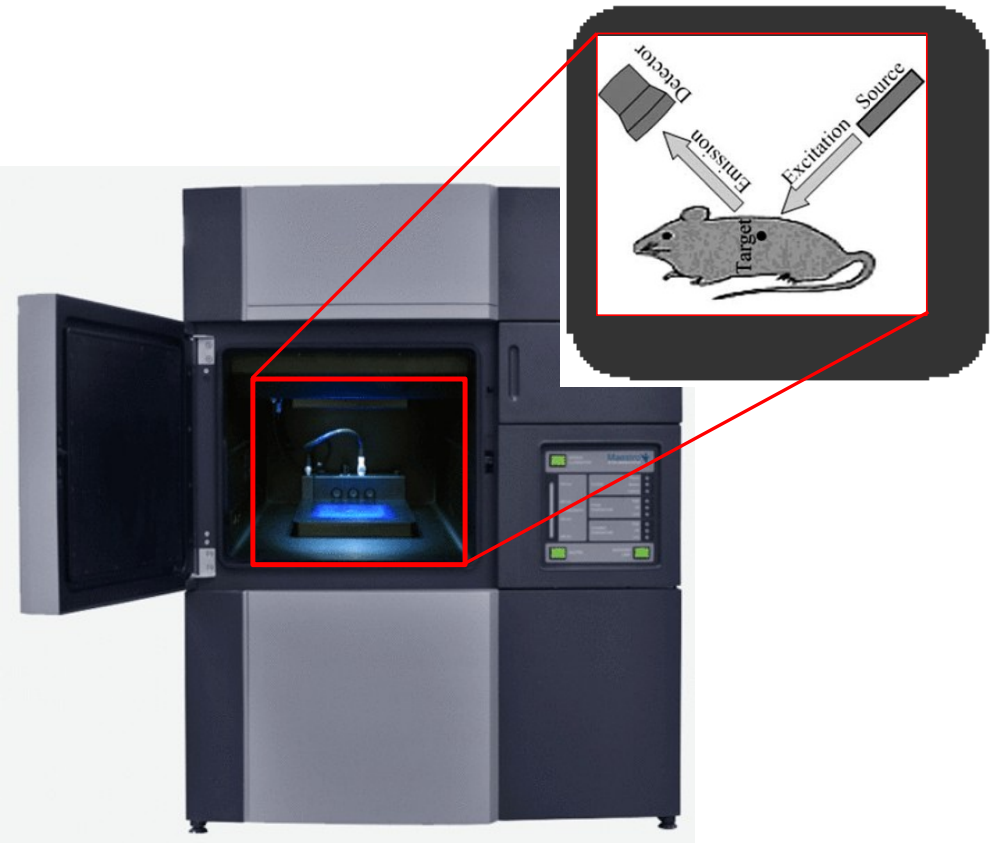

Figure 3.15 Image of Maestro^{TM} 2.0 and scheme of fluorescence imaging.

To evaluate the possibility of *in vivo* TDD, live whole-body fluorescence imaging of mice was explored. The permeability and efficacy of fast and controlled drug delivery of Cy5.5 through the skin of nude mice was investigated. The patch was placed on the chest of the mouse and a constant potential was applied for 1 h. with optical fluorescence measurements taken every 15 min (Figure 3.16a, b). Live imaging results within 15 min show the percentage of release was 40% greater than in the control. A fluorescence intensity of 3989 ($x10^6$ photon count $cm^{-2}s^{-1}$) was recorded in the first 15 min, compared to just 2411 in the control mouse (0 V). To demonstrate the patch stability and steady release, a constant potential was applied over two hours with fluorescence images

recorded at 0 h, 1 h, and 2 h. Our data confirmed steady release with minimal delivery fluctuations over 2h where the fluorescence intensity averaged 3200 ($x10^6$ photon count $cm^{-2}s^{-1}$).

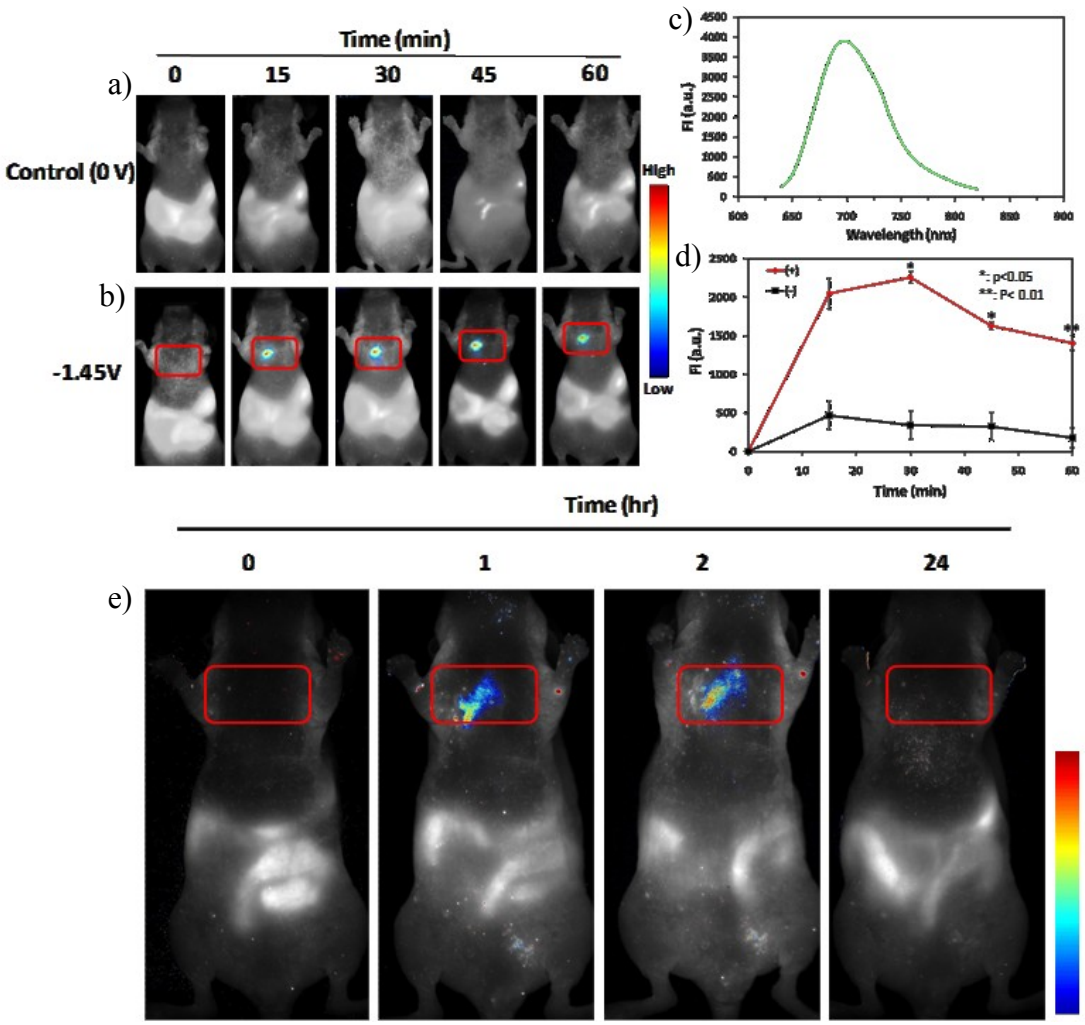

Figure 3.16 Live optical imaging of mice. Fluorescence imaging of Cy 5.5 delivery through the skin a) at 0 V and b) -1.45 V from 0 to 60 min was applied for control measurements. c) Fluorescence signals from the Maestro and d) multiple areas of the mouse were recorded. Fluorescence imaging of Cy5.5 delivery through the skin at e) 0, 1 and 2 h. The 24 h image was obtained 24 h after the patch was removed. The photoluminescence signal is easily distinguished from endogenous autofluorescence without any imaging process

since the patch was placed in a non-fluorescent area. All images used an exposure time of 100ms.

The patch was removed after 2 h and the mouse was imaged again 24 h after the removal of the patch (Figure 3.16e). This was performed in order to determine whether the dye molecules penetrated the skin and reached the dermis for systemic delivery. It was speculated that no visible fluorescence intensity after 24 h would mean the dye molecules reached the dermis and had circulated throughout the body. However, no visible fluorescence could also indicate that the dye molecules degraded over the 24 h or that they only diffused through the epidermis and not reach the dermis. The data obtained from surface fluorescence imaging was not adequate enough to inconclusively determine the transdermal delivery of the dye molecules therefore the use of two photo microscopy was explored.

3.3.3.2. *In vivo* microscopy imaging

Two-photon excitation microscopy is a fluorescence technique that provides imaging of living tissues up to about 1 mm. Two photon microscopy was pioneered by Winfriend Denk at Cornell University when he combined two-photon absorption with a laser scanner.[118] The main theory behind two photon microscopy is the simultaneous absorption of two photons. The two excitation photons have an energy much lower than the amount required to excite a fluorophore in one quantum event. The emission photon following the two

photon absorption is typically higher than any of the two excitation photons individually. The two-photon molecular excitation is possible through a very high local instantaneous intensity provided by the focusing of an laser scanning microscope combined with a femtosecond pulse laser.[119-121] The probability of near-simultaneous absorption of two photons is very rare therefore a Ti-sapphire laser is normally used. The laser has a pulse width of ~100 fs and repetition rate of 80 Hz, necessary for providing a photon density and flux required to achieve two-photon absorption. Due to two-photon absorption during excitation, the probability of fluorescent emission increases quadratically with excitation intensity so that fluorescence and photo bleaching are confined to the focal plan area.

Fluorophores commonly used in two-photon microscopy have excitation spectra in the visible electromagnetic range, while the excitation laser lies in the NIR to IR. The use of NIR light to excite fluorophores carry the same advantages as stated in section 3.3.3.1. Longer wavelengths scatter less than shorter resulting in higher resolution images. In addition, longer wavelengths can penetrate tissues more easily and cause less damage than shorter ones.[122]

In vivo delivery of dyes and spatial pattern of transdermal penetration were studied within the tissue of 6-8 week old male C57B6/L mice at high resolution with a custom-built two-photon microscope. FITC was loaded into the PEDOT nanotube patch and delivered through the skin at -1.45V for 30 minutes. Baseline images of the skin prior to drug delivery were obtained (Figure 3.17a and b) and 0 V was applied to the control set up throughout the experiment (Figure 3.17c and

d). Fluorescence images were taken every 10 minutes for 30 minutes (Figure 3.17e and f). Images for a 3D stacking profile were obtained every 10 µm for up to 60 µm below the surface of the skin. As seen in Figure 3.17e and f, no detectable fluorescence signal was present at 0 V. However, when the potential was applied, dye distribution was clearly observed in both the epidermal and dermal tissue, indicating the penetration of the dye across the dermal-epidermal barrier. The dyes show non-uniform spatial pattern, which could be attributed to the heterogeneous lipid distribution in the skin. In Figure 3.17e and f it is evident that higher concentrations of FITC were found in the dermis, a result of the hydrophobicity of the epidermis. It is hypothesized that the migration of FITC into the dermis may result from the hydrophilicity of the molecule in conjunction with the electric field provided from the applied potential forcing FITC deeper into the skin.

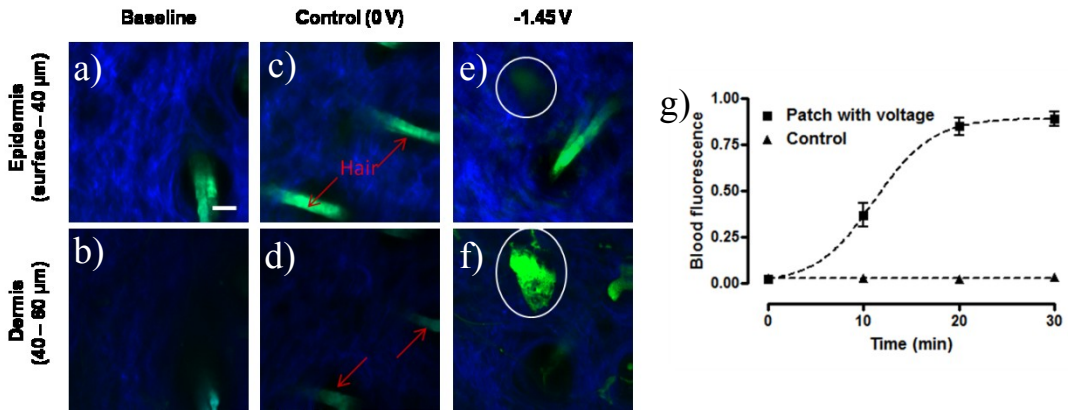

Figure 3.17 (a-f) *In vivo* two-photon fluorescence imaging. Analysis of the skin of B6 mice in response to the treatment with the FITC loaded PEDOT nanotube patch. 3D stacking of fluorescence images of FITC delivered to the epidermis (0–40 µm) and dermis (40–60 µm) (a, b) prior to attaching the patch, (c, d) at 0V, and

(e, f) at -1.45V. Autofluorescence of mouse hair are labeled (red arrows). FITC fluorescence (circled) is observed after 30 minutes of delivery in the e) epidermis and f) dermis with the voltage-applied, but not in the control. Scale bar is 20 μm. g) FITC fluorescence from blood samples taken from the mouse every 10 minutes for 30 minutes. Saturation of dye within the blood was recorded after 20 minutes.

Finally, blood samples were collected from the mouse every 10 minutes for 30 minutes (Figure 3.17) to demonstrate the ability of the nanotube patch to deliver drug molecules to the blood stream. Blood samples were obtained from the tail vein of the mouse. The samples were placed on a glass slide and the photon count was used to detect the fluorescence intensity in the blood. Within 10 minutes, the presence of FITC in the blood is clearly detectable, compared to the control where no detectable fluorescence intensity was found (Figure 6g, triangles). After about 20 minutes, the dye concentration in the blood stabilized to a constant level. This clearly demonstrates the ability of the patch to deliver drugs to the blood circulation in a fast and controlled manner.

Table 3.2 shows the comparison between the delivery mechanism and the time it took the delivered molecules to reach a steady state in the blood stream. Although the saturation time is dependent on the type of molecule, the times listed below are within range of the normal averages of *in vivo* delivery. The PEDOT patch demonstrates a delivery time comparable to oral dosage however, as address in Chapter 1, the required amount to reach a therapeutic concentration in the blood for oral delivery is much larger than for transdermal delivery.

Type of delivery	Potential (V)	Time	Release molecule
Chemical enhancers[123]	0	1 to 5 h	Hydrophobic and hydrophilic
Iontophoresis[124]	0.15 mA/cm^2	1 h	Hydrophilic
Oral[125]	0	20 min	Hydrophilic
Electrophoresis[126]	100 – 500 V	30 min	Hydrophilic
Microneedles[127]	0 V	2 h	Hydrophobic
PEDOT nanotube patch	1.2 – 1.45 V	20 min	Hydrophilic

Table 3.2 Comparison of different drug delivery mechanisms with the PEDOT nanotube transdermal patch system.

3.3.4. Conclusion

Overall, this study demonstrated that a nanotube patch delivery system can provide a fast, controlled and stable method of loading and delivering drugs *in vivo*. About 88% and 70% more of the model dye molecules were released with an applied potential compared to the control. The release of the model dyes was shown to be controlled by the strength of the applied potential. Live fluorescence imaging during transdermal delivery with nude mice demonstrated stable and steady release for up to two hours. *In vivo* two photon microscopy showed the ability of the PEDOT nanotube patch to deliver drugs through the epidermis and into the highly vascular dermis. Finally, blood samples confirmed the presence of dye molecules in the blood stream just after 10 minutes, with delivery saturation being achieved after 20 minutes.

Chapter 4: Functionalization of conductive polymers

This chapter has been reproduced in part with permission from: Nguyen, T.M., Cho, S., Varongchayakul N., Yoon, D., Zong, K., Seog J., and Lee, S.B. Electrochemical synthesis and modification of PMProDot nanotubes and their enhanced electrochemical properties. *Chem. Commun.,* 48, 2725-2727 (2012).

4.1 Introduction

Conductive polymer nanotubes have been of high interest in many fields of science because of their intrinsic electronic and physical properties, chemical stability, and significant potential in nano-sized electronic and electrochemical devices.[127-130] Moreover, CPs are inexpensive with an extensive range of applications. The ease in synthesis and versatility has created a large focus on the functionalization of conductive polymers. Such modifications can be used to generate both physical and chemical changes which can be applicable to biomedical applications. Multiple methods of functionalization will be focused in this chapter: 1) surface functionalization, 2) pre- polymerization, 3) post-polymerization, and 4) co-polymerization.[131-134]

4.1.1 Surface functionalization

Surface modifications of CP through the incorporation of biomolecules can lead to changes to the chemical and physical properties of the polymer. Changes to the chemical properties of CPs have occurred through the doping of biomolecules or the immobilization of bioactive polymers on the surface of the materials.[135] The use of different biomolecules has allowed biomedical researchers to utilize CP in

biological sensing, and turning on and off different cellular signaling pathways for several cellular processes. In some cases, the dopant can be used as a "tether" for further modification. For example, Song et al. doped PPy with poly(glutamic acid) which provides a carboxylic acid group available for further covalent linking to any amino group through carbodiimide chemistry.[136] George et al., previous mentioned in Chapter 1, utilized the biotin-streptavadin coupling to attach and release nerve growth factor (NGF) from PPy.[137]

Electrochemical properties of CP can be varied by changing the dopant concentration. Conductivities can vary as much as 15 orders of magnitude.[138] The choice of dopant corresponds to the desired application, but a major drawback to using a dopant is the possible diffusion of the dopant into the medium resulting in cytotoxicity and deterioration of the properties of the CP itself. For example, the uptake of positive ions from polyanionic dopants (e.g. poly(styrenesulfonate) (PSS)), has been found to affect protein adsorption and the cell cycle.[139] Although the range of possible dopants is endless as long as the selected molecule is charged, covalent methods are necessary for more permanent functionalization.

4.1.2 Pre-functionalization

The addition of the functional group to the monomer followed by electropolymerization represents the most straightforward and popular method of synthesizing functionalized CPs. Despite this useful strategy, the success depends on the compatibility of the functional group to the polymerization process. The synthesis of the monomer derivative often involves multiple steps using harsh

chemicals, which results in limited product yields. In addition, this approach often fails as the functional groups results in redox interferences.[140] To overcome these issues, some groups have focused on synthesizing monomer units that have the potential to be derivatized before or after polymerization.[141]

Chemical modifications to monomeric building blocks allow for structural control and tailoring of properties. Unfortunately, this strategy can fail due to steric demands or electronic instability of functional group inhibiting polymerization. On a practical level neither attachment of valuable nor sensitive groups to monomer units is efficient or cost effective.

4.1.3 Post-functionalization

Post- functionalization was introduced in the mid 1980s to circumvent the limitations of pre-functionalization. In post-functionalization, the polymer is modified after polymerization. Electrophilic substitution is a straightforward way to functionalize polyaniline (PANI).[142] However, sulfonation of PANI uses toxic and corrosive reactants, is highly sensitive to reaction conditions, and results in chain scission by hydrolysis. Alternative synthetic approaches, such as nucleophilic substitutions, have been pursued.

Despite some success, this approach is limited by chain stiffness and inter-chain interactions causing physical and electrostatic cross linking and branching. More importantly, the functional groups may disrupt the planarity of the conjugated system, which decreases the conductivity.

4.1.4 Co-polymerization (Chemical-grafting)

An alternative to the pre- and post-functionalization is to synthesize a reactive conductive polymer, and then attach the desired functional groups through chemical grafting. Copolymerization provides an additional variable by which the properties of the polymers can be tuned. Polymer systems containing reactive amino, carboxyl, or reactive esters have been developed and employed for this process.[141-145] It is highly desirable to develop polymers which allow for post-functionalization under mild and selective conditions without generating unnecessary byproducts.

The recent development of Click chemistry, especially one of the most popular, copper (I) catalyzed Huisgen reaction between azide and terminal alkyne, has provided a promising method for preparing functional polymers.[146] Ideally, Click reactions can be performed in water or organic solvents at room temperature. In polymer chemistry, it has been used for end-group functionalization, polymer-to-polymer coupling, and functionalization of linear polymers with selected groups, dendrons, and PEG.[147-151]

All the functionalization methods mentioned above provide multiple avenues to obtain finely tuned electronic and electrochemical properties for CPs. This versatility makes CPs an ideal candidate for a universal drug delivery system with the ability to deliver both imaging and drug moieties.

4.2. Materials and Methods

4.2.1 Chemical and materials

3,4-(2-methylene)propylenedioxythiophene (MProDot, provided from Zong lab at Chonbuk National University, 3,4-ethylenedioxythiophene (EDOT, Sigma Aldrich), acetonitrile (Fisher Scientific), and lithium perchlorate ($LiClO_4$, Acros) were used to synthesized PMProDot and PEDOT nanotubes within gold sputtered anodic aluminum oxide (AAO) (200 nm diameter, 60 μm thickness, Whatman) and polycarbonate membrane (PC, 220 nm diameter, GE Osmonics) with Pt foil (99.99%, Alfa Aesar) as the counter and Ag/AgCl as the reference electrode. Styrene (Sigma-Aldrich) and 9-vinylcarbazole (Sigma-Aldrich) were used for co-polymerization with PMProDot. Dopamine hydrochloride (Sigma-Aldrich), Tris (pH 8.5) (Agros), and methanol (VWR) was used to functionalize PEDOT. Millipore water was obtained by a Milli-Q A10 system.

4.2.2 Template synthesis of PMProDot nanotubes

The synthesis of MProDot was previous achieved and published by Yoon et al. from Chonbuk National University in South Korea (Figure 4.1).[152] Briefly, the reaction mixture of diethyl 3,4-dihydroxythiophene-2,5-dicarboxylate (2.0 g, 7.69 mmol) **1**, 3-chloro-2-chloromethyl-2-propene (0.96 g, 7.69 mmol) **2**, and K_2CO_3 (3.2 g, 23.1 mmol) in dimethylformamide (DMF, 80 mL) was reacted for 12 hours at 130 ^oC. The reaction mixture was cooled to room temperature and poured into ice-water. The precipitate was collected through filtration and the

recrystallization in hot methanol gave **3** in a 70 % yield. The compound **3** was subjected to hydrolysis in a 3 M NaOH solution at 70 ^{o}C for 3 hours and acidified with conc. HCl to pH = 1 to give **4** in a 95 % yield. Decarboxylation of **4** in the presence of copper chromite (0.2 g, catalyst) at 155 ^{o}C for 15 hours gave MProDOT **5** in a 55% isolated yield after column chromatography on silica gel.

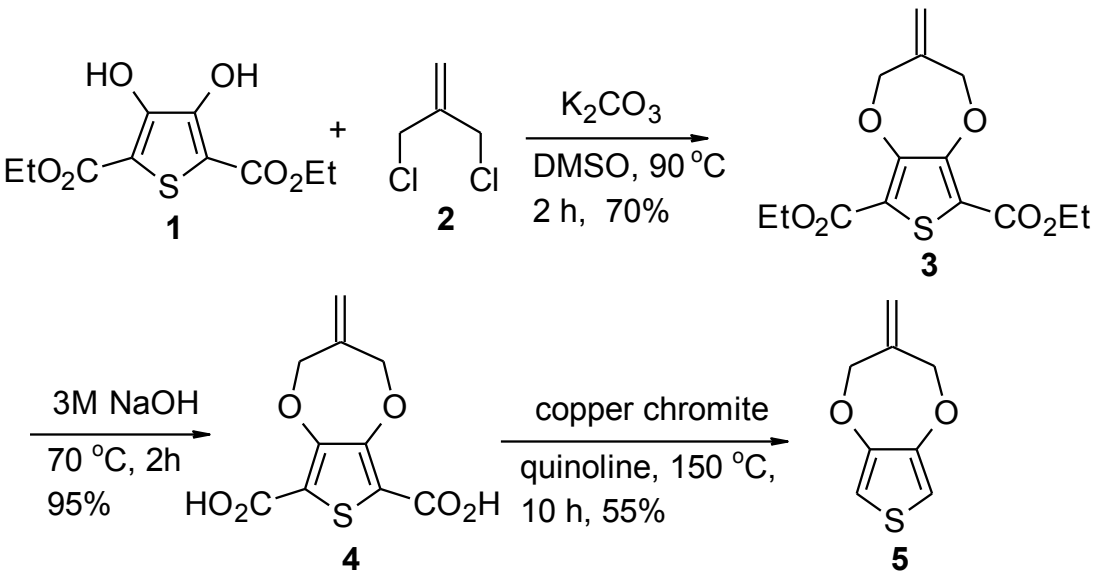

Figure 4.1 Synthetic route for MProDot.[152]

PMProDot were electrochemically synthesized in commercial AAO membranes and PC membranes. PMProDot were grown in AAO for electron microscopy due to the ease in sample preparation. PC membrane was used for electrochromic studies due to its transparency. A Denton Vacuum Desktop III was used to sputter a thin layer of gold as the working electrode (ca. 100 nm thick) on one side of the membrane template. Copper tape (3M) was attached to the gold to provide contact on the working electrode. The three electrode cell set

up is illustrated in Figure 2.2. An electroactive window with a 60% porosity consideration (1.26 cm^2) was defined by using acid resistant tape. The entire cell is placed in a 50 mM solution of MProDot in 100 mM $LiClO_4$ in acetonitrile. A potential of 1.3V is applied to the system until the charge reached 200 mC. All electrode potentials were measured relative to a Ag/AgCl reference electrode using Pt foil as a counter electrode, if not specified otherwise. The deposited mass of PMProDot nanotubes was controlled by fixing the total charge passed during electropolymerization. The wall thicknesses of the nanotubes were controlled by fixing the potential time. During polymerization, the electrode window color changed from white to dark blue.

Electrochemical synthesis of PEDOT was performed as described in section 2.2.2.

4.2.3 Functionalization of PMProDot and PEDOT nanotubes

Template embedded PMProDot nanotubes were placed in a solution of polystyrene (PS) or polyvinylcarbazole (PVK) for copolymerization. The copolymerization of polystyrene (PS) was achieved as published by Zong et al. by scanning the potential between -0.6 to +1.5 V at 10 mV/s in 600 mM styrene in 100 mM $LiClO_4$ in acetonitrile solution.[152] The copolymerization of PMProDot with PVK was achieved by applying a potential of 0.75 V in 600 mM PVC in 100 mM $LiClO_4$ in acetonitrile.

PEDOT nanotubes also remained embedded in the AAO template during post-functionalization. The template was immersed in a solution of 2 mg of

dopamine per milliliter of 10 mM, Tris pH 8.5 in methanol. A dopamine film thickness of 50 nm is achieved after 24 h as published by Lee et al.[171] The PEDOT nanotubes were immersed in the dopamine solution for approximately 5 h. The thickness of the polydopamine layer on top of PEDOT was approximately 10 nm of polydopamine.

4.2.4 Characterization of PMProDot nanotubes

The PMProDot nanostructures were investigated using a field-emission scanning electron microscope (SEM; Hitachi S-4700, operated at an acceleration voltage of 5 keV) and transmission electron microscope (TEM; Zeiss EM10CA, operated at 80 keV). TEM and SEM sampling method were previous described in detail (Section 2.2.4). Briefly, the template was dissolved in 3 M NaOH for 15 min to expose the PMProDot nanotubes. After rinsing them with de-ionized water repeatedly, the samples were dispersed in ethanol and sonicated. The nanotubes precipitated to the bottom of the microvial. For SEM sampling, 6 μL of the nanotube solution were dropped on carbon tape and dried in air before observation. For TEM sampling, 6 μL of the nanomaterial solution was dropped and dried on a TEM grid.

Electron microscopic sampling and characterization of PEDOT nanotubes are as presented in Section 2.2.4.

For spectroscopic characterization of PMProDot, all polymers were polymerized on an ITO surface of 1 cm^2. ITO was placed in a solution of 50 mM solution of MProDot in 100 mM $LiClO_4$ in acetonitrile. A potential of 1.3V is

applied to the MProDot solution until the charge reached 200 mC. If the total charged passed was greater than 200 mC there is a higher probability of having a nanowire/nanotube hybrid instead of only nanotubes. During electrochemical polymerization, the ITO surface changed from transparent to dark blue. The polymerization of PVK for spectroscopic studies was performed in a similar manner. ITO (1 cm^2) was immersed in 600 mM vinylcarbazole solution and a potential of 1.7 V was applied until the charge reached 200 mC. During polymerization of PVK, the ITO surface changed from transparent to dark green. The polymer samples remained on the ITO surface for UV-Vis spectroscopy characterization. For IR spectroscopy studies, the polymer samples were scraped off the ITO for analysis.

The mechanical properties of PMProDot and PVK-modified PMProDot film were tested by Atomic Force Microscopy nanoindentation technique. The PMProDot film was prepared as above. PVK was grafted on the PMProDot film by applying a potential of 0.75V. The force vs. indentation curves were obtained using an AFM (MFP-3D AFM, Asylum Research) at 1 Hz rate. The silicon tip, CSR-10, (VISTA Probes, nanoScience Instruments) with spring constant of 34.53 nN/nm was used to indent the film locally. Inverse optical lever sensitivity (87.56 nm/V) was obtained using ITO substrate which was incompressible within the tested force range.

Electrochromic responses were measured by applying a switching potential of -1.0 V and +1.0 V with a potentiostat (CH instrument 660 A) (Figure 4.2). The response times of PMProDot film were investigated on ITO and

nanotubes were investigated in PC membrane. The color-switching rate of the electrochromic device was measured using a reflectance measurement system (Ocean Optics Inc.), composed of a 600 nm laser (LS-1), a standard reflection probe (R400-7), and a holder (R PH-1). The reflected light was detected with a photomultiplier tube (PMT) and analyzed using an oscilloscope (Tektronics, TDS1012).

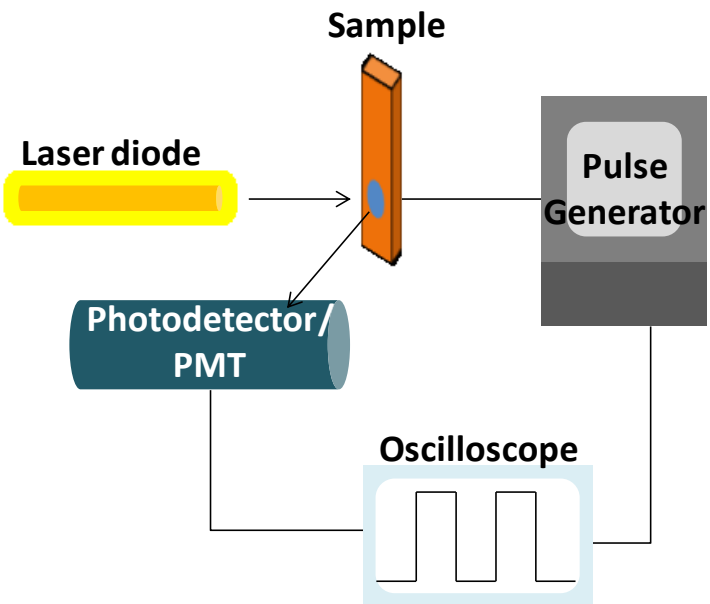

Scheme 4.1 Block diagram schematic of the setup used for measuring electrochromic the response time.

4.3. Results and discussion

In this section, the characterization of PMProDot co-polymerized with PS and PVK is thoroughly addressed. Zong et al. had previous reported extensive studies on the co-polymerization of PS on PMProDot films therefore this section will concentrate primarily on the co-polymerization of another vinyl monomer, PVK, on PMProDot film and nanotubes.

This section will also address the functionalization of PEDOT with polydopamine via post- functionalization. The functionalization of PEDOT with the versatile polydopamine will provide the possibility of exploring for a universal transdermal drug delivery system.

4.3.1. Characterization of functionalized PMProDot

Figure 4.2 shows TEM and SEM images of PMProDot nanotubes prepared in a similar manner as PEDOT nanotubes. It is hypothesized that the gold sputtered on the bottom of the AAO and PC membranes form a ring-shaped electrode that can define the tubular shape of most conductive polymer nanotubes synthesized electrochemically. Controlling the amount of charge per unit area during electropolymerization regulates the amount of PMProDot loaded in the pores of the template. Figure 4.2 b shows the SEM image of PMProDot nanotubes following the removal of the membrane template. Without the template to support the nanotubes, the structures collapse and aggregate from the strong surface tension generated at the interface of the nanotubes and solvent during evaporation. Although the top of the nanotubes are aggregated, the open porous structure of the nanotubes remains evident.

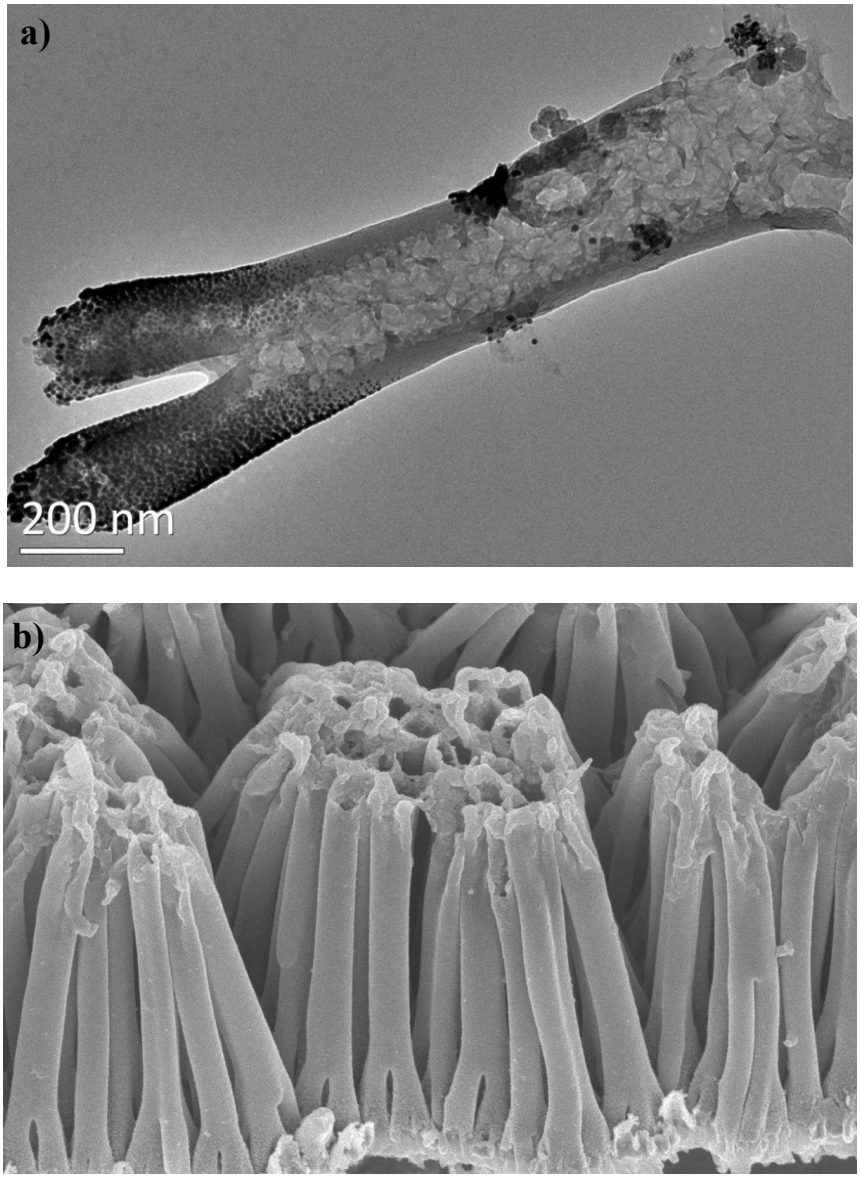

Figure 4.2 a) TEM and b) SEM images of PMProDot nanotubes prepared in AAO membrane with 200 nm pore diameter at 1.3V in 50 mM solution.

The following sections include characterization PMProDot nanotubes functionalized via one-step modification with PS and PVK. The accelerated copolymerization to PMProDot was achieved through the highly reactive methylene group on MProDot. Zong et al. had previous published the accelerated

co-polymerization of PS on PMProDot films. The methylene group was the chosen point of functionalization due to the versatility of vinyl groups. It has been demonstrated that the methylene groups on MProDot does not polymerize at potential of 1.3 V or less. Therefore the intact methylene group is available for electrochemical grafting with other vinyl monomers following polymerization of MProDot.

4.3.1.1 Quartz crystal microbalance

Quartz crystal microbalance (QCM) analysis was utilized to investigate the accelerated copolymerization of PVK on PMProDot. The electrochemical polymerization of PVK was achieved at a +1.7 V however the polymerization potential decreased significantly to 0.75 V in the presence of PMProDot. Figure 4.3 displays a plot of change in mass versus time for the electrochemical polymerization of vinylcarbazole on bare gold working electrode and on PMProDot surface at 0.75 V. During the electrochemical polymerization of vinylcarbazole at 0.75 V, a negative mass change was observed even though there was a very small mass increase initially recorded. This was caused by desorption of vinylcarbazole off the electrode surface which is normally observed at a lower positive potential than the polymerization potential.[154] In contrast, a mass increase was observed on the PMProDot electrode surface at the same potential. This represents the accelerated polymerization of vinylcarbazole and confirms the facile coupling ability of the methylene group on PMProDot.

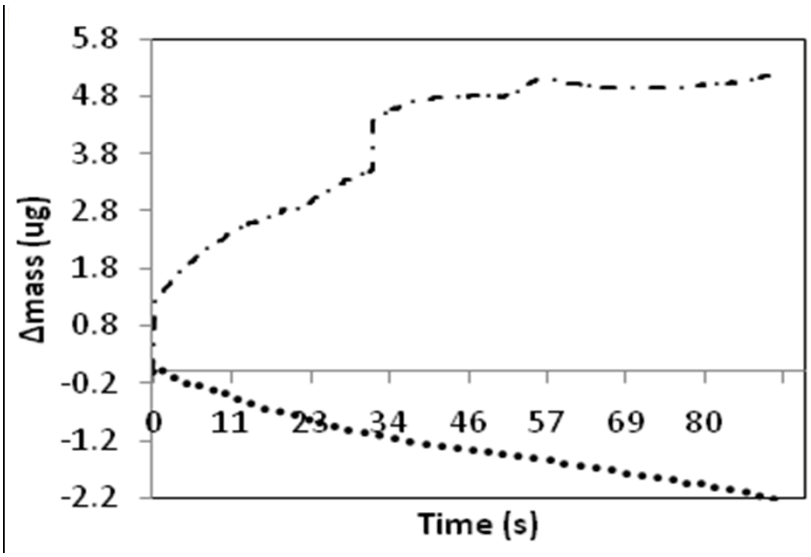

Figure 4.3 Plot of QCM mass change (polycarbonate/quartz crystal) vs. time of electrochemical deposition of PVK on planar electrode (dotted) and on PMProDot surface (dashed) at 0.750 V.

4.3.1.2 Spectroscopy

The IR spectrum of the PMProDot nanotubes shows a C=C stretching band of thiophene ring at 1486 cm^{-1}, a C—S stretching at 853 cm^{-1}, and a C—O bending band at 934 cm^{-1} (Figure 4.4a). The IR spectrum of PVK shows the C-H aromatic stretching at 3100cm^{-1}, characteristic ring vibration band at 1452 cm^{-1}, C-H deformation of vinylidene 1329 cm^{-1}, and C-H plane deformation of aromatic ring at 1220 cm^{-1}, respectively.[155, 156] IR analysis of the composite of PVK with PMProDot shows combinations of IR bands from individual polymers (Figure 4.4c). Zong et al. previously published the characteristic peak from sp^2 C—H of PS at 3020-3050 cm^{-1} for the FTIR spectrum of PS-treated PMProDot (Figure 4.4 d).[152]

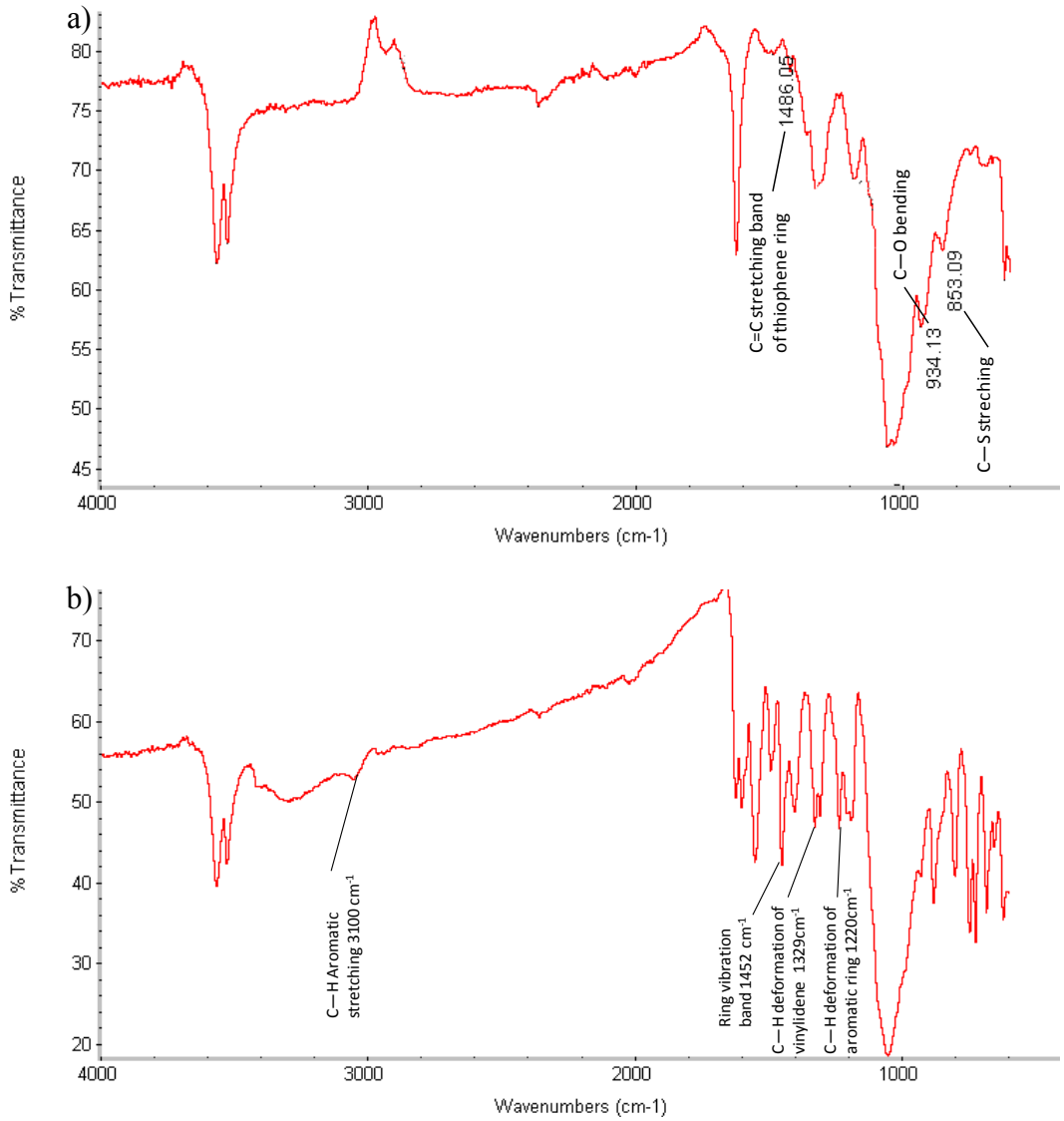
a)
% Transmittance
80
75
70
65
60
55
50
45
4000
3000
2000
1000
Wavenumbers (cm-1)
C=C stretching band of thiophene ring
1486.05
C—O bending
934.13
853.09
C—S streching
b)
% Transmittance
70
60
50
40
30
20
4000
3000
2000
1000
Wavenumbers (cm-1)
C—H Aromatic stretching 3100 cm-1
Ring vibration band 1452 cm-1
C—H deformation of vinylidene 1329cm-1
C—H deformation of aromatic ring 1220cm-1

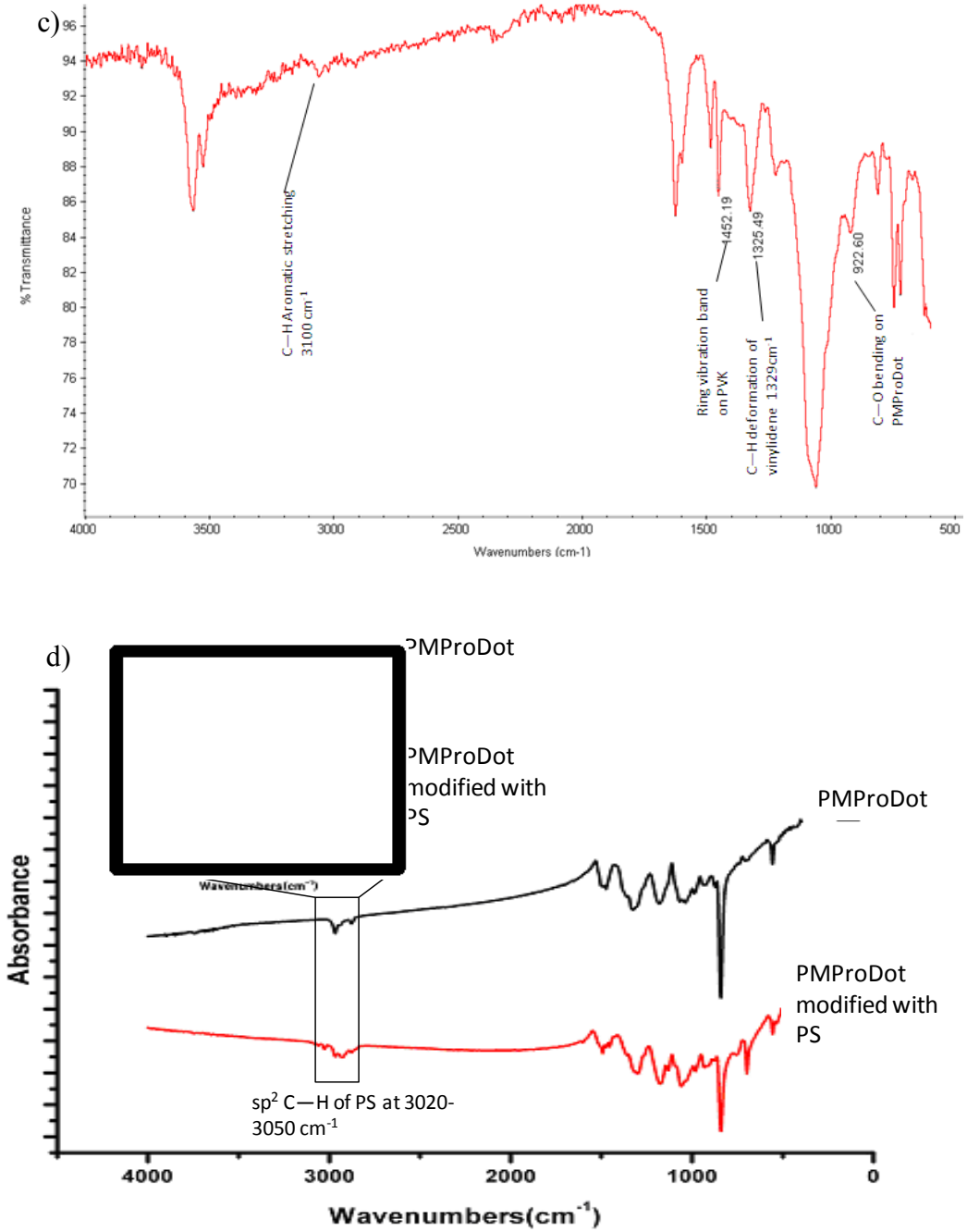

Figure 4.4 IR spectra of a) PMProDot, b) PVK, c) PMProDot modified with PVK, and d) PMProDot modified with PS, inset displays magnification at wave numbers 3020-3050cm^{-1}.[152]

Figure 4.5 shows the UV-Vis absorption spectra for oxidized PMProDot and PVK and PS copolymerized on PMProDot. The spectrum of oxidized PMProDot shows a strong absorption band at ca. 700 nm. The absorption band blue-shifted following the coupling of PS to ca. 470 nm and to ca. 350 nm as a result of the coupling with PVK. It should be noted that the absorption of the carbazole group extend up to 370 nm.[157] These absorbance shifts are due to the shortening of the chain length following the addition of substituents to the polymer backbone.[158, 159]

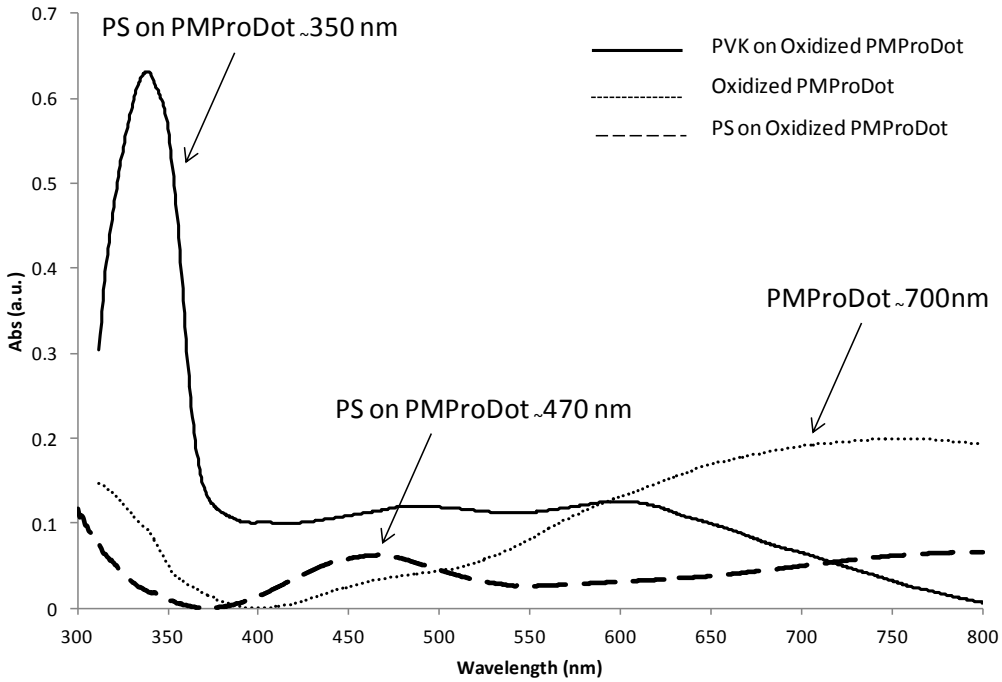

Figure 4.5 Absorbance spectra of oxidized PMProDot (dotted), oxidized PMProDot composed with PS (dash) and oxidized PMProDot composed with PVK (solid). All polymers were prepared on ITO. Blue shift following coupling of PS is expected due to the shortening of the chain length following addition of substituents to the polymer backbone.

4.3.1.3 Electrochromics

To easily assess the enhanced electrochemical properties of PMProDot following modification, the variation in electrochromic properties of PMProDot coupled with PS and PVK was investigated. The effect of electrochromism has been known for many years and it is based on the fact that certain materials change color depending on their redox state.[73, 160] The electrochromic behavior is due to an electron transfer reaction that takes place during the electrochemical oxidation and reduction of the polymer.

The evaluation of electrochromic properties of a polymer is an easy and visible method to detect changes in electrochemical properties. The speed in which the electron transfer occurs can be referred to as the "response time". The measurement of the response time provides information on the electrochemical changes to the conductive polymer. The strong coloration and color contrast between oxidized and reduced PMProDot is a visible assessment of the polymer's charging and discharging speed. The response time was investigated on 200 mC of PMProDot deposited as a film on ITO glass and as nanotubes in flexible PC membranes. As seen in Fig 4.6 a and b, PMProDot in full reduction and oxidation state shows a deep blue purple and transparent pale blue, respectively. There were no visible color changes following the modification with vinyl monomers. The color-switching response time was measured optically from reflectivity response at 600 nm wavelength as a function of time.

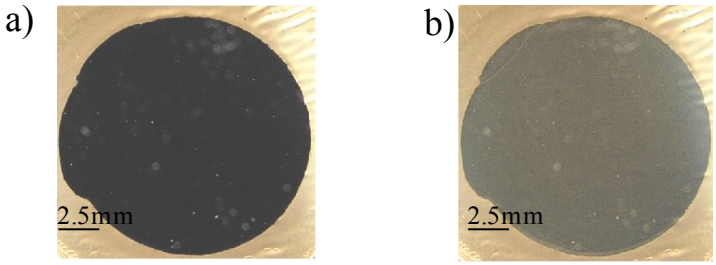

Figure 4.6 Electroactive window (scale bar is 2.5 mm) of full (a) reduction state and (b) oxidation of PMProDot.

Here, the response time is defined as the time required for the polymer to reach 90% of its full response. In general, it is the time that it takes ions to diffuse into the polymer film (i.e. reach saturation concentration in polymer film). The response time is obtained by measuring the time it takes for the polymer (and copolymer) to go from pale blue (100% reflectance) to dark blue (0% reflectance). The gold surface in the PC membrane acts as the working electrode. The reflectance is measured by shining the laser at the electrochemical window and measuring the intensity of the reflectance off the gold surface. The PMProDot is grown from the gold surface, therefore when PMProDot is pale blue, more light is reflected back and the reflectance is higher. When PMProDot is reduced and becomes dark blue, the polymer absorbs light from the laser therefore a lower reflectance is measured. The entire electrochemical cell is placed in 100mM lithium perchlorate in acetonitrile during electrochromic measurements. The color of the PMProDot and modified PMProDot range from pale blue (fully oxidized) to deep blue (fully reduced) when an alternating potential of 1.0 V and -1.0 V is applied. The speed in which the polymer becomes fully reduced or oxidized is

measured optically from the reflective response as a function of time at those applied potential. There have been multiple papers published by Lee et al. and others which thoroughly explain how the response time is measured and what it tells us about the electrochemical properties of the polymer.[69-72, 162]

In order to ensure ion saturation to measure 100% reflectance (the plateau in Figure 4.7), the switching time measurements is varied each sample. However, despite the difference in the measurement time, the only important part is the time it takes the polymer to go from 0% reflectance to 90% reflectance (i.e. response time). This time does not change and is independent of how long the polymer is fully oxidized. The signature "rectangle" graph depicts one cycle of switching, from full reduction to full oxidation back to full reduction. The times obtained for Figure 4.9 is at the first moment the graph passes the 90% reflectance line (red circle in Figure 4.7), mostly achieved before 1 sec.

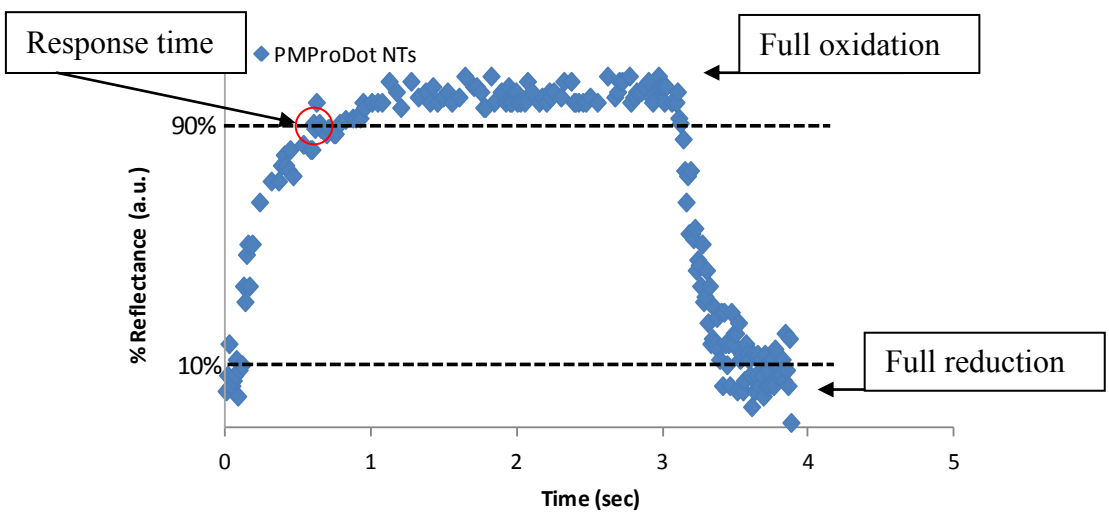

Figure 4.7 Labeled points of interests on an electrochromic graph of one redox cycle of PMProDot.

Figure 4.8 displays comparison of the response times of PMProDot on ITO, as bare nanotubes and modified with PS and PVK. As expected, the response time of 200 mC PMProDot film is more than twice as slow as the nanotube structure. The high surface area to volume ratio of the nanotube structure compared to thin film significantly decrease the diffusion time of counterions. The diffusion rate of the counter ions can further be improved with modification to PMProDot by reducing cross linking and branching associated with polymerization. The grafting of PS and PVK with PMProDot resulted in response times that were two times faster than unmodified PMProDot nanotubes. It is hypothesize that the decrease in response time is a result from the rigidity supplied by PS and PVK which can create ordered polymer chains allowing counterions to diffuse in and out of the interstitial spaces at a much faster rate. Further analysis on the rigidity of PMProDot following functionalization is addressed in the next section.

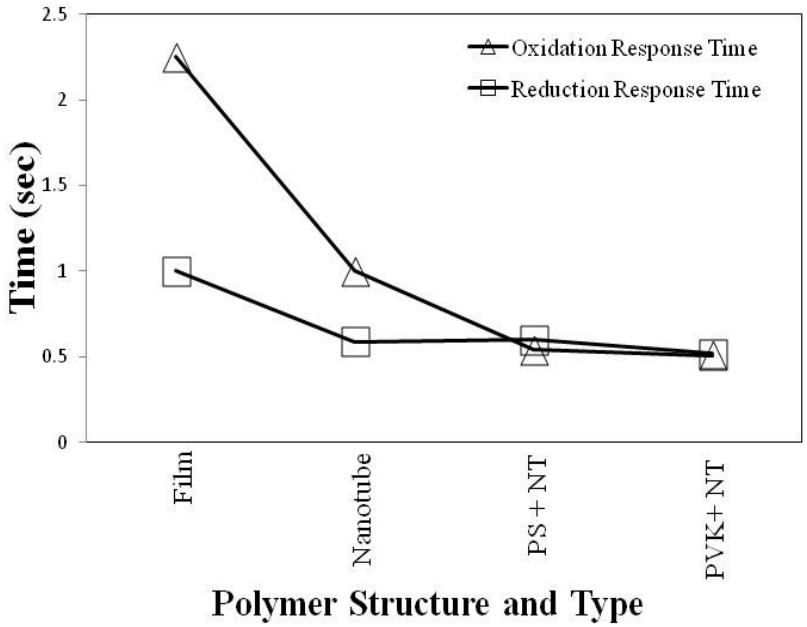

Figure 4.8 Response times of PMProDot film, PMProDot nanotube, and PMProDot co-polymerized with PS and PVK. The time resolution of the measurement was in microseconds. The polymer was cycled 100 times and the average response time was recorded.

Due to the faster response time of the polymer after copolymerization, the modification must be occurring throughout the bulk polymer rather than primarily on the surface. If copolymerization only occurred on the surface, the nanotubes wall thickness would increase causing the electrochromic response time to increase as well. Whereas this electrochromic study focused on two types of vinyl monomers, it seems feasible to replace them with many other types of vinyl monomers to fine tune the electrochemical properties of conductive polymer for other desired applications.

4.3.1.4. Atomic force microscopy

Scheme 4.2 shows a proposed schematic by Zong et al. following PMProDot copolymerization with PS, the schematic can generally be applied to the copolymerization with PVK as well. The retention of planarity of the polymer backbone with the addition of PS and PVK creates larger interstitial spacing which can allow counter ions to move easier and faster during the doping process. The rigidity, in this case, is defined as the stiffness of the polymer. A rigid polymer would not deform easily during redox cycles making the pathways for dopant ions less hindered resulting in faster response times.

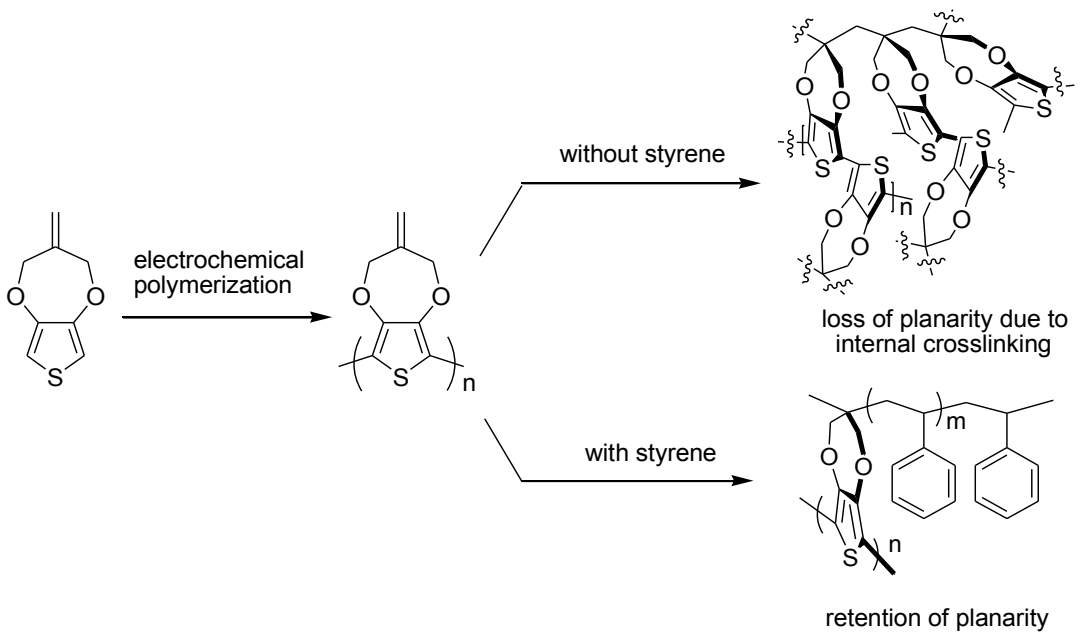

Scheme 4.2 Proposed schematic by Zong et al. of structures of PMProDot when methylene groups are involved in cross-linking or PST grafting.[152]

The increased rigidity hypothesis is supported by AFM measurements of the Young's modulus of PMProDot and PMProDot co-grafted with PVK (Figure

4.11). The elastic modulus of the polymer films were obtained using the method developed by Guo et al.[163] The force as a function of indentation is expressed in the following equation:

$$F^{2/3} = C + \left[\frac{4}{3}\frac{E \cdot R^{1/2}}{(1-\sigma^2)}\right]^{2/3} \cdot \Delta \qquad (4.1)$$

Where F is the loaded force, Δ is the indentation, R is the curvature of the tip, σ is the Poisson Ratio, E is the Young's modulus of the sample and C is the constant obtained from the fitting. Here, the nominal tip radius (20 nm) was used as specified by the manufacturer and the Poisson Ratio is approximated to be 0.3, which is a good estimate for conventional polymers. The force versus indentation profile near the contact point (Δ = 30 nm) is plotted and fitted with the above equation using Origin8 software (OriginLab, USA) (Figure 4.9a, b). In this small indentation region, the material is assumed to behave elastic without adhesion.

(a)

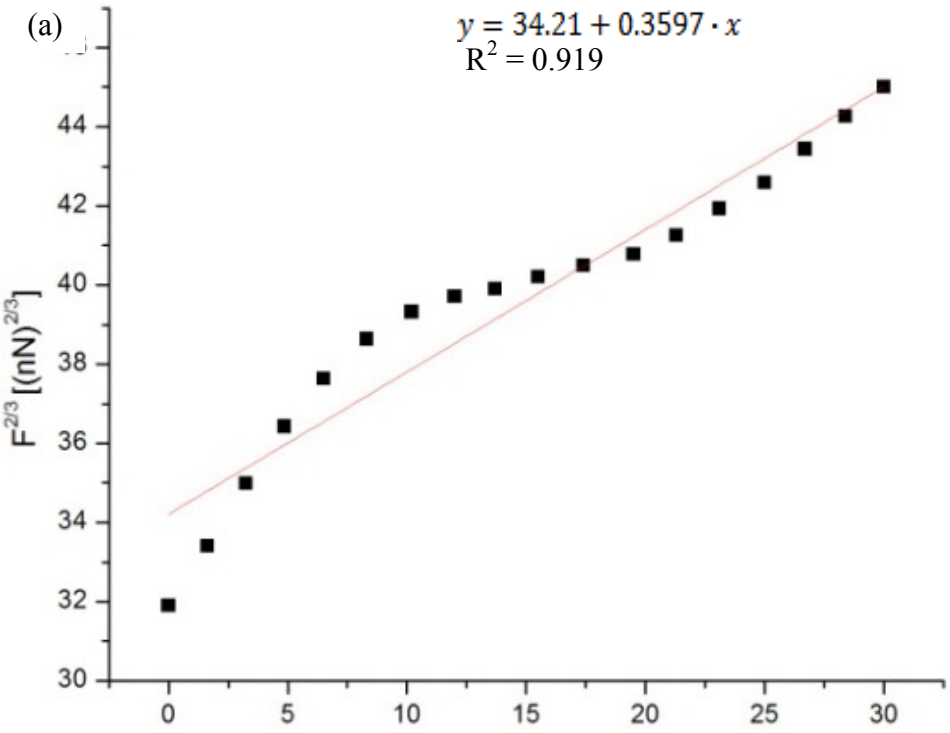

Separation Distance (nm)

(b)

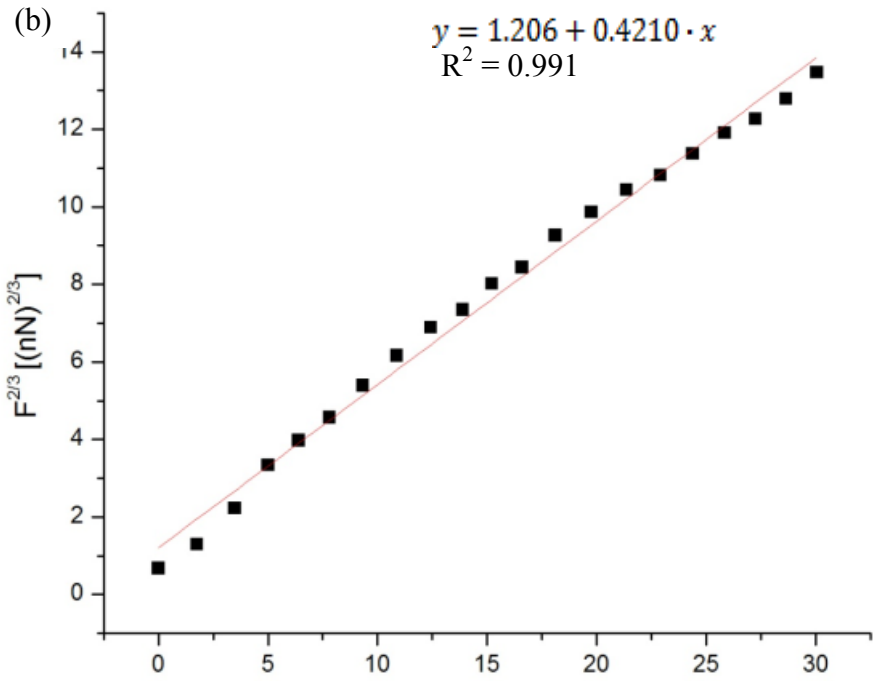

Separation Distance (nm)

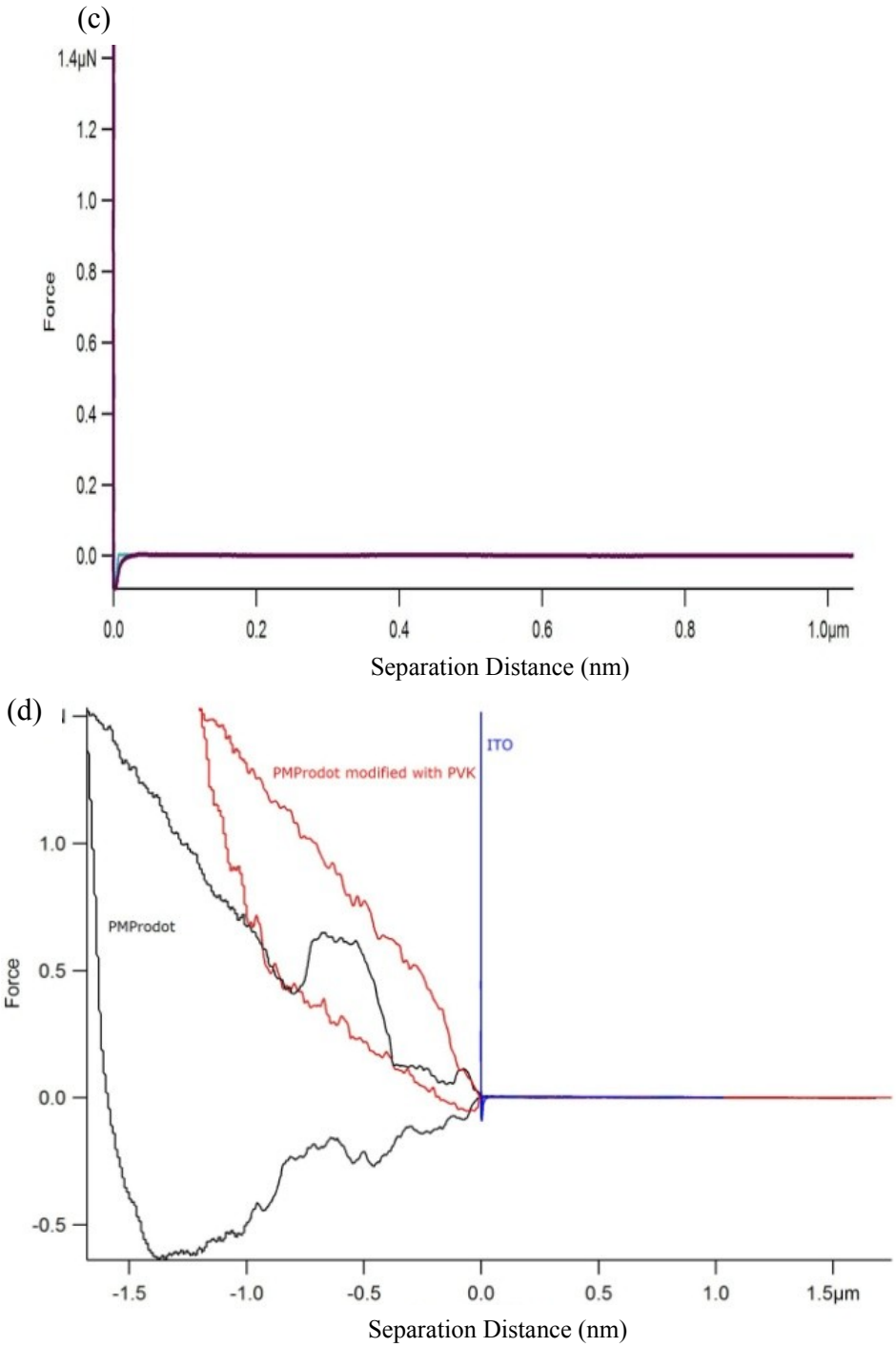

Figure 4.9 AFM Nanoindentation data and analysis. Force vs. Distance fitting for a) PMProDot and b) PMProDot grafted with PVK. Force curve of c) ITO (Control) and d) for PMProDot film, PMProDot grafted with PVK, and ITO.

ITO showed incompressible behavior in the force range that was tested (up to 1 μN) (see Figure 4.9c). From this measurement, the inverse optical lever sensitivity was obtained and used to calculate an indentation depth during the measurements. Only a short indentation length (up to 30 nm) was evaluated since the model only applies when the material behaves like an elastic material. The large indentation data (Figure 4.9c and d) showed characteristic behaviors for each sample. As mentioned, ITO (Figure 4.9c) was not compressed at all during the force range tested whereas PMProDot and PMProDot grafted with PVK showed over 1μm indentation. Figure 4.9d clearly shows very different initial slopes between the films were, however as the tip indents deeper, the slope becomes similar. The indentation depth of PMProDot decreased when the same area was repeatedly indented. This suggests that the material is brittle and likely to be damaged during repeated tapping with the AFM tip. In sharp contrast, PMProDot grafted with PVK showed repeatable force vs. indentation profile hysteresis, indicating that no permanent damage is caused during the large indentation. This behavior is hypothesized to occur due to the grafting copolymerization of PVK in PMProDot. The graft copolymerization of PVK decreases the cross linking between PMProDot chains which can increase the rigidity of the polymer and allow for faster doping of counter ions. The hysteresis seen in Figure 4.9d is likely due to the adhesion between the tip and substrate during the large indentation.

The Young's modulus for PMProDot and PMProDot copolymerized with PVK were measured to be 32.9 MPa, and 41.7 MPa, respectively, confirming the PVK modification increased the rigidity of the PMProDot.

4.3.2. Characterization of functionalized PEDOT

During polymerization, PEDOT becomes insoluble making further functionalization very difficult. Combining the conductive properties of PEDOT and the advantages of polydopamine will permit the use of PEDOT for upload and release of many different types of drug molecules for a wide range of treatments.

Lee et al. has developed a simple and versatile strategy for surface modification of multiple classes of materials. Their approach is based on the adhesive proteins secreted by mussels, 4-dihydroxyl-L-phenylalanine (DOPA), as they attach to wet surfaces, which are rich in 3.[153] DOPA forms strong covalent and noncovalent interactions with substrates and performs as a binding agent for coating inorganic surfaces, including the electropolymerization of dopamine on conducting electrodes.[164-171] Lee et al. identified dopamine as a small-molecule compound that is capable of achieving adhesions to a wide spectrum of materials with the crucial existence of a catechol and amine group (Figure 4.10). The group demonstrated that DOPA can spontaneously deposit thin polymer films on virtually any bulk material surface. Due to the elusiveness of coatings to organic surfaces, DOPA was chosen as the polymer of interest for the post-polymerization functionalization of PEDOT.

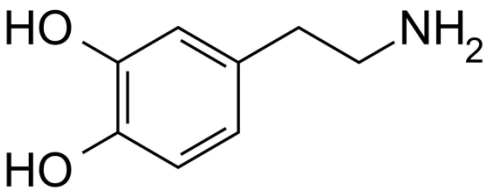

Figure 4.10 Dopamine molecular structure.

Lee et al. developed a very simple "dipping method" to coat surfaces with dopamine (Scheme 4.3). Since the polymerization of dopamine occurs at a very slow rate, clumping of the polydopamine is non-existence, making this process ideal for modification of template embedded PEDOT nanotubes.

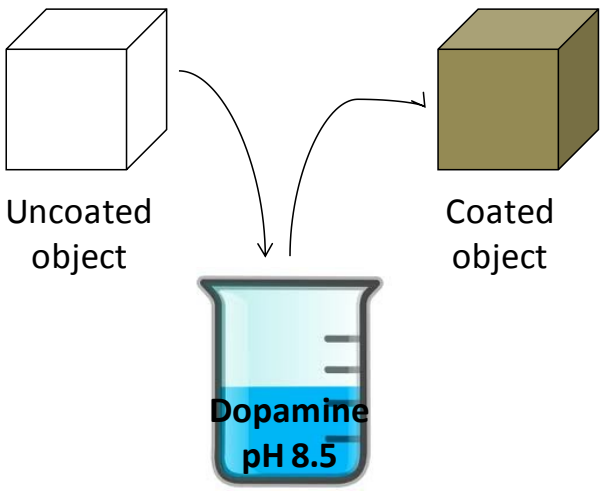

Scheme 4.3 Illustration of thin film deposition of polydopamine by dip-coating method.

The presence of nitrogen in dopamine and lack of nitrogen in PEDOT makes energy-dispersive X-ray spectroscopy (EDS) the fastest and most efficient way to characterize the functionalization. Initially, the functionalized nanotubes were characterized via EDS mapping (see Figure 4.11). The mapping showed the concentration of nitrogen in vacuum was still too high to differentiate exclusively

between the nitrogen atoms on the nanotubes and in the vacuum, although a slightly higher concentration of nitrogen atoms on the nanotubes shows a visible tubular structure.

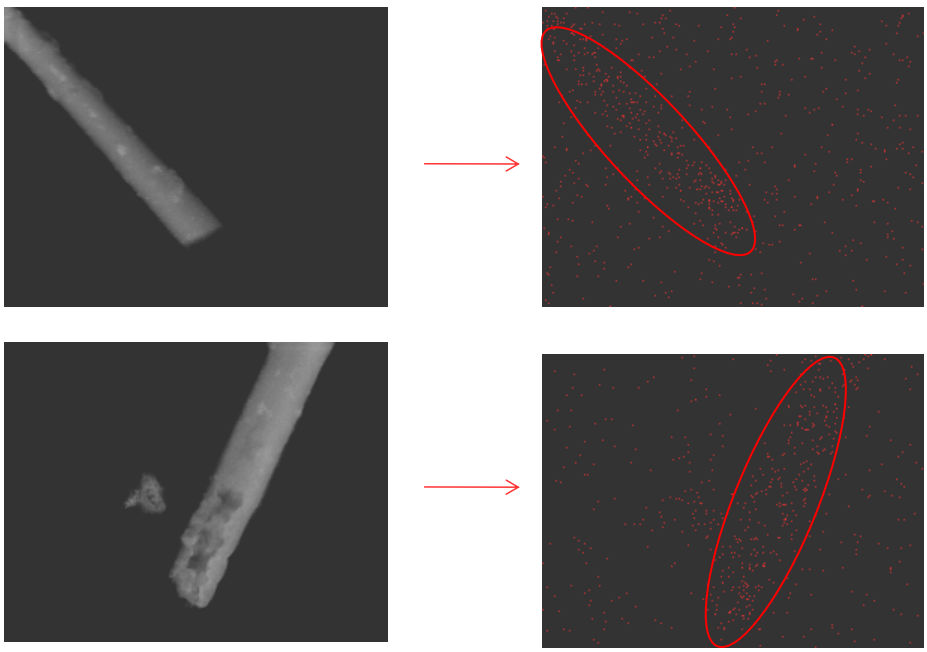

Figure 4.11 EDS mapping of nitrogen atoms on functionalized PEDOT nanotubes. Red ovals indicate region of interest.

Due to the inconclusive results from EDS mapping, area scans were performed on the functionalized PEDOT nanotubes instead. Figure 4.12 shows the EDS spectrum of the N_{1s} scan of PEDOT following 5 h polymerization of polydopamine. EDS spectrum obtained in a section without PEDOT was used as a control (See Figure 4.13).

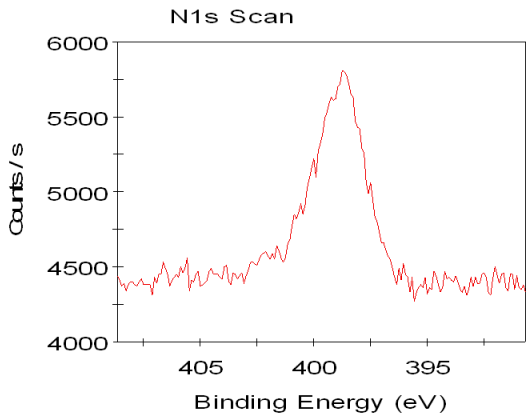

Figure 4.12 EDS N_{1s} spectrum of PEDOT nanotubes functionalized with dopamine for 5 h. N_{1s} has a binding energy of ~399 eV.

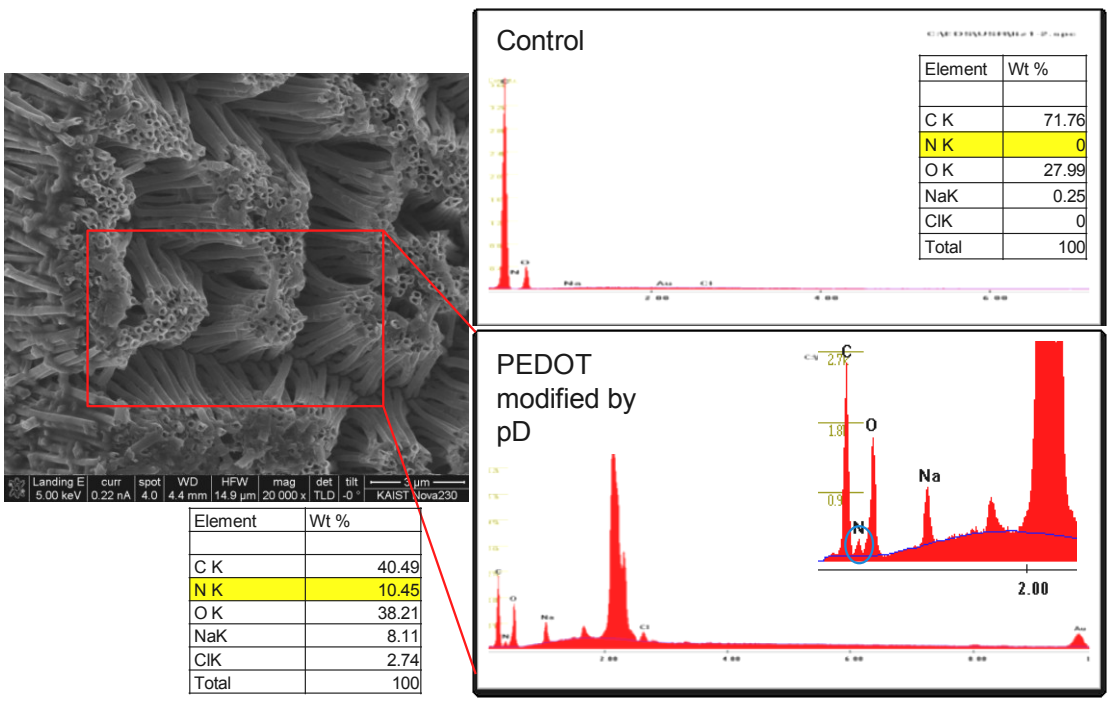

Element	Wt %
C K	71.76
N K	0
O K	27.99
NaK	0.25
ClK	0
Total	100

Element	Wt %
C K	40.49
N K	10.45
O K	38.21
NaK	8.11
ClK	2.74
Total	100

Figure 4.13 Full EDS spectra of PEDOT modified with polydopamine (p^D) and non-nanotube area as the control.

4.4. Conclusion

In this chapter, different methods of functionalization to conductive polymer were address, namely post-polymerization and co-polymerization (chemical-grafting). PMProDot nanotubes were synthesized and co-polymerized with PS and PVK through the accelerated grafting capability of the methylene group on the monomer. The functionalization was characterized with QCM, spectroscopy, electrochromics, and AFM. The functionalized PMProDot nanotubes responded two times faster to potential changes compared to the unfunctionalized counterparts.

The functionalization of PEDOT with polydopamine through post-polymerization was also addressed. Future prospects include the incorporation of dopamine with other drug molecules then polymerized on PEDOT nanotubes. In addition, with the proper choices of secondary reactants, polydopamine coatings can act as a scaffold for the addition of other chemicals allowing for upload and release of drug molecules independent of ionic charge.

Ultimately, this section addressed how the functionalization of the conductive polymers provides promising results that demonstrate the ability of the patch system to fine tune to control release rates of drug delivery accordingly. The ease in functionalization and biocompatibility of polydopamine can pave the way towards a universal controlled TDDS.

Chapter 5: Conclusions and Future Work

"*One never notices what has been done; one can only see what remains to be done."* – Marie Curie

5.1 Conclusions

In this thesis, I invented and fabricated a transdermal drug delivery system (TDDS) composed of PEDOT nanotubes. The success of the patch integrates the unique characteristics PEDOT nanotubes of nanotubes, such as facile template synthesis, robust mechanical properties, well-controlled dimension, high surface area to volume ratio, and extremely fast response times. The electrostatic attraction and repulsion mechanism for upload and release of dye molecules is a well established interaction. In Chapter 2, it was demonstrated that update and release of drugs can be controlled by varying the potential that is applied to the TDDS. The positively charged backbone of PEDOT during oxidation allows for the uptake of anionic dye molecules, while the reduction of PEDOT expels the molecules.

The PEDOT nanotube structure surpasses its film counterparts in fast and controlled drug delivery, as described in Chapter 3. There was an initial release of dyes with an applied potential, however there was almost no difference in the cumulative percent of dye release over 24 hours between -1.2 V and 0 V for films. In comparison, the PEDOT nanotubes provided 70 to 88% greater release with an applied potential than without. Most importantly, Chapter 3 reports the first conductive polymer nanotube transdermal patch drug delivery experiments

performed *in vivo*. Within 15 minutes, live fluorescence imaging revealed the fluorescence intensity from the delivery of Cy5.5 was 40% greater with an applied potential than with 0 V. The patch was shown to remain stable and provide a steady release for up to 2 h. Two-photon microscopy provided the technology to image *in vivo* delivery of dyes and spatial pattern of transdermal penetration in live mice. 3-D stacking images revealed the delivery of FITC penetrated across the dermal-epidermal barrier into the vascular dermis, while no fluorescence signal was detectable at 0 V. Finally, Chapter 3 demonstrated successful *in vivo* transdermal delivery into the blood stream within 10 minutes and saturation of delivery within 20 minutes.

In Chapter 4, the functionalization of PMProDot and PEDOT were thoroughly discussed and characterized. PMProDot nanotubes were synthesized for the first time and functionalized with PS and PVK. The functionalization of PMProDot decreased the polymer's response time by half. This knowledge can be used to fine tune transdermal drug delivery rates to accommodate for potency of different drugs and on-demand delivery for specific treatments. The facile functionalization of PEDOT nanotubes with the versatile polydopamine opens the possibility creating a universal transdermal drug delivery patch system. The idea is to design a TDDS that can be used for not only anionic drugs, but for any drug regardless of its ionic charge and hydrophobicity.

5.2 Future works

In this thesis, the PEDOT nanotube TDDS is shown to be a very promising candidate for biomedical applications. The works performed have proven the *in vivo* transdermal delivery system to be successful. The TDDS needs to be optimized for upload and release of drugs not limited by charge, size, or hydrophobicity. Despite promising *in vivo* results, experiments need to be performed with real drug molecules to demonstrate the possibility of clinical applications. For therapeutic applications, growth hormones should be utilized in order to delivery drugs at a rate that mimic the body's endocrine system. Clonidine is a high potency drug used to treat a variety of medical conditions including high blood pressure, ADHD, opioid detoxification, and menopausal symptoms. Each treatment requires a specific dose, time, and frequency therefore it would be beneficial to use Clonidine as the model drug for the PEDOT nanotube patch.

With the successful delivery of FITC into the blood stream, the PEDOT nanotube transdermal patch can become a universal multimode delivering and imaging system. Together with an external power source, efficacious delivery of therapeutic drugs and imaging moieties can be achieved. Finally, a truly universal, fast, and controlled drug *in vivo* and imaging delivery system can be achieved.

References

1. Prausnitz, M. R.; Langer, R., Transdermal drug delivery. *Nature Biotechnology* 26, 1261-1268 (2008).
2. Prausnitz, M. R.; Mitragotri, S.; Langer, R., Current status and future potential of transdermal drug delivery. *Nature Reviews Drug Discovery* 3, 115-124 (2004).
3. Benson, H. A. E., Transdermal drug delivery: Penetration enhancement techniques. *Current Drug Delivery* 2, 23-33 (2005).
4. Leduc, S. Introduction of medicinal substances into the depth of tissues by electric current. *Ann. d'Electrobiol*. 3, 545–560 (1900).
5. Fellinger, K. & Schmidt, *J. Klinik and therapies des chromischen gelenkreumatismus*. Maudrich Vienna, Austria 549–552 (1954).
6. Gerstel, M. S. & Place, V. A. Drug delivery device. US Patent 3,964,482 (1976).
7. Gora, M. L., Nicotine transdermal system. *Annals of Pharmacotherapy* 27, 742-750 (1993).
8. Prausnitz, M. R., A practical assessment of transdermal drug delivery by skin electroporation. *Advanced Drug Delivery Reviews* 35, 61-76 (1999)
9. Bramson, J.; Dayball, K.; Evelegh, C.; Wan, Y. H.; Page, D.; Smith, A., Enabling topical immunization via microporation: a novel method for pain-free and needle-free delivery of adenovirus-based vaccines. *Gene Therapy* 10 (3), 251-260 (2003).
10. Cramer, M. P.; Saks, S. R., Translating Safety, Efficacy and compliance into economic value for controlled-release dosage forms. *Pharmacoeconomics*, 5, 482-504 (1994).
11. Michaels, A. S.; Chandrasekaran, S. K.; Shaw, J. E., Drug Permeation through human skin – theory and *in vitro* experimental measurements. *Aiche Journal*, 21, 985-996 (1975).
12. Scheuple, R.J., Mechanism of percutaneous absorption. 2. Transient diffusion and relative importance of various routes of skin penetration. *Journal of Investigative Dermatology* 48, 79-88 (1967).
13. Anderson, R. L.; Cassidy, J. M., Variations in physical dimensions and chemical composition of human stratum corneum. *Journal of Investigative Dermatology* 61, 30-32 (1973).
14. Holbrook, K. A.; Odland, G. F., Regional differences in thickness (cell layers) of human stratum-corneum-ultrastructural analysis. *Journal of Investigative Dermatology* 62, 415-422 (1974).
15. Champion, R. H.; Burton, J. L.; Burns, D. A.; Breathnach, S. M., *Textbook of Dermatology*. Blackwell Science: London, 1998.
16. Flynn, G. L., *Transdermal drug delivery: Development issues and research initiatives*. Marcel Dekker: New York, 1991.

17. Elias, P. M.; Feingold, K. R., Coordinate regulation of epidermal differentiation and barrier homeostasis. *Skin Pharmacology and Applied Skin Physiology* 14, 28-34 (2001).
18. Segre, J. *Unlocking Skin's Many Secrets*. http://skinipedia.org/skin-studies/human-skin-secrets2.html.
19. Higuchi, W. I., Analysis of data on medicament release from ointments. *Journal of Pharmaceutical Sciences* 51, 802-804(1962).
20. Brown, M. B.; Martin, G. P.; Jones, S. A.; Akomeah, F. K., Dermal and transdermal drug delivery systems: Current and future prospects. *Drug Delivery* 13, 175-187 (2006).
21. Barry, B. W., Action of skin penetration enhancers – The lipid protein partitioning theory. *International Journal of Cosmetic Science* 10, 281-293 (1988).
22. Barry, B. W., Lipid-protein- partitioning theory of skin penetration enhancement. *Journal of Controlled Release* 15, 237-248 (1991).
23. Williams, A. C.; Barry, B. W., Terpenes and the lipid protein partitioning theory of skin penetration enhancement. *Pharmaceutical Research* 8, 17-24 (1991).
24. Francoeur, M. L.; Golden, G. M.; Potts, R. O., Oleic acid and its effects on stratum-corneum in relation to (trans)dermal drug delivery. *Pharmaceutical Research* 7, 621-627 (1990).
25. Yamane, M. A.; Williams, A. C.; Barry, B. W., Terpene penetration enhancers in propylene glycol water co-solvent systems: Effectiveness and mechanism of action. *Journal of Pharmacy and Pharmacology* 47, 978-989 (1995).
26. Cornwell, P. A.; Barry, B. W.; Bouwstra, J. A.; Gooris, G. S., Modes of action of terpene penetration enhancers in human skin differential scanning calorimetry, small-angle X-ray diffraction and enhancer uptake studies. *International Journal of Pharmaceutic* 127, 9-26 (1996).
27. Lashmar, U. T.; Hadgraft, J.; Thomas, N., Topical application of penetration enhancers to the skin of nude-mice-a histopathological study. *Journal of Pharmacy and Pharmacology* 41, 118-121 (1989).
28. Akimoto, T.; Aoyagi, T.; Minoshima, J.; Nagase, Y., Polymeric percutaneous drug penetration enhancer - Synthesis and enhancing property of PEG/PDMS block copolymer with a cationic end group. *Journal of Controlled Release* 49, 229-241 (1997).
29. Akimoto, T.; Kawahara, K.; Nagase, Y.; Aoyagi, T., Polymeric transdermal drug penetration enhancer: The enhancing effect of oligodimethylsiloxane containing a glucopyranosyl end group. *Journal of Controlled Release* 77, 49-57 (2001).
30. Guy, R. H.; Kalia, Y. N.; Delgado-Charro, M. B.; Merino, V.; Lopez, A.; Marro, D., Iontophoresis: electrorepulsion and electroosmosis. *Journal of Controlled Release*, 64, 129-132 (2000).

31. Wang, Y. M.; Allen, L. V.; Li, L. C.; Tu, Y. H., Iontophoresis of hydrocortisone across hairless mouse skin-investigation of skin alteration. *Journal of Pharmaceutical Sciences* 82, 1140-1144 (1993).
32. Turner, N. G.; Kalia, Y. N.; Guy, R. H., The effect of current on skin barrier function in vivo: Recovery kinetics post-iontophoresis. *Pharmaceutical Research* 14, 1252-1257 (1997).
33. Kalia, Y. N.; Naik, A.; Garrison, J.; Guy, R. H., Iontophoretic drug delivery. *Advanced Drug Delivery Reviews* 56, 619-658 (2004).
34. Banga, A. K.; Bose, S.; Ghosh, T. K., Iontophoresis and electroporation: comparisons and contrasts. *International Journal of Pharmaceutics* 179, 1-19 (1999).
35. Pikal, M. J., The role of electroosmotic flow in transdermal iontophoresis. *Advanced Drug Delivery Reviews* 46, 281-305 (2001).
36. Wang, Y. P.; Thakur, R.; Fan, Q. X.; Michniak, B., Transdermal iontophoresis: combination strategies to improve transdermal iontophoretic drug delivery. *European Journal of Pharmaceutics and Biopharmaceutics* 60, 179-191 (2005).
37. Ledger, P. W., Skin biological issues in electrically enhanced transdermal delivery. *Advanced Drug Delivery Reviews* 9, 289-307 (1992).
38. Kost, J.; Langer, R., Responsive polymeric delivery systems. *Advanced Drug Delivery Reviews* 46, 125-148 (2001).
39. Weaver, J. C.; Vaughan, T. E.; Chizmadzhev, Y., Theory of electrical creation of aqueous pathways across skin transport barriers. *Advanced Drug Delivery Reviews* 35, 21-39 (1999).
40. Prausnitz, M. R., A practical assessment of transdermal drug delivery by skin electroporation. *Advanced Drug Delivery Reviews* 35, 61-76 (1999).
41. Prausnitz, M. R.; Bose, V. G.; Langer, R.; Weaver, J. C., Electroporation of mammalian skin – a mechanism to enhance transdermal drug delivery. *Proceedings of the National Academy of Sciences of the United States of America* 90, 10504-10508 (1993).
42. Vanbever, R.; Preat, V., In vivo efficacy and safety of skin electroporation. *Advanced Drug Delivery Reviews* 35, 77-88 (1999).
43. Nickoloff, J. A., Electroporation Protocols for Microorganisms. Humana Press: Totowa, NJ, 1995.
44. Prausnitz, M. R.; Gill, H. S.; Park, J.-H., *Microneedles for Drug Delivery in Modified Release Drug Delivery.* Informa Healthcare: New York, 2008; Vol. 2.
45. Norden, B.; Krutmeijer, E. *Conductive Polymer*. http://nobelprize.org/nobel_prizes/chemistry/laureates/2000/chemadv.pdf (accessed 2009 25/09).

46. Peng, H.; Soeller, C.; Travas-Sejdic, J., Novel conducting polymers for DNA sensing. *Macromolecules* 40, 909-914 (2007).
47. Geetha, S.; Rao, C. R. K.; Vijayan, M.; Trivedi, D. C., Biosensing and drug delivery by polypyrrole. *Analytica Chimica Acta* 568, 119-125 (2006).
48. Thompson, B. C.; Moulton, S. E.; Ding, J.; Richardson, R.; Cameron, A.; O'Leary, S.; Wallace, G. G.; Clark, G. M., Optimising the incorporation and release of a neurotrophic factor using conducting polypyrrole. *Journal of Controlled Release* 116, 285-294 (2006).
49. Spires, J. B.; Peng, H.; Williams, D. E.; Wright, B. E.; Soeller, C.; Travas-Sejdic, J., The effect of the oxidation state of a terthiophene-conducting polymer and of the presence of a redox probe on its gene-sensing properties. *Biosensors & Bioelectronics* 24, 928-933 (2008).
50. Sershen, S.; West, J., Implantable, polymeric systems for modulated drug delivery. *Advanced Drug Delivery Reviews* 54, 1225-1235 (2002).
51. Zinger, B.; Miller, L. L., Timed release of chemicals form polypyrrole film. *Journal of the American Chemical Society* 106, 6861-6863 (1984).
52. Massoumi, B.; Entezami, A., Controlled release of sulfosalicylic acid during electrochemical switching of conducting polymer bilayers. *European Polymer Journal* 37, 1015-1020 (2001).
53. Massoumi, B.; Entezami, A., Electrochemically controlled binding and release of dexamethasone from conducting polymer bilayer films. *Journal of Bioactive and Compatible Polymers* 17, 51-62 (2002).
54. Pyo, M.; Maeder, G.; Kennedy, R. T.; Reynolds, J. R., Controlled-release of biological molecules from conducting polymer-modified electrodes – the potential – dependent release of adenosine 5'-triphosophate from poly(pyrrole adenosine 5'-triphosphate) films. *Journal of Electroanalytical Chemistry* 368, 329-332 (1994).
55. Fan, Q.; Sirkar, K. K.; Michniak, B., Iontophoretic transdermal drug delivery system using a conducting polymeric membrane. *Journal of Membrane Science* 321, 240-249 (2008).
56. George, P. M.; LaVan, D. A.; Burdick, J. A.; Chen, C. Y.; Liang, E.; Langer, R., Electrically controlled drug delivery from biotin-doped conductive polypyrrole. *Advanced Materials* 18, 577-581 (2006).
57. Li, Y. L.; Neoh, K. G.; Kang, E. T., Controlled release of heparin from polypyrrole-poly(vinyl alcohol) assembly by electrical stimulation. *Journal of Biomedical Materials Research Part A* 73A, 171-181 (2005).
58. Luo, X. L.; Cui, X. T., Electrochemically controlled release based on nanoporous conducting polymers. *Electrochemical Communications* 11, 402-404 (2009).

59. Luo, X. L.; Cui, X. T., Sponge-like nanostructured conducting polymers for electrically controlled drug release. *Electrochemically Communications* 11, 1956-1959 (2009).
60. Abidian, M. R.; Kim, D. H.; Martin, D. C., Conducting-polymer nanotubes for controlled drug release. *Advance Materials* 18, 405-409 (2006).
61. Martin, C. R., Template synthesis of electronically conductive polymer nanostructures. *Accounts of Chemical Research* 28, 61-68 (1995).
62. Martin, C. R.; Vandyke, L. S.; Cai, Z. H.; Liang, W. B., Template synthesis of organic microtubules. *Journal of American Chemical Society* 112, 8976-8977 (1990).
63. Brumlik, C. J.; Martin, C. R., Template synthesis of metal microtubules. *Journal of the American Chemical Society* 1991, 113 (8), 3174-3175.
64. Cao, Y.; Kovalev, A. E.; Xiao, R.; Kim, J.; Mayer, T. S.; Mallouk, T. E., Electrical Transport and Chemical Sensing Properties of Individual Conducting Polymer Nanowires. *Nano Letters* 8, 4653-4658 (2008).
65. Hernandez, R. M.; Richter, L.; Semancik, S.; Stranick, S.; Mallouk, T. E., Template fabrication of protein-functionalized gold-polypyrrole-gold segmented nanowires. *Chemistry of Materials* 16, 3431-3438 (2004).
66. Liu, R.; Lee, S. B., MnO2/Poly(3,4-Ethylenedioxythiophene) Coaxial Nanowires by One-Step Coelectrodeposition for Electrochemical Energy Storage. J*ournal of the American Chemical Society (Communication)* 130, 2942-2943 (2008).
67. Xiao, R.; Il Cho, S.; Liu, R.; Lee, S. B., Controlled electrochemical synthesis of conductive polymer nanotube structures. J*ournal of the American Chemical Society* 129, 4483-4489 (2007).
68. Liu, R.; Duay, J.; Lee, S. B., Electrochemical Formation Mechanism for the Controlled Synthesis of Heterogeneous MnO_2/Poly(3,4-ethylenedioxythiophene) Nanowires. *ACS Nano* 5, 5608-5619 (2010).
69. Liu, R.; Il Cho, S.; Lee, S. B., Poly(3,4-ethylenedioxythiophene) nanotubes as electrode materials for a high-powered supercapacitor. *Nanotechnology* 19, 21570 (2008).
70. Cho, S. I.; Kwon, W. J.; Choi, S.-J.; Kim, P.; Park, S.-A.; Kim, J.; Son, S. J.; Xiao, R.; Kim, S.-H.; Lee, S. B., *Advance Materials*, 17, 171-175 (2005).
71. Cho, S. I.; Lee, S. B., Fast Electrochemistry of Conductive Polymer Nanotubes: Synthesis, Mechanism, and Application. *Accounts of Chemical Research* 41, 699-707 (2008).
72. Platt, J. R., Electrochromics, a possible change of color producible in dyes by an electric field, *Journal of Chemical Physics* 34, 862-863 (1961).

73. Sonmez, G.; Schottland, P.; Zong, K. K.; Reynolds, J. R., Highly transmissive and conductive poly[(3,4-alkylenedioxy)pyrrole-2,5-diyl] (PXDOP) films prepared by air or transition metal catalyzed chemical oxidation. *Journal of Materials Chemistry* 11, 289-294 (2001).
74. Ravi, S.; Chaikof, E. L., Biomaterials for vascular tissue engineering. *Regenerative Medicine* 5, 107-120.
75. Corradi, R.; Armes, S. P., Chemical synthesis of poly(3,4-ethylenedioxythiophene). *Synthetic Metals* 84, 453-454 (1997).
76. Deleeuw, D. M.; Kraakman, P. A.; Bongaerts, P. E. G.; Mutsaers, C. M. J.; Klaassen, D. B. M., Electroplating of conductive polymers for the metallization of insulators. *Synthetic Metals* 66, 263-273 (1994).
77. Gustafsson, J. C.; Liedberg, B.; Inganas, O., In-situ spectroscopic investigations of electrochromism and ion-transport in a poly(3,4-ethylenedioxythiophene) electrode in a solid-state electrochemical cell. *Solid State Ion* 69 (2), 145-152 (1994).
78. Vernitskaya, T. V.; Efimov, O. N., Polypyrrole: A conducting polymer (synthesis, properties, and applications). *Uspekhi Khimii* 66, 489-505 (1997).
79. Martin, C. R., Nanomaterials – a membrane based synthetic approach. *Science* 266, 1961-1966 (1994).
80. Bognitzki, M.; Hou, H. Q.; Ishaque, M.; Frese, T.; Hellwig, M.; Schwarte, C.; Schaper, A.; Wendorff, J. H.; Greiner, A., Polymer, metal, and hybrid nano- and mesotubes by coating degradable polymer template fibers (TUFT process). *Advance Materials* 12 (9), 637-640 (2000).
81. Parthasarathy, R. V.; Martin, C. R., Template-synthesized polyaniline microtubules. *Chemistry of Materials* 6, 1627-1632 (1994).
82. Martin, C. R., Template synthesis of electronically conductive polymer nanostructures. *Accounts of Chemical Research* 28, 61-68 (1995).
83. Wadhwa, R.; Lagenaur, C. F.; Cui, X. T., Electrochemically controlled release of dexamethasone from conducting polymer polypyrrole coated electrode. *Journal of Controlled Release* 110, 531-541 (2006).
84. Abidian, M. R.; Corey, J. M.; Kipke, D. R.; Martin, D. C., Conducting-Polymer Nanotubes Improve Electrical Properties, Mechanical Adhesion, Neural Attachment, and Neurite Outgrowth of Neural Electrodes. *Small*, 421-429 (2010).
85. Nguyen, T. M.; Cho, S.; Varongchayakul, N.; Yoon, D.; Seog, J.; Zong, K.; Lee, S. B., Electrochemical synthesis and one step modification of PMProDot nanotubes and their enhanced electrochemical properties. *Chemical Communications* 48, 2725-2727 (2012).
86. Dey, D.; Hussain, S. A.; Nath, R. K.; Bhattacharjee, D., Preparation and characterization of an anionic dye-polycation molecular film by electrostatic layer-by-layer adsorption process. *Spectrochimica*

Acta Part A-Molecular and Biomolecular Spectroscopy 70, 307-312 (2008).
87. Scheindlin, S., Transdermal drug delivery: Past, present, future. *Molecular Interventions* 4, 308-312 (2004).
88. Don, T. M.; Huang, M. L.; Chiu, A. C.; Kuo, K. H.; Chiu, W. Y.; Chiu, L. H., Preparation of thermo-responsive acrylic hydrogels useful for the application in transdermal drug delivery systems. *Material Chemistry and Physics* 107, 266-273 (2008).
89. Groenendaal, B. L.; Jonas, F.; Freitag, D.; Pielartzik, H.; Reynolds, J. R., Poly(3,4-ethylenedioxythiophene) and its derivatives: Past, present, and future. *Advance Materials* 12, 481-494 (2000).
90. Smela, E.; Inganas, O.; Lundstrom, I., Controlled folding of micrometer-size structures. *Science* 268, 1735-1738 (1995).
91. Smela, E., A microfabricated movable electrochromic "pixel" based on polypyrrole. *Advance Material* 11 (16), 1343-1345 (1999).
92. Gandhi, M. R.; Murray, P.; Spinks, G. M.; Wallace, G. G., Mechanism of electromechanical actuation in polypyrrole. *Synthetic Metals* 73, 247-256 (1995).
93. Yun, J.; Im, J. S.; Lee, Y.-S.; Kim, H.-I., Electro-responsive transdermal drug delivery behavior of PVA/PM/MWCNT nanofibers. *European Polymer Journal* 47, 1893-1902 (2011).
94. Svirskis, D.; Wright, B. E.; Travas-Sejdic, J.; Rodgers, A.; Garg, S., Evaluation of physical properties and performance over time of an actuating polypyrrole based drug delivery system. *Sensors Actuator B: Chemical* 151, 97-102 (2010).
95. Niamlang, S.; Sirivat, A., Electrically controlled release of salicylic acid from poly(p-phenylene vinylene)/polyacrylamide hydrogels. *International Journal of Pharmaceutics* 371, 126-133 (2009).
96. Schmidt, D. J.; Moskowitz, J. S.; Hammond, P. T., Electrically Triggered Release of a Small Molecule Drug from a Polyelectrolyte Multilayer Coating. *Chemistry of Materials* 22, 6416-6425 (2010).
97. Fan, Q.; Sirkar, K. K.; Michniak, B., Iontophoretic transdermal drug delivery system using a conducting polymeric membrane. *Journal of Membrane Sciences* 321, 240-249 (2008).
98. Kumar, A.; Welsh, D. M.; Morvant, M. C.; Piroux, F.; Abboud, K. A.; Reynolds, J. R., Conducting Poly(3,4-alkylenedioxythiophene) Derivatives as Fast Electrochromics with High-Contrast Ratios. *Chemistry of Materials* 10, 896-902 (1998).
99. Kligman A.M., and Christophers E. Preparation of isolated sheets of human stratum corneum. *Achieves Dermatology* 88, 702–705 (1963).
100. Lombry, C.; Dujardin, N.; Preat, V., Transdermal delivery of macromolecules using skin electroporation. Pharmaceutical Research 2000, 17 (1), 32-37
101. http://en.wikipedia.org/wiki/Two-photon_excitation_microscopy.

102. Bronaugh, R. L.; Stewart, R. F.; Congdon, E. R.; Giles, A. L., Methods for in vitro percutaneous- absorption studies. 1. Comparison with *in vivo* results. *Toxicology and Applied Pharmacology* 62, 474-480 (1982).
103. Bronaugh, R. L.; Maibach, H. I., *Percutaneous penetration of nitroaromatic compounds studies in vivo and in vitro in animals and humans.* In Rickert, D. E., 1985; pp 141-148.
104. Panchagnula, R.; Stemmer, K.; Ritschel, W. A., Animal models for transdermal drug delivery. *Methods and Findings in Experimental and Clinical Pharmacology* 19, 335-341 (1997).
105. Sato, K.; Sugibayashi, K.; Morimoto, Y., Species-differences in percutaneous absorption of nicorandil. *Journal of Pharmaceutical Sciences* 80, 104-107 (1991).
106. Schmook, F. P.; Meingassner, J. G.; Billich, A., Comparison of human skin or epidermis models with human and animal skin in in-vitro percutaneous absorption. *International Journal of Pharmaceutics* 215, 51-56 (2001).
107. Vecchia, B. E.; Bunge, A. L., *Dermal Absorption Models in Toxicology and Pharmacology, Chapter 15: Animal models: A comparison of permeability coefficients for excised skin from humans and animals*. Informa Healthcare, 2006; p 305-333.
108. Walker, M.; Dugard, P. H.; Scott, R. C., In vitro percutaneous absorption studies – a comparison of human and laboratory species. *Human Toxicology* 2, 561-562 (1983).
109. Meyer, W.; Schwarz, R.; Neurand, K., *The skin of domestic mammals as a model for human skin with special references to the domestic pig.* In Simon, G. A. Et Al., 1978; pp P39-52.
110. Gordon, C. J.; Gray, L. E.; Monteiro-Riviere, N. A.; Yang, Y.; Miller, D. B., Temperature regulation in adult hamsters and rats exposed perinatally to dioxin. *FASEB Journal* 10, A4 (1996).
111. Calabrese, E. J., Gastrointestinal and dermal absorption – interspecies differences. *Drug Metabolism Reviews* 15, 1013-1032 (1984).
112. Ntziachristos, V.; Ripoll, J.; Wang, L. H. V.; Weissleder, R., Looking and listening to light: the evolution of whole-body photonic imaging. *Nature Biotechnology* 23, 313-320 (2005).
113. Willmann, J. K.; van Bruggen, N.; Dinkelborg, L. M.; Gambhir, S. S., Molecular imaging in drug development. *Nature Reviews Drug Discovery* 7, 591-607 (2008).
114. Weissleder, R.; Ntziachristos, V., Shedding light onto live molecular targets. *Nature Medicine* 9, 123-128 (2003).
115. Weissleder, R.; Pittet, M. J., Imaging in the era of molecular oncology. *Nature* 452, 580-589 (2008).
116. Cherry, S. R., In vivo molecular and genomic imaging: new challenges for imaging physics. *Physics in Medicine and Biology* 49, R13-R48 (2004).

117. Gifford, A. N.; Rice, O. V.; Gatley, S. J.; Huemmer, C. L.; Rogoz, R.; Dejesus, O. T.; Shea, C. E.; Volkow, N. D., Effects of endogenous neurotransmitters on the in vivo binding of dopamine and 5-HT radiotracers in mice. *Journal of Nuclear Medicine* 42, 15P-15P (2001).
118. Denk, W.; Strickler, J. H.; Webb, W. W., 2-Photon laser scanning fluorescence microscopy. Science 248, 73-76 (1990).
119. Webb, W. W.; Wells, K. S.; Sandison, D. R.; Strickler, J. H.*, An International Conference on Digitized Video Microscopy*, B. B. Herman and K. Jacobson: Liss, New York, 1990.
120. Wells, K. S., Sandison, D.R., Strickler, J.H., Webb, W.W., *Handbook of Biological Confocal Microscopy*. J. Pawley: Plenum, New York, 1990.
121. Keller, H. E., *Handbook of Biological Confocal Microscopy*. J. Pawley, Ed.: Plenum, New York, 1990.
122. Konig, K., *Multiphoton Microscopy in Life Sciences*. J. Microsc.-Oxf. 2000, pp. 83-104.
123. Magnusson, B. M.; Walters, K. A.; Roberts, M. S., Veterinary drug delivery: potential for skin penetration enhancement. *Advanced Drug Delivery Reviews 50*, 205-227 (2001).
124. Holovics, H. J.; Anderson, C. R.; Levine, B. S.; Hui, H.-W.; Lunte, C. E., Investigation of drug delivery by iontophoresis in a surgical wound utilizing microdialysis. *Pharmaceutical Research* 25, 1762-1770 (2008).
125. Vanbever, R.; Langers, G.; Montmayeur, S.; Preat, V., Transdermal delivery of fentanyl: rapid onset of analgesia using skin electroporation. *Journal of Controlled Release* 50, 225-235 (1998).
126. Wermeling, D. P.; Banks, S. L.; Huclson, D. A.; Gill, H. S.; Glupta, J.; Prausnitz, M. R.; Stinchcom, A. L., Microneedles permit transdermal delivery of a skin-impermeant medication to humans. *Proceedings of the National Academy of Sciences of the United States of America* 105, 2058-2063 (2008).
127. Assink, R. A.; Arnold, C.; Hollandsworth, R. P., Preparation of oxidatively stable cation-exchange membranes by the elimination of tertiary hydrogens. *Journal of Membrane Science* 56, 143-151 (1991).
128. Wang, C. Q.; Li, G. T.; Guo, R. R., Multiple morphologies from amphiphilic graft copolymers based on chitooligosaccharides as backbones and polycaprolactones as branches. *Chemical Communications* 28, 3591-3593 (2005).
129. Wang, Y.; Jia, W. Z.; Strout, T.; Ding, Y.; Lei, Y., Preparation, Characterization and Sensitive Gas Sensing of Conductive Core-sheath TiO2-PEDOT Nanocables. *Sensors* 9, 6752-6763(2009).
130. Ramanavicius, A.; Ramanaviciene, A.; Malinauskas, A., Electrochemical sensors based on conducting polymer-polypyrrole. *Electrochim Acta* 51, 6025-6037 (2006)

131. Xu, J. J.; Tian, Y.; Peng, R.; Xian, Y. Z.; Ran, Q.; Jin, L. T., Ferrocene clicked poly(3,4-ethylenedioxythiophene) conducting polymer: Characterization, electrochemical and electrochromic properties. *Electrochemistry Communications* 11, 1972-1975 (2009).
132. Bu, H. B.; Gotz, G.; Reinold, E.; Vogt, A.; Schmid, S.; Blanco, R.; Segura, J. L.; Bauerle, P., "Click"-functionalization of conducting poly(3,4-ethylenedioxythiophene) (PEDOT). *Chemical Communications* 11, 1320-1322 (2008).
133. Li, Y.; Vamvounis, G.; Holdcroft, S., Tuning Facile Functionalization of Poly(3-hexylthiophene) via Electrophilic Substitution. *Macromolecules* 34, 141-143 (2001).
134. Inagi, S.; Hayashi, S.; Hosaka, K.; Fuchigami, T., Facile Functionalization of a Thiophene−Fluorine Alternating Copolymer via Electrochemical Polymer Reaction. *Macromolecules* 42, 3881-3883 (2009).
135. Cui, X. Y.; Lee, V. A.; Raphael, Y.; Wiler, J. A.; Hetke, J. F.; Anderson, D. J.; Martin, D. C., Surface modification of neural recording electrodes with conducting polymer/biomolecule blends. *Journal of Biomedical Materials Research* 56, 261-272 (2001).
136. Song, H. K.; Toste, B.; Ahmann, K.; Hoffman-Kim, D.; Palmore, G. T. R., Micropatterns of positive guidance cues anchored to polypyrrole doped with polyglutamic acid: A new platform for characterizing neurite extension in complex environments. *Biomaterials* 27, 473-484 (2006).
137. George, P. M.; LaVan, D. A.; Burdick, J. A.; Chen, C. Y.; Liang, E.; Langer, R., Electrically controlled drug delivery from biotin-doped conductive polypyrrole. *Advanced Materials* 18, 577-581 (2006).
138. Malhotra, B. D.; Singhal, R., Conducting polymer based biomolecular electronic devices. Pramana-*Journal of Physics* 61, 331-343 (2003).
139. Wong, J. Y.; Langer, R.; Ingber, D. E., Electrically conducting polymers can noninvasively control the shape and growth of mammalian cells. *Proceedings of the National Academy of Sciences of the United States of America* 91, 3201-3204 (1994).
140. Brisset, H.; Navarro, A.-E.; Moustrou, C.; Perepichka, I. F.; Roncali, J., Electrogenerated conjugated polymers incorporating a ferrocene-derivatized-(3,4-ethylenedioxythiophene). *Electrochemistry Communications*, 6, 249-253 (2004).
141. Mishra, S. P.; Sahoo, R.; Ambade, A. V.; Contractor, A. Q.; Kumar, A., Synthesis and characterization of functionalized 3,4-propylenedioxythiophene and its derivatives. *Journal of Materials Chemistry* 14, 1896-1900 (2004).
142. Yue, J.; Gordon, G.; Epstein, A. J., Comparison of different synthetic routes for sulfonation of polyaniline. *Polymer* 33, 4410-4418 (1992).

143. Li, G. T.; Bhosale, S.; Tao, S. Y.; Fuhrhop, J. H., Conducting polythiophenes with a broad spectrum of reactive groups. *Journal of Polymer Science Part A-Polymer Chemistry* 43, 4547-4558 (2005).
144. Li, G. T.; Yan, Q.; Nita-Lazar, A.; Haltiwanger, R. S.; Lennarz, W. J., Studies on the N-glycosylation of the subunits of oligosaccharyl transferase in Saccharomyces cerevisiae. *Journal of Biological Chemistry* 280, 1864-1871 (2005).
145. Li, G. T.; Zhou, X.; Zhao, G.; Schindelin, H.; Lennarz, W. J., Multiple modes of interaction of the deglycosylation enzyme, mouse peptide N-glycanase, with the proteasome. *Proceedings of the National Academy of Sciences of the United States of America* 102, 15809-15814 (2005).
146. Kolb, H. C.; Finn, M. G.; Sharpless, K. B., Click chemistry: Diverse chemical function from a few good reactions. *Angewandte Chemie-International Edition* 40, 2004-2021(2001).
147. Sumerlin, B. S.; Tsarevsky, N. V.; Louche, G.; Lee, R. Y.; Matyjaszewski, K., Highly efficient "click" functionalization of poly(3-azidopropyl methacrylate) prepared by ATRP. *Macromolecules* 38, 7540-7545 (2005).
148. Opsteen, J. A.; van Hest, J. C. M., Modular synthesis of block copolymers via cycloaddition of terminal azide and alkyne functionalized polymers. *Chemical Communications* 1, 57-59 (2005).
149. Lutz, J. F.; Borner, H. G.; Weichenhan, K., Combining atom transfer radical polymerization and click chemistry: A versatile method for the preparation of end-functional polymers. *Macromolecular Rapid Communications* 26, 514-518 (2005).
150. Helms, B.; Mynar, J. L.; Hawker, C. J.; Frechet, J. M. J., Dendronized linear polymers via "click chemistry". *Journal of the American Chemical Society* 126, 15020-15021 (2004).
151. Parrish, B.; Breitenkamp, R. B.; Emrick, T., PEG- and peptide-grafted aliphatic polyesters by click chemistry. *Journal of the American Chemical Society* 127, 7404-7410 (2005).
152. Yoon, D.; Ko, S.; Lee, Y.; Lee, S.; Pyo, M.; Zong, K., Poly(3,4-(2-methylene)propylenedioxythiophene) for Electrochemical Grafting of Polystyrene via Methylene Functionality. *Journal of Electrochemical Society* 155, H438-H442 (2008).
153. Lee, H.; Dellatore, S. M.; Miller, W. M.; Messersmith, P. B., Mussel-inspired surface chemistry for multifunctional coatings. *Science* 318, 426-430 (2007).
154. Mendez, A.; Diaz-Arista, P.; Salgado, L.; Meas, Y.; Trejo, G., *International Journal of Electrochemical Science* 2008, 3, 918.
155. Ballav, N.; Biswas, M., A conducting composite of polyN-vinylcarbazole and polythiophene. *Synthetic Metals* 132, 213-218 (2003).

156. Ballav, N.; Maity, A.; Biswas, M., Preparation and characterization of a conducting nanocomposite of polyN-vinylcarbazole with acetylene black. *Materials Chemistry and Physics* 87, 120-126 (2004).
157. Rivaton, A.; Mailhot, B.; Derderian, G.; Bussiere, P. O.; Gardette, J. L., Investigation of the Photophysical Processes and Photochemical Reactions Involved in PVK Films Irradiated at $\lambda > 300$ nm. *Macromolecules* 36, 5815-5824 (2003).
158. Gorman, C. B.; Ginsburg, E. J.; Grubbs, R. H., Soluble, highly conjugated derivatives of polyacetylene from the ring-opening metathesis polymerization of monosubstituted cyclooctatetraenes: synthesis and the relationship between polymer structure and physical properties. *Journal of American Chemical Society* 115, 1397-1409 (1993).
159. Wei, Y.; Focke, W. W.; Wnek, G. E.; Ray, A.; Macdiarmid, A. G., Synthesis and electrochemical of alkylring-substituted polyanilines. *Journal of Physical Chemistry* 93, 495-499 (1989).
160. Monk, P. M. S.; Mortimer, D. R.; Rosseinsky, D. R., Electrochromism, *Fundamentals and Applications*. VCH Verlagsgesellschaft mbH: Germany, 1995.
161. Cho, S. I.; Choi, D. H.; Kim, S.-H.; Lee, S. B., Electrochemical Synthesis and Fast Electrochromics of Poly(3,4-ethylenedioxythiophene) Nanotubes in Flexible Substrate. *Chemistry of Materials* 17, 4564-4566 (2005).
162. Liu, R.; Duay, J.; Lee, S. B., Heterogeneous nanostructured electrode materials for electrochemical energy storage. *Chemical Communications* 47, 1384-1404 (2011).
163. Hu, X.; Wang, T.; Wang, L.; Guo, S.; Dong, S., A general route to prepare one- and three-dimensional carbon nanotube/metal nanoparticle composite nanostructures. *Langmuir* 23, 6352-6357 (2007).
164. Yu, M. E.; Deming, T. J., Synthetic polypeptide mimics of marine adhesives. *Macromolecules* 31, 4739-4745 (1998).
165. Dalsin, J. L.; Hu, B. H.; Lee, B. P.; Messersmith, P. B., Mussel adhesive protein mimetic polymers for the preparation of nonfouling surfaces. *Journal of the American Chemical Society* 125, 4253-4258 (2003).
166. Statz, A. R.; Meagher, R. J.; Barron, A. E.; Messersmith, P. B., New peptidomimetic polymers for antifouling surfaces. *Journal of the American Chemical Society* 127, 7972-7973 (2005).
167. Paunesku, T.; Rajh, T.; Wiederrecht, G.; Maser, J.; Vogt, S.; Stojicevic, N.; Protic, M.; Lai, B.; Oryhon, J.; Thurnauer, M.; Woloschak, G., Biology of TiO2-oligonucleotide nanocomposites. *Nature Materials* 2, 343-346 (2003).
168. Xu, C. J.; Xu, K. M.; Gu, H. W.; Zheng, R. K.; Liu, H.; Zhang, X. X.; Guo, Z. H.; Xu, B., Dopamine as a robust anchor to immobilize functional molecules on the iron oxide shell of magnetic

nanoparticles. *Journal of the American Chemical Society* 126, 9938-9939 (2004).
169. Zurcher, S.; Wackerlin, D.; Bethuel, Y.; Malisova, B.; Textor, M.; Tosatti, S.; Gademann, K., Biomimetic surface modifications based on the cyanobacterial iron chelator anachelin. *Journal of the American Chemical Society*, 128, 1064-1065 (2006).
170. Li, Y. L.; Liu, M. L.; Xiang, C. H.; Xie, Q. J.; Yao, S. Z., Electrochemical quartz crystal microbalance study on growth and property of the polymer deposit at gold electrodes during oxidation of dopamine in aqueous solutions. *Thin Solid Films*, 497, 270-278 (2006).
171. Lee, H.; Scherer, N. F.; Messersmith, P. B., Single-molecule mechanics of mussel adhesion. *Proceedings of the National Academy of Sciences of the United States of America* 103, 12999-13003 (2006).